BACTERIAL STIMULATION ENHANCES THE PRO-METASTATIC CROSS-TALK OF NEUTROPHILS AND TUMOR CELLS

Dissertation
for
the doctoral degree of
Dr. rer. nat.

from the Faculty of Biology
University of Duisburg-Essen
Germany

Submitted by
Jagoda Agnieszka Szlachetko

Born in Bochnia, Poland

Date of submission: February 2023

The experiments underlying the present work were conducted at the research department of the clinic for otorhinolaryngology of the University Hospital Essen as part of the University of Duisburg-Essen.

1. **Examiner:**

   Prof. Dr. Sven Brandau

2. **Examiner:**

   Prof. Dr. Daniel R. Engel

3. **Examiner:**

Chair of the Board of Examiners:

Prof Dr. Nicole Dünker

Date of the Oral Examination:

13.06.2023

“If we knew what it was we were doing, it would not be called research, would it?”

Albert Einstein

Table of Contents

ABBREVIATIONS

Abbreviation	Full name
BAs	Bile Acids
Bcl-2	B-cell Lymphoma 2
Bcl-X	B-cell Lymphoma extra large
BSA	Bovine Serum Albumine
CAFs	Cancer Associated Fibroblasts
CAM	Chick Chorioallantoic Membrane
cDNA	Complementary Deoxyribonucleic Acid
cEMT	Complete Epithelial-Mesenchymal Transition
cMSCs	Control Mesenchymal Stromal Cells
CTCs	Circulating Tumor Cells
DAPI	4',6-diamidino-2-phenylindole
DNA	Deoxyribonucleic Acid
ECM	Extracellular Matrix
ELISA	Enzyme-linked Immunosorbent Assay
EMT	Epithelial-Mesenchymal Transition
FACS	Fluorescence-activated Cell Sorting
FAS	Fatty Acid Synthase
FCS	Fetal Calf Serum
fMLP	*n*-formylmethionine-leucyl-phenylalanine
G-CSF	Granulocyte Colony Stimulating Factor

G-CSFR	Granulocyte Colony Stimulating Factor Receptor
GFP	Green Fluorescent Protein
GM-CSF	Granulocyte-Macrophage Colony-Stimulating Factor
GMPs	Granulocyte-Monocyte Progenitors
HIF-1α	Hypoxia-Inducible factor 1-alpha
HMGB1	High Mobility Group Box 1 Protein
HNC	Head and neck cancer
HNSCC	Head and neck squamous cell carcinoma
HSP90β	Heat Shock Protein 90 beta
IL	Interleukin
JAK	Janus kinase
KRAS	Kirsten rat sarcoma virus
LB	Lysogeny broth
LPS	Lipopolysaccharide
LTA	Lipoteichoic acid
MACS	Magnetic-activated cell sorting
MAMPs	Microbe-associated molecular patterns
MDSCs	Myeloid-derived suppressor cells
MET	Mesenchymal-Epithelial Transition
MIC-A	MHC class I chain-related gene A
MIC-B	MHC class I chain-related gene B
MIF	Macrophage migration inhibitory factor
MIP-1β	Macrophage inflammatory protein

MMP-9	Matrix Metallopeptidase 9
MPO	Myeloperoxidase
MSC	Mesenchymal Stromal Cells
MYH9	Myosin heavy chain 9
NAD	Nicotinamide Adenine Dinucleotide
NE	Neutrophil Elastase
NETs	Neutrophil Extracellular Traps
NF-kβ	Nuclear factor 'kappa-light-chain-enhancer' of activated b-cells
NK	Natural killer cells
NLR	Neutrophil-Lymphocyte Ratio
NMR	Nuclear magnetic resonance
PAD4	Protein arginine deiminase 4
PBS	Phosphate-buffered saline
PD-1	Programmed cell death protein 1
PDGF	Platelet-derived growth factor
PDL-1	Programmed death-ligand 1
pEMT	Partial Epithelial-Mesenchymal Transition
PFA	Paraformaldehyde
PMA	Phorbol myristate acetate
PMN	Polymorphonuclear Neutrophils
PRR	Pattern Recognition Receptor
PVA	Poly(vinyl alcohol)
PVDF	Polyvinylidene fluoride

qPCR	Quantitative Polymerase Chain Reaction
QSX	Sulfhydryl Oxidase 1
RNA	Ribonucleic acid
ROS	Reactive Oxygen Species
RT	Room temperature
RT-PCR	Reverse Transcription - Polymerase Chain Reaction
SDS	Sodium Dodecyl Sulfate
STAT3	Signal transducer and activator of transcription 3
TAM	Tumor-associated Macrophages
TAN	Tumor-associated Neutrophils
TBS	Tris-buffered saline
TEM	Trans-endothelial migration
TGF-β	Transforming growth factor beta
TIMP	Tissue inhibitor of metalloproteinase
TLR	Toll-like receptor
TMB	3,3',5,5'-Tetramethylbenzide
TME	Tumor Microenvironment
tMSC	Tumor Mesenchymal Stromal Cells
TNF-α	Tumor necrosis factor alpha
uPA	Urokinase-type plasminogen activator
VEGF	Vascular endothelial growth factor
XIAP	X-linked inhibitor of apoptosis

LIST OF FIGURES

LIST OF TABLES

1. INTRODUCTION

1.1. DIVERSITY OF TUMOR MICROENVIRONMENT

The Tumor Microenvironment (TME) has been an underestimated part of tumor research. However, over the last decade scientists have started to unravel the role of this heterogeneous structure and appreciate its importance. Inside of TME, beside tumor cells, we can find a large compartment of stromal cells, fibroblasts, several different types of immune cells (both innate and adaptive) and bacteria. Not only is the quantity of these components important but also their distribution and functional reprogramming triggered by other parts of TME. Activated immune cells can either affect tumor cells directly by binding to the receptors on their surface or indirectly by releasing cytokines and chemokines. Those could either modify tumor cells or attract other immune cells to act either as a tumor-promotor or -repressor. This duality of function can be observed in most immune cells present in TME and certain switch is triggered by environmental signals. N1 neutrophils, M1 macrophages and DC1 dendritic cells can phagocyte tumor cells, while their N2, M2 and DC2 versions promote immune suppressive microenvironment of tumors. Th1 T cells and NK1 natural killer cells induce apoptosis of tumor cells by release of granzyme and perforin, while Treg, Th2 and NK2 release VEGF and cytokines to induce tumor growth (Kim et al., 2016, Vitale et al., 2021).

1.1.1. TME OF HEAD AND NECK TUMORS (HNC)

Head and Neck Squamous Cell Carcinoma (HNSCC), which includes cancers of oropharynx, larynx, hypopharynx, oral cavity and paranasal sinuses, is one of the most aggressive cancers with low survival rates (68% 5-year relative survival rate) and tendency to form short distance metastasis to local draining lymph nodes. The main risk factors are alcohol and tobacco intake, which are the cause of almost 75% of the cases. Furthermore, a gender and age dependence was observed, as most of the patients are male, above 50 years old. HNC tumors are highly heterogeneous and contain extracellular matrix (ECM), cancer associated fibroblasts (CAFs) and several types of immune cells. All mentioned cells not only provide intermediate metabolites and nutrients to tumor cells during stimulation in TME, but also release a net of cytokines, chemokines and growth factors

which then can influence further tumor growth and development (Fig. 1, Bhat et al., 2021, Chen P. et al., 2020, Nisar et al., 2021, Qin et al., 2021).

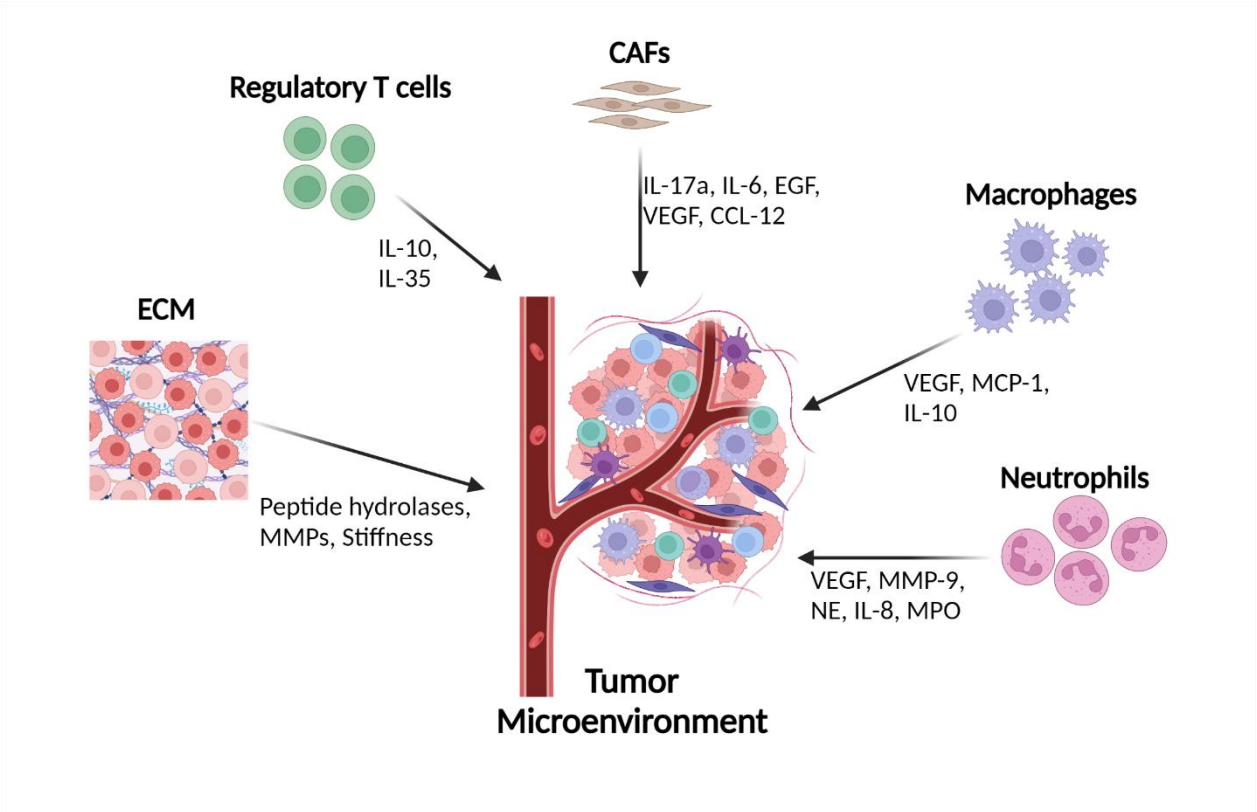

FIGURE 1: CHEMOKINE AND CYTOKINE-MEDIATED CROSSTALK IN HEAD AND NECK SQUAMOUS CELL CARCINOMA (HNSCC) TUMOR MICROENVIRONMENT (TME) (ADAPTED FROM: NISAR ET AL., 2021).

1.1.2. ROLE OF STROMAL CELLS INSIDE TME

CAFs are by definition fibroblasts, which can be found in close proximity to cancer cells. Based on their origin they can be divided into four groups: tissue-resident fibroblasts (activated by their closed proximity to the tumor) (i), cells which differentiated from other types of cells (endothelial cells, epithelial cells etc.) (ii), tumor cells which went through epithelial-mesenchymal transition (EMT) (iii) and mesenchymal stromal cells coming from bone marrow (iv). This simple classification got more complicated with the onset of single-cell RNAseq. These novel methods revealed that inside every stromal part of tumor at least few different groups of fibroblasts could be observed, which significantly differ from each other in their function in TME. Taking this novel information, it became even more important to study their interactions with tumor cells and search

for certain patterns of behavior among the groups, which could in the future help improving tumor therapy (Kanzaki et al., 2020).

CAFs are well-known for their pro-tumor abilities like increasing angiogenesis, promoting tumor proliferation, ECM remodeling and regulation of immune response. Most of these effects are caused indirectly via cytokines (angiogenesis) or matrix remodeling enzymes released by CAFs upon their activation in TME. It was also shown that CAFs can play an anti-tumor role and inhibit tumor growth and progression (Chen P. et al., 2021).

Another important role of stromal parts of tumors is their hospitality to and influence on several groups of immune cells. CAFs can decrease the influx of cytotoxic T-cells into the tumor. Additionally, when T cells reach the stromal areas, fibroblasts can via various cytokines either decrease their function or decrease the ability of dendritic cells to stimulate them. In both cases, CAFs work as immuno-suppressors and help tumor progression. CAFs can also serve as a friendly environment for immune-suppressive immune cells like regulatory T cells, MDSCs and macrophages. Better characterization of CAFs in this context is important in terms of improving immunotherapy approaches (Chen P. et al., 2021, Wang et al., 2020).

1.2. BACTERIAL COLONIZATION OF TUMORS

Most of the parts of human organism are to some extent colonized by bacteria. Populations of commensal bacteria in colon or vagina are known for their beneficial impact on immune system, but unfortunately, not all bacterial species are harmless. Bacterial communities in the gut and reproductive tract have been studied in detail. However, the bacterial component of the TME has been ignored despite that certain species are known to cause cancers (e.g. *Heliobacter pylori*) (Goodman et al., 2018, Poutahidis et al., 2016, Schwabe et al., 2013, Sepich-Poore et al., 2021, Wong-Rolle et al., 2021, Zitvogel et al., 2017).

1.2.1. DYSBIOSIS AND BARRIER FAILURE

Dysbiosis is an imbalance in microbial composition of human body, typically connected with decrease in beneficial bacteria, being overgrown by aggressive species.

Dysbiosis as a result of cancer-induced immunodeficiency is a sudden bacterial overgrowth limited to some parts of the body, which can cause certain qualitative and metagenomic changes in TME. Those changes include a decrease in health promoting symbionts combined with an increase in invasive and inflammation-inducing bacteria together with genotoxic bacteria, which produce

cancer-promoting metabolites. Bacteria are releasing pro-inflammatory MAMPs (like LPS) and certain metabolites, which can reach tumors with blood stream and promote their growth. Through this mechanism some microbiome-free tumors, like liver or pancreas can still be affected by bacteria (Azevedo et al., 2020, Goodman et al., 2018, Schwabe et al., 2013). Dysbiosis is also suspected to decrease effectiveness of the immunotherapy. Dysbiosis can occur through changes in diet (and obesity), intake of medications (antibiotics), inflammation or infections. Exact mechanisms are still unknown; however, it has been shown that antibiotic therapy in certain type of cancers could decrease some of their negative effects. However, in colon cancer the effect seems to be opposite and pre-antibiotic therapy increased tumor growth (Yu et al., 2021). Additionally, it should be considered that every antibiotic therapy is connected with not only killing 'bad' bacteria, but also the 'good' ones what can destabilize whole immune response of the organism.

As an effect of the imbalance in the tumor-bacteria interaction, two types of barrier failures can be observed: physical and functional. Physical barrier failure can be a tear either in mucosa layer or on the level of tight junctions. The functional barrier can be compromised when antibacterial defense systems are no longer active, which can be triggered by primary defects in genes encoding a functional barrier, or secondary defects caused by infections and carcinogenesis.

Both events lead to the inflammation, during which MAMP or PRR signaling is activated. This in turn leads to certain pathways in tumor cells, like NF-kB pathway, being induced. Which, through the release of cytokines along with factors like IL-6 and TNF, leads to increase of tumor proliferation and survival (Fig 2, Azevedo et al., 2020, Schwabe et al., 2013).

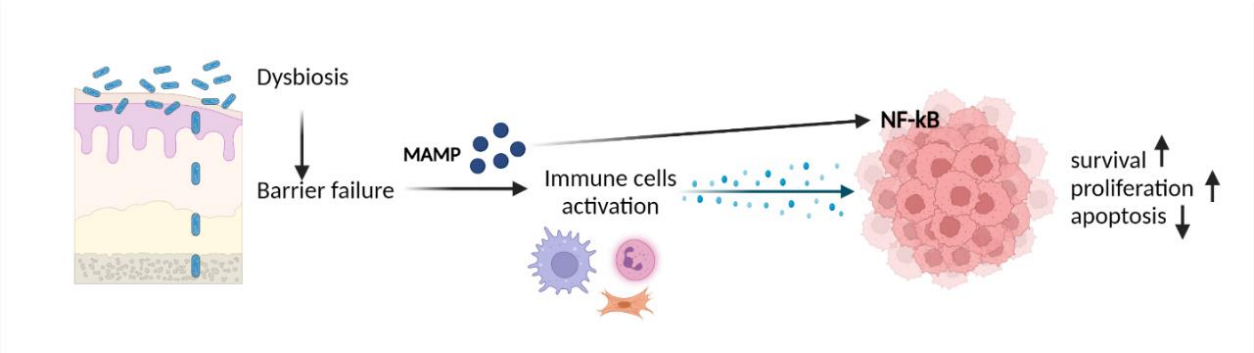

FIGURE 2: SCHEME OF POSSIBLE MECHANISMS BY WHICH MICROBIOME MODULATES CARCINOGENESIS.

1.2.2. ROLE OF THE BACTERIA INSIDE TUMOR CELLS

When tissues functional barriers are compromised, bacteria can colonize spaces in compartments and cells, they normally wouldn't be able to reach. Visualization of bacteria in TME revealed they reside mainly inside tumor and immune cells and not in the extracellular components. Bacteria, when present inside tumor cells can induce carcinogenesis, by causing chronic infection, immune evasion and immune suppression. Other mechanisms promoting the tumor progression can include the transformation of cells and the production of toxins, which by the induction of hormones leads to increase proliferation of tumor cells (Al-Hilu et al., 2020). Bacteria can also act via the molecules present on their cell walls, like LPS or LTA, which were shown to modulate anti-tumor immunity in liver. The indirect way of action is enacted by the release or processing of metabolites by bacteria (Azevedo et al., 2020, Zitvogel et al., 2017).

1.2.3. IMPACT OF THE MICROBIOME ON TUMOR THERAPY

Using murine models, it has been demonstrated that chemotherapy can influence the microbiome and in this way modulates the anti-tumor response. Cyclophosphamide, medication from the alkylating agents group, causes translocation of gram-positive bacteria into secondary lymphoid organs, which in turn increases the production of helper T-cells and enhances the response of the organism caused by memory T-cells (Yu et al., 2021). Another drug used in chemotherapy treatment of ovarian, breast and lung cancer and often affected by microbiome is Gemcitabine (belonging to class of medications called antimetabolites). It has been established that bacteria from Mycoplasma group can rapidly metabolize this compound, not leaving enough time for the drugs to start working and act on tumor cells (Azevedo et al., 2020). A similar pattern was visible with bacteria metabolizing Irinotecan (drug from antineoplastic class of medications, used in colon or rectal cancer therapy); however, here not the whole therapy was jeopardized, but there was a visible increase in side effects, notably diarrhea (Goodman et al., 2018). On the other hand, *Pseudomonas aeruginosa*, via its metabolite – lectin, was able to increase the effectiveness of doxorubicin-mediated cell death during the treatment (Chen et al., 2022). Changes in the microbiome caused by chemotherapy can also induce NF-kB, which then via IL-6 and TNF, promotes the inflammation and mucosal damage (Azevedo et al., 2020, Yu et al., 2021).

In case of radiotherapy, direct impact of microbiome is not known yet, but changes in the microbiome caused by this method of treatment are responsible for most of the adverse effects patients' experience. It was found out that with the use of probiotics, which should re-build

microbiome in the colon, most of the side effects, as nausea and diarrhea could be avoided (Yu et al., 2021).

The bacterial presence in tumors is also playing a role during immunotherapy. It was shown that LPS can enhance the innate immune response and boost the cytotoxicity of T cells against tumor cells. Additionally, in the case of anti-PD-1/PDL-1 immunotherapy it was observed that different bacteria strains affect differently the effectiveness of the treatment (Azevedo et al., 2020, Goodman et al., 2018).

1.2.4. BACTERIAL ABUNDANCE IN HNC TUMORS

Oral tumors, because of their location, are highly colonized by bacteria, which would suggest that the HNC microbiome can play an important role in the tumor development. The increased alcohol and tobacco consumption, can lead to dysbiosis even in a healthy oral cavity. There are a few bacteria strains characterized as strictly specific to this environment, and they are also thought to play a certain role in tumor therapy. *Fusobacterium nucleatum* and *Porphyromonas gingivalis* are anaerobic bacteria, which are commonly found in a disturbed oral cavity and as such can serve as a negative prognostic biomarker for HNC tumor. High abundance of those bacteria might impair effects of chemotherapy and upregulate the drug tolerance (Chen et al., 2022, Sun et al., 2020). They can also increase the number of tumor-infiltrating immune cells, which are forming a pro-inflammatory environment within tumor tissue (Whitmore et al., 2014). It was observed that originating from the oral cavity, these bacteria can easily travel with food through the digestive tract and find their new location in the colon or pancreatic cancer microenvironment. Both species were detected in those types of cancer and positively correlated with the tumor progression (Chen et al., 2022, Sun et al., 2020). Additionally *F. nucleatum* can activate p38, which leads to the increased secretion of MMP-9 and might induce tumor invasion and metastasis (Whitmore et al., 2014). Other bacteria strains that are often associated with HNC tumors are *Staphylococcus aureus*, *Streptococcus pneumoniae* and *Klebsiella pneumoniae* (Shiomori et al., 2007).

Presence of many different bacteria strains in the oral microbiome leads to chronic inflammation, and release of ROS and pro-inflammatory cytokines, like IL-1β, IL-6, IL-8, MMPs. All those factors are known to be involved in promoting tumor initiation, progression and finally metastasis. Another mechanism via which the microbiome influences HNC cancers is by inducting immunosuppression of the host. Furthermore, bacteria can release specific factors and proteins (e.g. E6, E7) which can decrease activation of T lymphocytes and cytotoxicity of NK cells. Bacteria can

also induce Epithelial Mesenchymal Transition (EMT) and in this way promote the tumor metastasis (Sun et al., 2020).

1.2.4.1. The role of *Staphylococcus aureus* infection in HNC tumors

Oro-pharyngeal and respiratory tract are mainly populated by commensal bacteria, but they can also be exposed to pathogenic bacteria due to infections (Sharma et al., 2018). In HNC tumors, the most frequent therapy is the surgery, putting the patients in the danger of serious tissue infections or even sepsis if the disintegration of the mucosal barriers occurs. Up to 90% of patients are suffering from wound infection after the surgery and surgical site infections occur in about 50% of cases, mostly being caused by *S. aureus* (Durand et al., 2015). Especially dangerous for the patients is the methicillin resistant *S. aureus* (MRSA) which complicates the course of disease and significantly decreases their recovery rate (Shiomori et al., 2007).

Staphylococcus aureus is not only a bacteria species which can infect the whole body as a consequence of the surgery, but it's also the one, which is present inside the primary tumor and can therefore influence metastatic properties of tumor cells. One of the examples is the induction of EMT by lipoteichoic acid (LTA) coming from *S. aureus* (Kim et al., 2017).

1.3. POLYMORPHONUCLEAR NEUTROPHILS IN TUMORS

Polymorphonuclear neutrophils (PMN) are the most abundant leukocytes in the human blood. They are the first defense line during an infection, because of their rapid response and the fast recruitment to the site of tissue injury. Because of their short life span (around 24h in the blood or a few days in the tissue) and specialized mechanism of action, they were for a long time ignored in the chronical diseases like cancer; however, when TME field started to emerge also the PMN were put into focus.

PMN develop in the bone marrow from granulocyte-monocyte progenitors (GMPs), which give rise to both neutrophils and monocytes. On the way to the full maturation, PMN follow certain development steps, as the expression of lineage marker CD66b, followed by the upregulation of CD11b and CD16. During granulopoiesis three types of granules are formed: azurophilic, which contain myeloperoxidase (MPO) and neutrophil elastase (NE), secondary with lactoferrin as well as tertiary containing gelatinases (like MMP-9) (Smith et al., 2018). During differentiation, PMN develop from myelocytes into banded and then segmented neutrophils. Under homeostatic conditions, this whole maturation process takes place in the bone marrow, so in the blood only

fully mature cells with segmented nuclei are found. However, in the tumor tissue and blood coming from tumor patients also immature PMN were found, which suggests the operation of so-called emergency hematopoiesis with the pre-mature release of cells which are not fully developed into the bloodstream (Coffelt et al., 2016, Hedrick et al., 2022, Nicolas-Avila et al., 2017, Shaul et al., 2017, Wu et al., 2020). This observation highlights the importance of understanding the PMN heterogeneity in the bone marrow, blood and tumor tissue and principles affecting the response of the organism to the disease (Ng et al., 2019). The main factor regulating the induction of granulopoiesis is the granulocyte colony-stimulating factor (G-CSF) and its receptor – G-CSFR. Endothelial cells or fibroblasts produce G-CSF as a response to the inflammation event. It binds to its receptor on the surface of PMN, activating several pathways essential for cancer inflammation and granulopoiesis (JAK, STAT3). In addition, G-CSF is responsible for the release of mature PMN (Liang et al., 2016). PMN released to the blood are then attracted by tumors via CXCR2 ligands: CXCL1, CXCL2, CXCL5 and CXCL8 or by GM-CSF. Tumors lacking those factors have limited PMN number and grow slower (Coffelt et al., 2016, Fridlender et al., 2012, McFarlane et al., 2021, SenGupta et al., 2021, Wu et al., 2020). PMN were shown to exhibit different pro- or anti-tumor features in primary and metastatic tumor sites.

1.3.1. PRO-TUMORAL FUNCTIONS OF PMN

Tumor-associated neutrophils (TAN) had significantly upregulated cytokines (CXCL-8) and chemokines, which suggest their role in the recruitment of immune cells (also themselves) into TME. Nonetheless, they can also support tumorigenesis in multiple different ways (Fridlender et al., 2012, Giese et al., 2019, Nicolas-Avila et al., 2017). For example, releasing ROS can induce oxidative DNA damage at the time of the carcinogen exposure and in this way promote the tumorigenesis. PMN can also support tumor growth via release of certain compounds, like IL-1β or NE, which were shown to degrade insulin substrate receptors and trigger lung cancer proliferation. They are a source of angiogenesis promoting factors like VEGF, MMP-9, Bv8, CXCL1, CXCL8, IL-1β, IL-6, uPA (Liang et al., 2016). In the azurophilic granules, PMN store MPO, which catalyzes the HOCl formation which in turn may induce mutagenesis in the adjacent epithelial cells (Mukaida et al. 2020). Another pro-tumor function of PMN is their ability to change the functionality of other immune cells, like induction of T cells exhaustion, inhibition of CD8+ T cell expansion via production of arginase 1 or activation of γδ T cells that promotes inflammation and tumor growth. Regarding pro-metastatic functions of PMN, they are able to cluster together with tumor cells and facilitate their transport via the blood stream (Hedrick et al., 2022, Nicolas-

Avila et al., 2017, Shaul et al., 2017). Using blockade of CXCR2 or depletion of its ligands, it was shown that the migration of PMN into tumor, depends on CXCR2 expression and modulates tumor growth (Nicolas-Avila et al., 2017)

All of these pro-tumor features made PMN a negative prognostic marker for tumor patients. High Neutrophil-to-Lymphocyte Ratio (NLR) is associated with poorer responses to chemo- and radiotherapy as well as with worse overall progression-free survival of cancer patients (Hedrick et al., 2022, Nicolas-Avila et al., 2017, Templeton et al., 2014, Wu et al., 2020).

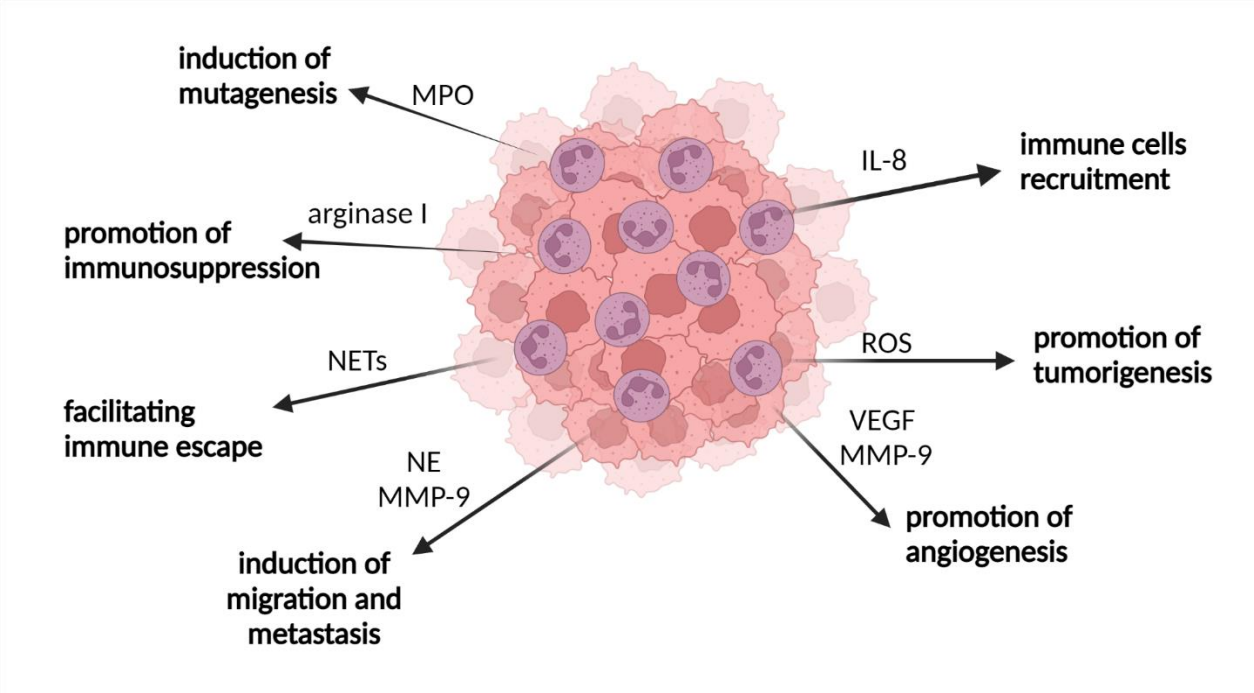

FIGURE 3: SCHEME OF THE PRO-TUMORIGENIC FUNCTIONS OF PMN.

1.3.1.1. Neutrophil Extracellular Traps (NETs)

Together with phagocytosis and degranulation, release of NETs (NETosis) is one of the major strategies of PMN in fight with a potential danger. NETosis can be either suicidal or non-lytic, and is triggered through toll-like receptors (TLR2 and TLR4) by lipopolysaccharide (LPS), HMGB1, dectin 2 or through FcaRI signaling. The formation of NETs is also related to the regulation of PAD4 and ROS (Chen T. et al., 2021, Liu et al., 2020, Masucci et al., 2020, Jorch et al., 2017). NETs are web-like structures, which contain cytosolic and granule proteins (like NE, MPO, MMP-9) assembled on decondensed chromatin, the majority of which comes from the nucleus. Their

main function is to trap and neutralize pathogens appearing in the body, but recently they were demonstrated to influence also chronic diseases like cancer.

First, NETosis can be induced by specific properties of TME, like high concentration of G-CSF, IL-8 or LPS of microbiota origin. Similar to PMN themselves, also NETs, may act pro- or anti-tumorigenic. By capturing tumor cells and preventing them from travelling and metastasizing, NETs can prevent tumors from spreading (Papayannopoulos, 2018). However, in certain patients capturing of circulating tumor cells has an opposite effect and actually promotes metastasis by anchoring tumor cells in a new location (Cools-Lartigue et al., 2013, Jorch et al., 2017, Masucci et al., 2020). A well-known anti-tumor mechanism is directly killing tumor cells, mainly due to MPO present in NETs. Another element of this structure, the histones, can damage the epithelial cells and blood vessels feeding the tumor (Liu et al., 2020, Papayannopoulos, 2018). The pro-tumoral activity of NETs includes induction and promotion of tumors growth as well as induction of their migratory properties and metastatic abilities via NE, MMP-9 and cathepsin G presence (Papayannopoulos, 2018, Liu et al., 2020).

1.3.1.2. NE and MMP-9

Neutrophil elastase (NE) is stored in azurophilic granules and is released via PMN, predominantly during the degranulation or NETosis. Its main role is to help clearing pathogens during infection. However, it was also shown to play an important role in TME and act as a biomarker of a patient prognosis. In several cancers, high levels of NE were shown to promote the tumor induction, progression (via an increase of VEGF and PDGF in the tumor cells), invasiveness and tendency to metastasize (Fridlender et al., 2012, Liu et al., 2020). NE can promote metastasis via induction of EMT by the downregulation of epithelial marker e-cadherin and the activation of β-catenin signaling. Tumor proliferation can be promoted via the activation of PI3K (through degradation of IRS-1) while entering tumor cells. NE can also regulate the activity of MMP-9 and hence influence angiogenesis (Lerman et al., 2018).

Due to the lack of expression of tissue inhibitor of metalloproteinase (TIMP), PMN are the rich source of MMP-9 (Liang et al., 2016). MMP-9 can promote tumor metastasis and angiogenesis via degradation of ECM (Liu et al., 2020). Additionally, it promotes the migration and invasion of tumor cells by the degradation of the basement membrane (Furumaya et al., 2020). In lung cancer, it was also shown that MMP-9 prevented tumor cell death. What is interesting, is that the level of

MMP-9 RNA is high in native PMN and its decreasing in TAN, suggesting that this protein is more important in the first stages of the tumor development (Fridlender et al., 2012).

1.3.2. ANTI-TUMORAL FUNCTIONS OF PMN

PMN are firmly associated with cancer-related inflammation (Mantovani et al., 2008) and in most scenarios promote tumor progression. However, under special conditions, PMN may also limit tumor growth. PMN were shown to block the early proliferation by forced EMT, or to directly kill tumor cells via release of H_2O_2 and an induction of lethal Ca^{2+} ions influx (Furumaya et al., 2020, Hedrick et al., 2022). During the initiation of the tumor, they were shown to switch their function to anti-tumor upon TGF-β blockade and via releasing of pro-inflammatory factors like IL-8, TNF-α and IL-6 as well as stimulating T cells response (Nicolas-Avila et al., 2017). PMN can delay tumorigenesis by presenting certain tumor antigens to cytotoxic CD8+ T cells (McFarlane et al., 2021).

1.3.3. CROSS-TALK BETWEEN PMN AND MICROBIOTA

Recently, microbiota have been recognized as an important component of the TME. This triggered interest in understanding how those commensal bacteria can influence PMN and other tumor-associated immune cells. First, the microbiota can influence PMN in TME by breaking the epithelial barrier and facilitating microbial translocation. Such a sudden event leads to the emergency activation of PMN (Smith et al., 2018). Microbial components derived from the microbiota, as LPS or LTA can induce IL-17, which triggers the production of G-CSF. G-CSF is a regulator of the PMN differentiation, also playing role in the PMN release from the bone marrow (pre-maturely as an effect of the emergency granulopoiesis), and ultimately enhances the PMN recruitment by cancer cells. Moreover, bacterial derived compounds can prime PMN, enhance their migration, cytokine release and production of ROS (Smith et al., 2018, Zhang et al., 2019). It was shown that LPS is able to activate the T cell suppressive activity in PMN (Furumaya et al., 2020). In addition, the aging of PMN can be regulated by microbiota via TLR/MyD88 pathways (Zhang et al., 2019).

1.3.4. TAN IN HEAD AND NECK CANCERS

Similarly, to other types of cancers, also in HNC the high infiltration of PMN into the tumor tissue is connected with a poor survival of patients. Upon other pro-tumorigenic mechanisms, we can find decreased ROS presence and increased expression of CCL4, lactoferrin and MMP-9, which has impact on angiogenesis, tumor cells survival and migration (Dumitru et al., 2012, Trellakis et al.,

2011). Oral TAN can also increase cortactin phosphorylation and promote cancer migration (Dumitru et al., 2013). The microbiome is playing a big role in oral cancers and it has been shown that several oral pathogens can promote pro-tumor phenotype of PMN.

For HNC tumors, PMN are being considered as a fast diagnostic tool, as they can be easily collected from saliva (Magalhaes et al., 2014).

1.4. METASTASIS

Metastasis is a process during which tumor cells are moved from the initial tumor to a new, distant location. Metastasis is the primary cause of death for most patients with cancer, when surgery and radiotherapy are no longer therapeutic options. The process consists of three important steps: invasion, survival and arrest of tumor cells in the bloodstream followed by metastatic colonization. The invasion starts with changes in tumor cell adherence to other cells, mediated by cadherins and to the extracellular matrix, which is mostly mediated by integrins. During the invasion, a change in cadherin expression profile can be observed, from e-cadherin, which is typical for epithelial cells to n-cadherin, characteristic for mesenchymal phenotype and responsible for the binding to the stromal cells. In the next step, the recruitment of the several proteases starts allowing degradation of the extracellular matrix and setting the stage for the invasion. When tumor cells escape to the bloodstream they still need to survive in such a challenging environment. Besides survival, tumor cells must also arrest and extravasate from the circulatory system, which mostly occurs via the endothelial retraction. Finally, the leftover cells have to colonize new tissues. The success of this operation depends on how permissive the new microenvironment already is, and how fast it can perform angiogenesis to feed arriving cells. Considering statistics, just 1 in 100 micro-metastasis events progresses into macroscopic metastases (El-Kenawi et al., 2020, Klein, 2020, Lambert et al., 2017, Quail et al., 2013, Steeg, 2006, Valastyan et al., 2011, Wan et al., 2013, Zhuang et al., 2019).

1.4.1. WHAT TRIGGERS METASTASIS?

The exact mechanisms, which trigger metastasis, are still not well described. However, in the last 20 years more and more studies begun to appear. First, some mechanisms will be specific for just certain types of tumors due to their inherent diversity. For example, in the oral cancer, two chemokine receptors were found to play an important role in metastasis to the lymph nodes: CXCR4 and CCR7. Presence of both chemokines strongly correlates with a more invasive and more aggressive tumor phenotype, poorer survival and higher metastasis rate (Hoon et al., 2011).

In addition, tumor cells are never alone and TME was found to have impact on the metastasis induction via induction of translational and transcriptional changes in tumor cells. Hypoxia can induce translational changes in VEGF expression, promote angiogenesis and activate HIF-1α-dependent transcriptional changes inside immune cells (like triggering immunosuppressive activity in macrophages). The overexpression of KRAS and MYC can increase the translation of the immunosuppressive ligand – PDL-1, which can in turn lead to the tumor immune escape (Albini et al., 2008, El-Kenawi et al., 2020, Micalizzi et al., 2021, Smith et al., 2013).

In early 2000s cancer stem cell term was used for the first time. This described tumor-initiating cells, which have the capacity to self-renew and when isolated, are still capable of giving rise to all types of cellular phenotypes observed in original tumor. However, these cells still have to be activated to initiate tumors. A few proteins and pathways were seen to cause cell renewal in both normal and tumor cells: namely Bmi-1, Wnt/β-catenin, Hedgehog and Notch. Another important aspect are the alterations in adhesive properties of tumor cells. They let them ignore tissue architecture and proceed into the malignant form as well as increase resistance to extracellular death signals by overexpression of BCL2, BCL-X, XIAP (Gupta et al., 2006).

Moreover, once the tumor cells go through the basement membrane and enter stroma, mesenchymal stem cells and various immune cells start to interact with them. Stromal cells can induce angiogenesis, essential for the tumor survival, via secretion of VEGF, CXCL12 (which is often connected with metastasis and poor survival in oral cancers), FGF and repression of anti-angiogenic Thrombospondin-1 (Guo et al., 2018, Hoon et al., 2011, Quail et al., 2013, Smith et al., 2013, Yang et al., 2017). Besides these, stromal cells can further increase invasiveness of tumor cells by secretion of IL-1β, IL-6, IL-4, IL-8, TGF-β, PDGF and MMPs (Guo et al., 2018, Smith et al., 2013, Valastyan et al., 2011, Wan et al., 2013). MSCs can also suppress the T cell response via several different pathways, including signaling via PD-L2 and FAS ligand expression and the recruitment of immunosuppressive immune cells (El-Kenawi et al., 2020, Yang et al., 2017).

Another goal of tumor cells on their way to metastasize is to avoid cytotoxic cells, like NK cells, which high numbers are mostly correlated with a good prognosis for the patients. This can happen via the downregulation of NK activating ligands like MIC-A and MIC-B or physical masking of tumor cells by platelets when they are still in the circulation. While still in blood circulation, the metastasis can also be promoted by PMN. The binding between integrins, expressed on PMN, and ligands, expressed by endothelial cells, allow them to form a bridge between CTCs (Circulating

Tumor Cells) and endothelium, which increases CTCs proliferation. Another pro-metastatic function of PMN is the release of NETs, which can inhibit the NK cell-mediated cytotoxicity and via release of factors like MMP-9, HMGB1, and NE promote extravasation (Smith et al., 2013, Yang et al., 2017, Zhuang et al., 2019).

1.4.2. Epithelial-Mesenchymal Transition

One of the main phenotypic changes of the pro-metastatic cells is Epithelial-Mesenchymal Transition (EMT), which allows cells transformation from epithelial to a more invasive mesenchymal phenotype and in result gain of aggressive abilities. Because of the constant changes in TME and the need of high plasticity of cells, EMT is not so often visible in its complete form (cEMT); more often cells are gaining just some of the EMT specific traits. This process is called partial EMT (pEMT) and is highly reversible (Fig. 4). When the promotor signal disappears, cells are coming back to their epithelial form in the process called Mesenchymal-Epithelial Transition (MET). MET is important especially in the context of metastasis, as cells when they reach their destination have to form a new tumor at the metastatic site.

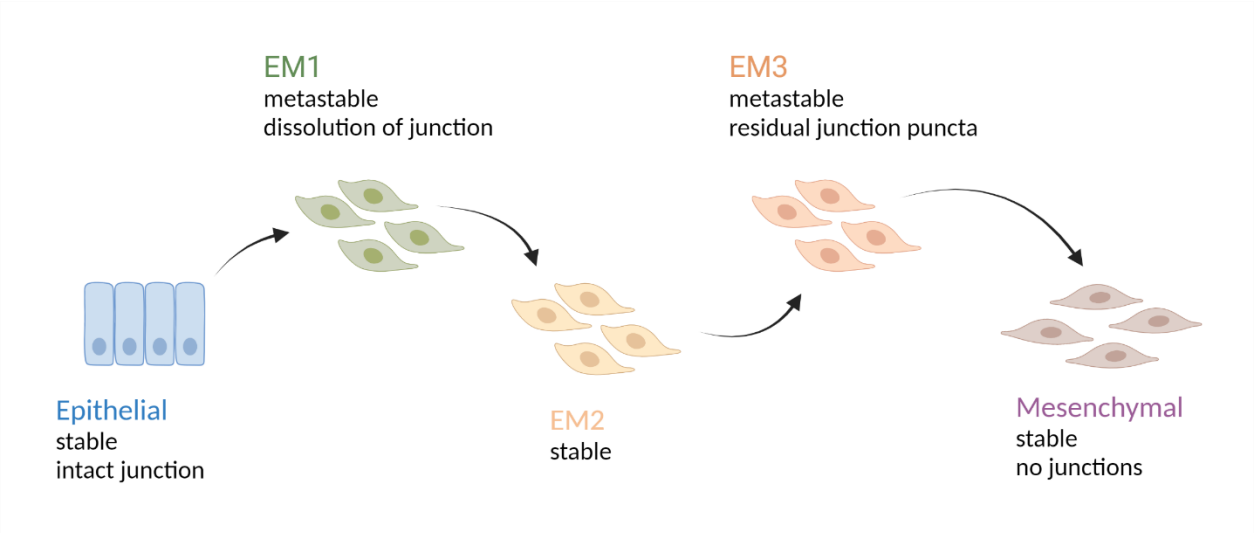

Figure 4: A scheme of the transition through different stages of EMT (adapted from: Nieto et al., 2016).

Start of the EMT can be triggered by signals from the microenvironment such as TGF-β, TNF-α, IL-6/STAT, WNT or NOTCH signaling pathways and is mostly driven by so called EMT transcription factors: Snail, Slug, Twist and Zeb. However, total upregulation of all the factors is not required. Upon the EMT induction, we can observe the downregulation in epithelial markers,

like e-cadherin and an upregulation in mesenchymal ones, like n-cadherin or Vimentin, noticeable changes in morphology are clearly visible under the microscope (Bakir et al., 2020, Micalizzi et al., 2021). The overexpression of those mesenchymal proteins is critical for enhancing cell migration, by the formation of new membrane protrusions and expression of metalloproteinases, which results in ECM degradation (Yeung et al., 2017).

EMT transitioning cells were also shown to influence the composition of immune cells in TME helping the metastatic progression. They can, for example, secrete inflammatory soluble factors, like IL-6, IL-8 and induce expression of their receptors CXCR1 and CXCR2. Those two cytokines are known to be chemoattractants for certain immune cells, like TANs, which are connected with poor prognosis in most solid tumors and their blockage decrease the metastasis forming potential. IL-8 increase is not only an effect of EMT but also can be the cause of the transition, as it was shown that blockade of IL-8 significantly reduced the number of EMT cells in tumors. Cells, which overexpress SNAIL1, were shown to induce immunosuppressive T-cells and non-responsive CD8+ T-cells, which resulted in increased metastasis. EMT cells also displayed an increased expression of PDL-1, which is another way of inhibiting cytotoxic T cells (Chou et al., 2021). It was shown that EMT-like cells have an impact on immune cells, but several studies showed that immune cells in TME can induce EMT by themselves. Via TNF-α, IL-6 and TGF-β the activated effector T cells were able to induce spindle-shaped morphology of cells with a reduced e-cadherin expression and less invasive behavior (Dominguez et al., 2017). TAMs presence in TME induces EMT via increase in the level of TGF-β and the release of cytokines like IL-1β, IL-6, and MMPs, which are known for increasing invasiveness of cells. PMN can promote EMT via JAK2/STAT3 signaling, which is activated by IL-17a. It was also shown that they can induce EMT via NETosis and NE released during this process (Chou et al., 2021, El-Kenawi et al., 2020).

AIM OF THE STUDY

Many immune and stromal cells are reprogrammed and functionally modulated within the TME. These cells can change the biological properties of tumor cells and enhance their capacity to invade and metastasize.

The goal of this project is to develop an in vitro system that mimics the interaction of tumor and stromal cells with PMN, under conditions of bacterial stimulation. It is hypothesized that bacterial stimulation functionally modulates and perhaps enhances, the bi-directional interaction between tumor cells and non-malignant cells within the TME.

To this end, we designed an assay of sequential stimulation of tumor cells and PMN allowing us to probe the system (described in Chapter 3.2 and 4.1). Invasive, migratory and metastatic capacity of stimulated tumor cells were tested in several *in vitro* setups, in an *in ovo* CAM as well as in an orthotopic murine model. Bacterial colonization, PMN abundance and vimentin (mesenchymal marker) intensity were quantified in the HNC patient tissue and a correlative analysis was performed to support the *in vitro* experimentation.

In conjunction, these experiments aim at defining the functional impact of bacterial stimulation and tumor-PMN cross-talk on the biology and metastatic features of tumor cells.

2. MATERIALS

2.1. CONSUMABLE SUPPLIES

Consumables	Manufacturer	Location
6 well cell culture multiwell plate	Sarstedt	Nümbrecht Germany
12 well cell culture multiwell plate	Greiner bio-one	Frickenhausen Germany
24 well cell culture multiwell plate	MerckMillipore	Darmstadt Germany
96 well cell culture plate round bottom	Greiner bio-one	Frickenhausen Germany
96 well cell culture plate flat bottom	Sarstedt	Nümbrecht Germany
Biosphere®pipette tips 10µL	Sarstedt	Nümbrecht Germany
Biosphere®pipette tips 100µL	Sarstedt	Nümbrecht Germany
Biosphere®pipette tips 1000µL	Sarstedt	Nümbrecht Germany
Biosphere®pipette tips 20µL	Sarstedt	Nümbrecht Germany
Biosphere®pipette tips 200µL	Sarstedt	Nümbrecht Germany
Casy Cups	Omni life Science	Bremen Germany
Cell culture flasks T25	Sarstedt	Nümbrecht Germany
Cell culture flasks T75	Sarstedt	Nümbrecht Germany
Cell culture flasks T175	Sarstedt	Nümbrecht Germany
Celltrix 100µm	Sysmex	Norderstedt Germany
Cover slips round 12mm	Carl Roth	Karlsruhe Germany
Filtropur BT 50, Bottle top filter	Sarstedt	Nümbrecht Germany

Immuno PlatesMaxisorp F96 Nunc	VWR	Darmstadt Germany
LS Columns	Miltenyi	Bergisch Gladbach Germany
Multiply&Strip pro 4 tubes chain with lid	Sarstedt	Nümbrecht Germany
Millex-GP Filter Unit	MerckMillipore	Darmstadt Germany
Pipette tips clear (300µL)	Sarstedt	Nümbrecht Germany
PP sealing foil	Kisker-Biotech	Steinfurt Germany
PVDF Western Blotting Membrane	Roche Applied Science	Wiesbaden Germany
Reaction tubes 0.5mL	Sarstedt	Nümbrecht Germany
Reaction tubes 1.5mL without cap	Sarstedt	Nümbrecht Germany
Reaction tubes 1.5mL	Sarstedt	Nümbrecht Germany
Reaction tubes 2.0mL	Sarstedt	Nümbrecht Germany
Reagent and centrifuge tubes 15mL	Sarstedt	Nümbrecht Germany
Reagent and centrifuge tubes 50mL	Sarstedt	Nümbrecht Germany
RTCA E-Plates 16	Agilent	Waldbronn Germany
S-Monovette® 10mL 9NC (Citrat)	Carl Rot	Nümbrecht Germany
Superfrost Plus glass slides	Langenbrinck	Karlsruhe Germany
TC 24 well insert 3µm Falcon	Sarstedt	Nümbrecht Germany
Tissue culture plate 24 well	Sarstedt	Nümbrecht Germany
Transfer pipette 3.5mL sterile	Sarstedt	Nümbrecht Germany

2.2. EQUIPMENT

Equipment	Manufacturer	Location
Amersham Imager 600 (used in the Cardio Science Lab, West German Heart- and Vascular Center, Clinic for Cardiology and Angiology, University Hospital Essen)	Cytiva	Freiburg Germany
Analytical balance AE260	Mettler-Toledo	Giessen Germany
Applied Biosystems StepOne plus	ThermoScientific	Karlsruhe Germany
Autoclave VX75	Systec	Linden Germany
BD FACS CANTO II	BD Biosciences	Heidelberg Germany
Casy Cell Counter + Analyzer System version TT	Omni life Science	Bremen Germany
Centrifuge Mikro 200R	Hettich Zentrifugen	Tuttlingen Germany
Centrifuge Universal 320	Hettich Zentrifugen	Tuttlingen Germany
Centrifuge Universal 420R	Hettich Zentrifugen	Tuttlingen Germany
CO_2 Incubator HERAcell 240 und 240i	Thermo Scientific	Langenselbold Germany
ELISA-Washer ELx50	Agilent	Ketsch Germany
Eppendorf Research pipette 0.5-10µL	Eppendorf	Hamburg Germany
Eppendorf Research pipette 20-200µL	Eppendorf	Hamburg Germany
GFL Water bath	Lauda	Lauda-Königshofen Germany
Heating block Neoblock 1	Neolab	Heidelberg Germany
Ice box 2.5L	Carl Roth	Karlsruhe Germany

Incu-Shaker-Mini	Benchmark	Sayreville USA
Incubator & shaker TH30	Edmund Bühler	Hamburg Germany
InLab Routine Pro pH electrode	Mettler-Toledo	Giessen Germany
Laminar flow hood MSC-Advance 1.8	Thermo scientific	Langenselbold Germany
Liquid nitrogen tank LD25	Taylor-Wharton	Wiesbaden Germany
Leica confocal microscope SP8 (used in IMCES)	Leica	Wetzlar Germany
Minishaker 3D	Kisker-Biotech	Steinfurt Germany
MyCycler PCR machine	BioRad	Munich Germany
Pipetman-Pipette P10	Gilson	Limburg-Offheim Germany
Pipetman-Pipette P100	Gilson	Limburg-Offheim Germany
Pipetman-Pipette P1000	Gilson	Limburg-Offheim Germany
Pipetman-Pipette P20	Gilson	Limburg-Offheim Germany
Pipetman-Pipette P200	Gilson	Limburg-Offheim Germany
Precision analytical balance AZ612	Sartorius	Göttingen Germany
QuadroMACSTM Separator	Miltenyi	Vernon Hills USA
Scotsman AF80 ice flaker	Scotsman	Vernon hills Illinois USA
Screw Top Bottles clear 50-2000mL	Carl Roth	Karlsruhe Germany
Seven Easy pH-Meter	Mettler-Toledo	Giessen Germany
Staining boxes acc. to Schiefferdecker	Carl Roth	Karlsruhe Germany
Synergy 2Multi-Mode Reader	Agilent	Ketsch Germany
UVP ChemiDoc-It®Imager	Analytik Jena	Jena Germany

Variomag Powertherm (magnetic stirrer & heat plate)	HP Medizintechnik GmbH	Oberschleissheim Germany
VortexMixer VTX-300L	Kisker-Biotech	Steinfurt Germany
Western blot transfer Wet/Tank Blotting Systems	Bio-Rad	München Germany
xCelligence DP (used in the Molecular Tumor Immunology Lab and Tumor Metabolism Lab, Clinic for Dermatology, University Hospital Essen)	Agilent	Waldbronn Germany
Zeiss Axioscope 2 and Zeiss AxioObserver.Z1 (used in IMCES)	ZEISS	Jena Germany

2.3. CHEMICALS

Chemicals and reagents	**Manufacturer**	**Location**
0.9% Sodium chloride solution	Fresenius Kabi	Bad Homburg Germany
123counting beads	Thermo Fisher Scientific	Darmstadt Germany
40% Acrylamide/Bis solution	Bio-Rad	München Germany
Ammonium persulfate	Serva Electrophoresis	Heidelberg Germany
Aqua B. Braun	B.Braun	Melsungen Germany
BD CST Beads	BD Bioscience	Heidelberg Germany
BD Cytofix Cytoperm	BS Bioscience	Heidelberg Germany
BD FACS Flow Sheat Fluid	BD Bioscience	Heidelberg Germany

BD FACSRinse Solution	BD Bioscience	Heidelberg Germany
BD Shutdown Solution	BD Bioscience	Heidelberg Germany
Biocoll separating solution 1.077g/mL	Merck	Berlin Germany
CASYton	Omni life science	Bremen Germany
Cell culture medium DMEM	Thermo Fisher scientific	Darmstadt Germany
Cell culture medium RPMI 1640	Thermo Fisher scientific	Darmstadt Germany
Collagenase Type 2	Cellsystems	Troisdorf Germany
Collagen V	Sigma-Aldrich	Taufkirchen Germany
DAPI	BioLegend	Fell Germany
Dihydrorhodamine 123	Thermo Fisher Scientific	Darmstadt Germany
Dispase 2	Sigma-Aldrich	Taufkirchen Germany
Fluoromount G	Thermo Fisher Scientific	Darmstadt Germany
Penicillin/Streptomycin	Thermo Fisher Scientific	Darmstadt Germany
Paraformaldehyde	Sigma-Aldrich	Taufkirchen Germany
PhosphoSTOP	Sigma-Aldrich	Taufkirchen Germany
Poly(vinyl alcohol)	Sigma-Aldrich	Taufkirchen Germany
Poly-D-Lysine	Sigma-Aldrich	Taufkirchen Germany

Protease inhibitor I	Merck Millipore	Darmstadt Germany
Protease inhibitor III	Merck Millipore	Darmstadt Germany
TEMED	Bio-Rad	München Germany

2.4. READY TO USE REACTION SYSTEMS

Kit	**Manufacturer**	**Location**
10x PermWash buffer	BD Bioscience	Heidelberg Germany
Acetaldehyde Detection Kit	Sigma-Aldrich	Taufkirchen Germany
Annexin V:PE Apoptosis Detection Kit	BD Bioscience	Heidelberg Germany
BD Cytofix/Cytoperm	BD Bioscience	Heidelberg Germany
Clarity Max Western ECL Substrate	Bio-Rad	München Germany
dNTP-Mix, 10mM each 1mL	Thermo Fisher Scientific	Darmstadt Germany
Ethanol Detection Assay	Sigma-Aldrich	Taufkirchen Germany
Giemsa solution	Merck AG	Darmstadt Germany
IL8/CXCL8 DuoSet ELISA	BioTechne	Wiesbaden Germany
Lexogen QuantSeq 3' mRNA-Seq Library Prep Kit FWD	Lexogen	Vienna Austria
Luna® Universal qPCR Master Mix	New England Biolabs	Frankfurt Germany
MACS Buffer	Miltenyi	Bergisch Gladbach Germany
May-Grünwald solution	Merck AG	Darmstadt Germany
MIF DuoSet ELISA	BioTechne	Wiesbaden Germany

MIP1b DuoSet ELISA	BioTechne	Wiesbaden Germany
MMP-9 DuoSet ELISA	BioTechne	Wiesbaden Germany
Neutrophil Elastase Activity Assay Kit	Cayman Chemicals	Michigan USA
NE DuoSet ELISA	BioTechne	Wiesbaden Germany
NK Cell Isolation Kit	Miltenyi	Bergisch Gladbach Germany
NucleoSpin® RNA II	MACHEREY-NAGEL GmbH & Co	Düren Germany
Roti Histo Kit II	Carl Roth	Kalrsruhe Germany
SuperScript II RT	Thermo Fisher Scientific	Darmstadt Germany

2.5. BIOLOGICAL MATERIAL

2.5.1. TUMOR CELL LINES

Cell line	**Origin**	**Reference**
A549	Human lung adenocarcinoma	RRID:CVCL_0023
Colo699	Human lung adenocarcinoma	RRID:CVCL_1992
FaDu	Human pharynx squamous cell carcinoma	RRID:CVCL_1218
FaDu-eGFP	Human pharynx squamous cell carcinoma	FaDu cell line transduced with pCL7EGwo-eGFP by AG Giebel (UK Essen, Germany)
H1975	Human lung adenocarcinoma	RRID:CVCL_DG25
H23	Human lung adenocarcinoma	RRID:CVCL_1547

H460	Metastasis of human lung large cell carcinoma	RRID:CVCL_0459
HMEC-1	Human microvascular endothelial immortalized cell line - 1	RRID:CVCL_0307
PCI1	Human laryngeal squamous cell carcinoma	RRID:CVCL_C167
PCI13	Human oral cavity squamous cell carcinoma	RRID:CVCL_C182
UD-SCC3	Human laryngeal squamous cell carcinoma	RRID:CVCL_E326
UM-SCC17b	Metastasis of human laryngeal squamous cell carcinoma	RRID:CVCL_7725
UM-SCC22b	Human hypopharynx carcinoma	RRID:CVCL_7732

2.5.2. IMMORTALIZED MSC CELL LINES

Cell line	**Origin**	**Reference**
C2545 SV40-DsRed	Mucosa of oral cavity, patient nr 2545 (ENT department, UK Essen)	Cells immortalized by Kirsten Bruderek (Group of Prof. Brandau, UK Essen)
C2627 SV40-DsRed	Mucosa of oral cavity, patient nr 2627 (ENT department, UK Essen)	Cells immortalized by Kirsten Bruderek (Group of Prof. Brandau, UK Essen)
C2665 SV40-DsRed	Mucosa of oral cavity, patient nr 2665 (ENT department, UK Essen)	Cells immortalized by Kirsten Bruderek (Group of Prof. Brandau, UK Essen)

2.5.3. *BACTERIA*

Strain	ATCC number	Reference
Klebsiella Pneumoniae	ATCC 700603	Provided by Dr. Jan Kehrmann, Department of Microbiology, University Hospital Essen
Staphylococcus Aureus	ATCC 25923	
Streptococcus Pneumoniae	ATCC 6305	

2.5.4. *BIOLOGICAL COMPOUNDS*

Biological compound	Manufacturer	Location
BSA	AppliChem	Darmstadt Germany
FCS	Sigma-Aldrich	Taufkirchen Germany

2.6. PRIMERS

Target	Direction	Sequence	Tm [°C]	Amplicon [bp]
b-actin	Forward	AGCGGGAAATCGTGCGTG	60	307
	Reverse	CCTTGGCCTCAGAGAGCTGG		
Catenin-b	Forward	CACAAGCAGAGTGCTGAAGGTG	61	146
	Reverse	CCTCATGTTTGTGCAGGAGA		
MMP-9	Forward	CTATGTACCGCTTCACTGAGGG	60	267
	Reverse	TGTCCATTTTCTCCTTCTCTGGA		
n-cadherin	Forward	CCTCCAGAGTTTACTGCCATGAC	60	149
	Reverse	GACTCAAAGGCACAGTAGTGGC		
Slug	Forward	AGATGCATATTCGGACCCAC	53	258

	Reverse	GGGTACATGGTGGTGCCG		
Snail	Forward	AATCGGAAGCCTAACTACAGCGAG	58	400
	Reverse	ATCTGGCGTTCCAGGGACTCAT		
TCF	Forward	GGCATACACCTACTCAACTACGG	61	155
	Reverse	GTAGGATCTCCGCCACTGATTC		
Twist	Forward	TGTCCGCGTCCCACTAGC	58	93
	Reverse	TGGGCGGTGTAGAATCAGAGTC		
Vimentin	Forward	AGGCAAAGCAGGAGTCCACTGA	64	100
	Reverse	GATTCCTGAGAGTCCAAAGACAG		

2.7. INHIBITORS AND ENDONUCLEASES

Inhibitor/Endonuclease	**Target**	**Working concentration**	**Manufacturer**
Blebbistatin	Myosin-9	10µM, 50µM	PeproTech
DNAse I	DNA	0.5U/mL	Sigma-Aldrich
GM6001	MMP-9	10µM	Tocris, Biotechne
Sivelestat	NE	10µM	Sigma-Aldrich

2.8. CELL STIMULI

Cell stimulus	**Working concentration**	**Manufacturer**	**Location**
fMLP	1µM	Sigma-Aldrich	Taufkirchen Germany
IL-2	200U/mL	PeproTech	Hamburg, Germany
Ionomycin	1µg/mL	Sigma-Aldrich	Taufkirchen Germany

LPS	1/10/100ng/mL	InvivoGen	Toulouse France
LTA	1/10/100ng/mL	Sigma-Aldrich	Taufkirchen Germany

2.9. ANTIBODIES

2.9.1. ANTIBODIES FOR WESTERN BLOT

Target	**Isotype**	**Clone**	**Working concentration/Dilution**	**Manufacturer**
Beta-Tubulin	Mouse IgG2b	D10	40ng/mL	Santa Cruz Biotech.
EpCam	Rabbit IgG	D4K8R	50ng/mL	Cell signaling
Fatty Acid Synthase	Rabbit IgG	C20G5	1:1000	Cell signaling
GAPDH	Rabbit IgG	14C10	8.4ng/mL	Cell signaling
HSP90β	Polyclonal rabbit IgG		1:1000	Cell signaling
MYH9	Polyclonal rabbit IgG		117ng/mL	Proteintech
S100A12	Polyclonal Goat IgG		1µg/mL	Biotechne
uPA	Mouse IgG1	H77A10	100ng/mL	Santa Cruz Biotech.
QSX	Polyclonal rabbit IgG		300ng/mL	Proteintech

2.9.2. ANTIBODIES FOR FACS

Target	Isotype	Fluorochrome	Clone	Working concentration	Manufacturer
CD274 (PD-L1)	mouse IgG1	PerCP-eFlour710	MIH1	4µg/mL	eBioscience
EpCAM/Trop1 (CD326)	mouse IgG1	PE	1B7	2.5ng/mL	eBioscience
MICA	mouse IgG2b	APC	159227	50ng/mL	BioTechne
MHC-1	mouse IgG2a	PE	W6/32	500ng/mL	BioLegend

2.9.3. ANTIBODIES AND REAGENTS FOR IMMUNOFLUORESCENCE STAININGS

Target	Isotype	Clone	Working concentration	Maunfacturer
CD66b	mouse IgG1	80H3	1µg/mL	BioRad
DAPI			0.14µg/mL	BioLegend
Ki67	mouse IgG1	MIB-1	0.46µg/mL	Agilent Dako
Vimentin	Mouse IgM	VIM 13.2	4.25µg/mL	Sigma-Aldrich

2.9.4. ANTIBODIES USED FOR ANIMAL EXPERIMENTS

Antibody	Identifier	Manufacturer
Anti-Mouse/Rat Asialo GM1 Polyclonal Antibody	AB_10090118	Cedarlane

Normal Rabbit Serum	CLS403	Cedarlane

2.10. CELL TRACKERS

Cell tracker	Working concentration	Manufacturer	Location
CMDFA	10µM	Thermo Scientific	Karlsruhe, Germany
Deep Red Tracker	1µM	Thermo Scientific	Karlsruhe, Germany

2.11. BUFFERS, SOLUTIONS AND MEDIA

Buffer	Recipe
1x Phosphate buffer saline, PBS	150mM sodium chloride 2.7mM potassium chloride 8.1mM sodium dihydrogen phosphate 1.5mM potassium dihydrogen phosphate pH 7.3
1x Tris buffered saline, TBS	20mM TRIS 1.5M sodium chloride pH 7.2-7.4
5x SDS sample buffer	50mM TRIS-HCl pH 6.8, 2% SDS) 10% glycerol 1% β-mercaptoethanol 12.5mM EDTA 0.02% bromophenol blue
Blocking buffer (NETs assay)	3% cold water fish gelatin 1% BSA 0.5% Tween-20 1x PBS

Blocking buffer (R&D ELISA)	1% BSA 0.2M Sucrose 7.7mM Sodium azide 1x PBS
Cell culture medium	RPMI 1640 10% fetal calf serum 1% Penicillin/Streptomycin
Cell culture medium MSCs	44.5% RPMI 1640 44.5% DMEM 10% fetal calf serum 1% Penicillin/Streptomycin
ELISA washing buffer	0.05% Tween 20 in PBS
IL-8 Reagent Diluent (R&D ELISA)	1% BSA in PBS pH 7.3 005% Tween 20
Laemmli running buffer	1.9M Glycine 34.7mM SDS 247.1mM Tris
LB medium	1% Trypton 0.5% Yeast extract 1% NaCl pH 7.0
Reagent Diluent (R&D ELISA)	1% BSA in PBS pH 7.3

SDS lysis buffer 25mM HEPES (pH 7.3 PAN Biotech)	0.1% SDS 1% Triton X-100 10mM EDTA 10mM Sodium pyrophosphate 10mM Sodium fluoride 125mM Sodium chloride
TBS-T	1x TBS 0.1% Tween-20
TMB Solution	0.48% TMB 10% Acetone 90% EtOH 0.6% H_2O_2
TMB Substrate Buffer	0.63% Citric acid 0.02% Kathon pH 4,1
Western Blot Transfer Buffer	25mM TRIS 192mM Glycine 20% MeOH
Zymography buffer	50mM TRIS pH 7.5 200mM sodium chloride 5mM calcium chloride 1% Triton-X-100

2.12. SOFTWARE

Software	**Manufacturer**	**Location**
Adobe Illustrator 2020	Adobe System GmbH	München Germany
BD FACSDiva 8 and 10	BD Bioscience	Heidelberg Germany

Definiens Tissue Studio	Definiens Inc.	München, Germany
Fiji ImageJ 1.52i	Wayne Rasband, National Institute of Health	Bethesda USA
FlowJo 10	BD Bioscience	New Jersey USA
Gen5	Fisher scientific	Schwerte Germany
GraphPad Prism V 7+8	GraphPad Software, Inc.	La Jolla USA
LightCycler 3	Roche Apllied Science	Wiesbaden Germany
Microsoft Office 2010	Microsoft GmbH	Unterschließheim Germany
R studio	R studio	Boston, USA
RTCA	Agilent	Waldbronn Germany
Stepone Software V2.3	Thermo Fisher Scientific	Darmstadt Germany
ZEN (black, blue edition)	Zeiss	Jena Germany

3. METHODS

3.1. PRIMARY CELLS ISOLATION

3.1.1. ISOLATION OF HUMAN PMN

PMN from healthy donors were isolated via density gradient centrifugation. Venous blood was collected in 3.2% trisodium blood collection tubes (S-Monovette). Diluted blood (1:1 with PBS) was carefully loaded on Biocoll solution. Density centrifugation was performed at 300xg for 30min, with minimal acceleration and gentle breaking. The layer of peripheral mononuclear cells (PBMC) was harvested for isolation of NK cells and the pellet containing PMN and erythrocytes was collected into a fresh tube. Next, erythrocytes were sedimented by adding the same volume of 1% PVA for 20-30 minutes. Upper layer containing PMN was collected, washed with PBS and pelleted by centrifugation at 300xg for 5min. The remaining erythrocytes were lysed in 0.2% NaCl for 1min and a subsequent readjustment of osmolarity was performed by addition of 1.2% NaCl. The PMN's pellet was re-suspended in culture medium.

3.1.2. ISOLATION OF HUMAN NK CELLS

NK cells were isolated by magnetic-activated cell sorting (MACS). After density centrifugation, PBMC layer was collected and washed several times with PBS for removal of platelets. To enrich lymphocytes before MACS separation, monocytes were depleted by plastic adherence. Therefore, PBMC were incubated for 1h at a maximum density of $5x10^6$cells/mL in a cell culture flask. The non-adherent lymphocytes were collected. For the isolation of NK cells, lymphocytes were first labelled with 10µL NK Cell Biotin-Antibody Cocktail and 40µL MACS Buffer per 10^7 cells. This cocktail contains antibodies against antigens not expressed by NK cells. After 5 minutes of incubation at 4ºC, 20µL of NK cell Microbeads Cocktail and 30µL MACS Buffer were added and incubated for additional 10min at 4ºC. Sorting was performed using LS-MACS columns placed in the QuadroMACS Separator. The column was equilibrated by addition of 3mL MACS Buffer. The cell suspension was applied onto the column and column was washed 3 times with 3mL MACS Buffer. All flow-through fractions containing the unlabeled NK cells were collected in the collection tube below the column. The collection tube was centrifuged at 460xg for 10min and isolated NK cells were re-suspended in the culture medium.

3.1.3. ISOLATION OF TISSUE RESIDENT MSCS FROM TUMOR OR ORAL CAVITY MUCOSA

Specimens from tumor tissue or oral cavity mucosa were obtained during surgical procedures performed at the Department of Otorhinolaryngology of the University Hospital Essen, Germany. This study was approved by the local ethics committee.

Tumor or oral cavity mucosa tissue was cut in 1-2mm small pieces and digested in Ringer´s solution containing 5.1mg/mL Collagenase Type 2 solution. After 40min of incubation at 37°C under gentle shaking conditions, the partially digested tissue was centrifuged, pellet re-suspended in 33.4mg/mL Dispase 2 Ringer´s solution and incubated for additional 40min. Afterward cell suspension was centrifuged, pellet re-suspended in MSC culture medium and filtered through 100µm Celltrix. The single cells suspension was plated into T25 cell culture flask and maintained at 37°C, 5% CO_2 . To prevent contamination of tumor derived MSC by the fungal microorganisms, 1.25µg/mL Fungizone was added for the first culture period.

3.1.4. ESTABLISHMENT OF IMMORTALIZED RED FLUORESCENT ORAL MSC FOR IMAGING

Primary MSC cells reach senescence after 7-10 passages and re-establishment of fresh cultures from explanted tissue is needed. This can lead to significant variation of cultivated cells. In order to have consistent material for imaging experiments, MSC from different patients were first immortalized with SV40 Lentivirus particles. $0.02x10^6$ MSC in passage 1-3 were plated in 12 well plates approximately 24h prior transduction. On the next day MSC medium containing 8µg/mL polybrene was prepared and $3.6x10^6$ of pLenti-SV40 (no selection) particles were added. Medium of MSC was aspirated and cells were transduced for 24 hours with polybrene/SV40 mixture. Afterwards, transduction medium was removed, cells were washed several times with PBS and fresh medium was added. After additional 10 passages, the immortalized MSC were transduced with 30µL DsRed Lentivirus particles in MSC/polybrene medium for 24 hours. Transduction medium was removed, cells were washed several times with PBS and fresh medium containing 0.4µg/mL puromycin for selection was added.

DsRed Lentivirus particles were produced by transfection of Lenti-X 293T cells with Lenti-X™ Packaging Single Shots (VSV-G) and 7µg of pLVX-DsRed-Monomer-N1 Vector for 48h. Supernatant containing Lentivirus particles was harvested and concentrated by precipitation using Lenti-X™ Concentrator. Virus particles were stored in aliquots at -80°C until usage.

Genetic modification of MSC was performed by Kirsten Bruderek.

3.2. SUPERNATANT PRODUCTION

3.2.1. PRODUCTION OF BACTERIA-TUMOR SUPERNATANT

Tumor cells were seeded in the concentration of $2x10^6$/mL in culture medium without antibiotics. Bacteria were cultured in LB medium until they reached OD = 0.6. For OD measurement bacteria solution was transferred to 96 well plate and OD value was determined with the Synergy2 plate reader. After approximately 4h of adherence, tumor cells were stimulated with 10^6/mL bacteria (MOI 0.5) for 12h at 37°C, 5% CO_2. Supernatant of the co-culture was harvested and remaining bacteria were removed by two steps of centrifugation at 2760xg for 15min and filtration through 0.2µm filter. Additionally to prevent further bacterial contaminations, 1% of Penicillin/Streptomycin solution was added. Collected supernatant was then stored in -80°C.

3.2.2. PRODUCTION OF SUPERNATANTS WITH INACTIVATED BACTERIA

To study the effect of living vs dead microorganisms in the induction of tumor cells, bacteria were inactivated either by 40min incubation at 70ºC or by 30min incubation with 40% Ethanol. Afterwards, bacteria were centrifuged at 2000xg for 10min and pellet was resuspended in culture medium lacking antibiotics and co-cultured with tumor cells. All other steps were performed according to standard supernatant production protocol (3.2.1)

3.2.3. PRODUCTION OF BACTERIA-TUMOR-PMN SUPERNATANT

PMN were isolated from blood of 3-4 healthy donors and stimulated in the concentration of 10^6/mL with previously prepared bacteria-tumor supernatant. After 20h of incubation at 37°C, 5% CO_2 supernatants were harvested, centrifuged two times at 2760xg for 15min and filtered with 0.2µm filter. Afterwards supernatants from all the PMN donors were pooled and stored in -80°C.

3.2.4. PRODUCTION OF BACTERIA-TUMOR-PMN SUPERNATANTS WITH INHIBITORS/ENZYMES

To understand the role of PMN in our supernatant system we used an inhibitor of neutrophil elastase – Sivelestat (10µM), MMP-9 inhibitor - GM6001 (10µM) and DNAse I (0.5U/mL). Inhibitors/enzymes were added, in mentioned concentrations, during stimulation of PMN with bacteria-tumor supernatant.

3.2.5. PRODUCTION OF TUMOR SUPERNATANT

Tumor cells were seeded in the concentration of $2x10^6$/mL in culture medium. After 24h of incubation at 37°C, 5% CO_2 supernatant was harvested and spinned down at 1840xg for 10min. Supernatants were stored at -20°C.

3.2.6. PRODUCTION OF TUMOR-PMN SUPERNATANT

PMN were isolated from blood of at least 3 healthy donors and stimulated with tumor supernatant in a concentration of 10^6/mL for 20h at 37°C, 5% CO_2. Next, supernatants were harvested, centrifuged two times at 2760xg for 15min and filtered with 0.2µm filter. Afterwards supernatants from all the PMN donors were pooled and stored at -80°C.

3.2.7. PRODUCTION OF TUMOR-MSC SUPERNATANT (PRIMED STROMA)

MSCs isolated from different patients were cultured in tumor supernatant at concentration of $0.5x10^6$/mL. After 24h incubation at 37°C, 5% CO_2 supernatants were harvested, centrifuged at 1840xg for 10min and stored at -20°C.

TABLE 1: DETAILED DESCRIPTION OF SUPERNATANTS USED FOR STUDY

Abbreviation	**Tumor cell line**	**Bacteria strain**	**Neutrophils (PMN)**
SAF	FaDu	*S. aureus*	No
SAFP	FaDu	*S. aureus*	Yes
SPF	FaDu	*S. pneumoniae*	No
SPFP	FaDu	*S. pneumoniae*	Yes
SAH	H460	*S. aureus*	No
SAHP	H460	*S. aureus*	Yes
KPH	H460	*K. pneumoniae*	No
KPHP	H460	*K. pneumoniae*	Yes
SAP	PCI1	*S. aureus*	No

SAPP	PCI1	*S. aureus*	Yes
SPP	PCI1	*S. pneumoniae*	No
SPPP	PCI1	*S. pneumoniae*	Yes

3.3. FUNCTIONAL ASSAYS

3.3.1. NK CYTOTOXICITY ASSAY

$0.2x10^6$/mL tumor cells were stimulated with selected supernatants in a 12-well plate for 3 days in 37°C, 5% CO_2.

NK cells were isolated and stimulated in a concentration of 10^6/mL with 200U/mL IL-2 for 2 days in 37°C, 5% CO_2.

Stimulated tumor cells and IL-2-activated NK cells were seeded at a 1:1 ratio in a 96 well flat bottom plate and co-cultured for 24h at 37°C, 5% CO_2. To assess the tumor cell death, whole supernatant of the co-culture was transferred into a new 96 well plate. Adherent tumor cells were dislodged and combined with the transferred supernatant. Plate was centrifuged at 460xg for 5min and cells were stained with Annexin/7AAD kit (according to manufacturer instruction). Cell analysis was performed with BD FACS Canto II and FlowJo 10.

3.3.2. MIGRATION ASSAY

To obtain a confluent monolayer, tumor cells were seeded at a concentration of 10^6/mL in culture medium or selected supernatants, in a 12 well plate, for 24h. Mechanical scratching of the wound was performed using a pipette tip. Medium and supernatants were aspirated and wells were carefully replenished. Pictures of the gaps were taken at time 0h and 16h to calculate percent of migration. Scratch closure was analyzes with ImageJ.

3.3.3. ENZYME-LINKED IMMUNOSORBENT ASSAY (ELISA)

Levels of secreted cytokines in supernatants were analyzed by ELISA. 96-well NUNC plates were coated with 50µL capture antibody, diluted in PBS, at 4°C overnight. On the next day coating solution was removed and unspecific binding was blocked by adding 200µL blocking solution. Plate was incubated for 1h in room temperature. After washing the plate with 3 x 200µL washing buffer, 50uL of sequentially diluted standards or supernatants in different dilutions were applied. After 2h of incubation at room temperature, plate was washed and 50µL of biotinylated detection

antibody solution was added for following 2h. After washing, 50µL of HRP coupled Streptavidin solution was added for 20min incubation. Plate was washed and 100µL of TMB substrate solution was added. HRP catalyzed 3,3´5,5´ TMB to TMD diamine, which is of blue color. This reaction was stopped after 5-10min by adding 2N H_2SO_4. Absorbance was measured at 450nm with Synergy2. Concentrations were calculated according to the standard curve that derived from the standard dilutions.

3.3.4. ZYMOGRAPHY

Zymography was used to measure activity of MMP-9. Supernatants were collected and incubated with Zymogram sample buffer, containing 80mM Tris pH 6.8, 1% sodium dodecylsulfate (SDS), 4% glycerol and 0.006% bromophenol blue. Proteins were separated using 10% SDS-Polyacrylamide Gel Electrophoresis (SDS-PAGE) containing 0.2% gelatin as a substrate for MMP-9. Samples were renatured by removal of SDS, with washing in 2.5% Triton-X-100 for 1h at room temperature under shaking conditions. In order to let the enzymatic reaction proceed, samples were incubated in the Zymography reaction buffer (Table 2.19) for 16 hour at 37°C. To visualize digested bands, the gel was stained with Coomassie blue solution (0.5% Coomassie blue, 30% methanol and 10% acetic acid) for 2h at room temperature, under gentle shaking, followed by multiple destaining steps in a solution containing methanol and 10% acetic acid (until digested bands were visible). Photo of the gel was taken and bands intensity was calculated with ImageJ.

3.3.5. WESTERN BLOT

Tumor cells were stimulated with conditioned supernatants for 72h at 37°C, 5% CO_2. FaDu cells were lysed at a concentration of 10^7/mL with SDS-lysis buffer containing additionally: 1% protease inhibitor cocktail I, 1% protease inhibitor cocktail III, and 10% PhosStop. Cell debris were removed by centrifugation and the lysates were incubated at 95°C for 10min in SDS-sample buffer. Samples were separated by SDS-PAGE, followed by transfer to a PVDF membrane. Incubation with primary antibodies was performed over night at 4°C in 4% BSA in 1xTBS + 0.1% Tween-20, followed by incubation with secondary antibodies for 1 hour at room temperature in 4% BSA. Chemiluminescent detection was performed with an Amersham imager 600. Expression level was analyzed using Fiji ImageJ 1.53c and normalized to GAPDH.

3.3.6. TUMOR CELLS PROLIFERATION WITH XCELLIGENCE

$0.2x10^6$/mL FaDu or H460 tumor cells were stimulated with supernatants or culture medium for 72h at 37°C, 5% CO_2. Afterwards, cells were detached and $8x10^3$ FaDu or $10x10^3$ H460 cells per

well, were seeded on the E-plates in medium or supernatants. Proliferation was monitored for 90h with measurement taken every 5min. Data analysis was performed with RTCA software.

3.3.7. NE ACTIVITY ASSAY

Activity of NE was determined in the supernatants with a commercial assay. Samples and Standard were diluted with Assay Buffer and applied on a black 96-well plate. In the next step the non-fluorescent elastase substrate (Z-Ala-Ala-AlaAla)2Rh110 was added, and incubated for 1.5h at 37°C. The substrate is selectively cleaved by elastase to yield the highly fluorescent compound R100. The fluorescence signal was detected in Synergy2 at an excitation wavelength of 485nm and an emission wavelength of 525nm.

3.3.8. ROS ASSAY

10^6/mL PMN were cultured in stimulating supernatants or culture medium for 3h at 37°C, 5% CO_2. Afterwards 123DiRhodamin was added at a final concentration of 2.5µg/mL and samples were incubated for 15min at 37°C, 5% CO_2. The non-fluorescent 123DiRhodamin penetrate into the cells and is oxidized by ROS to the green-fluorescent Rhodamine123. To stop the reaction, samples were placed on ice for 15min and were immediately analyzed on a BD FACSCanto II flow cytometer using BD FlowJo Software.

3.3.9. ANNEXIN ASSAY

10^6/mL PMN were cultivated in conditioned supernatants or culture medium for 24h. Cells were harvested and resuspended in 50µL Annexin Binding Buffer with Annexin V-PE (1:100) and 7AAD (1:100). After 20min of incubation at room temperature, 200µL of Annexin Binding Buffer was added and cells were immediately analyzed with BD FACSCanto II flow cytometer and BD FlowJo Software.

3.3.10. CHEMOTAXIS

Isolated PMN were adjusted to the cell concentration of $2.5x10^6$/mL in culture medium. 700µL of medium or supernatants were added into the wells of 24 well plate, followed by placing 3µm inserts inside the wells. 200µL of PMN suspension was applied per insert. PMN migration was performed for 3h at 37°C, 5% CO_2. Afterwards inserts were removed; supernatants with migrated PMN were harvested and mixed with counting beads. Frequency of migrated PMN was quantified with BD FACSCanto II flow cytometer using BD FlowJo Software.

In case of bidirectional chemotaxis PMN were resuspended in the corresponding supernatants instead of culture medium.

3.3.11. TRANS-ENDOTHELIAL MIGRATION ASSAY

$0.2x10^6$ cells of the immortalized microvascular endothelial cell line cdc.HMEC-1were seeded on 3µm trans-well inserts, coated with $2.5µg/cm^2$ collagen V, and cultured for 2 days to build a monolayer. This inserts were used for chemotaxis assays described in 3.3.10.

3.3.12. PMN KILLING ASSAY

5 hours prior tumor cell - PMN co-culture, $8x10^3$ FaDu or $10x10^3$ H460 tumor cells were seeded on the E-plates in the culture medium. Adherence of tumor cells was tracked with measurement taken every 10min. In the meantime, 10^6/mL isolated PMN were stimulated with culture medium or supernatants for 30min or with 5nM PMA for 3 hours. Stimulated PMN were added to tumor cells in a 5:1 ratio and their impact on tumor cells survival was monitored for 72 hours. Measurement were taken every 3min. Data analysis was performed with RTCA software.

3.3.13. NETS FORMATION

Assay was performed on 0.01% poly-D-lysine coated coverslips in 24-well plate. PMN were cultured in the respective culture medium or conditioned supernatant and incubated for 30min at 37°C, 5% CO_2. Cells were fixed by adding 16% PFA for 15min, followed by permeabilization step with 0.5% Triton x-100. Afterwards samples were blocked with blocking buffer (Table 2.19) for 20 min at room temperature. To visualize NETs formation slides were stained with 0.3µM DAPI for 30min at room temperature in the dark. Samples were mounted with Fluoromount–G Mounting medium and analyzed with a Zeiss Axioscope 2 and Zeiss AxioObserver.Z1.

3.3.14. CONJUGATES FORMATION ASSAY

Tumor cells were stimulated with conditioned supernatants for 72h at 37°C, 5% CO_2 and isolated NK cells were activated with 200 U/mL IL-2 for 48h. Both cell types were stained for 30min with either 10µM Cell Tracker CMDFA or 1µM Deep Red under serum free conditions. Afterwards, cells were co-cultured in culture medium (in target: effector cell ratio of 4:1) for 30min at 37°C. To break loose contact between cells, samples were moderately vortexed for 1s and ice-cold 0.5% PFA was added. Formation of conjugates (CMFDA/Deep Red double positive events) was immediately analyzed on a BD FACSCanto II flow cytometer using BD FlowJo Software.

3.3.15. SPHEROID ASSAY

To set up spheroids, 96 well flat bottom plates were coated with 1.5% agarose solution.

$0.01x10^6$ FaDu or $0.02x10^6$ cMSC-SV40 DsRed were seeded per well and cultured for 3 days at 37°C, 5% CO_2. Spheroids were transferred separately into new wells (one spheroid per well) and cultured at 37°C, 5% CO_2 prior adding PMN. Isolated PMN were labelled with 0.5µM CMFDA and added to spheroids in a ratio of 10:1. After 8h migration, spheroids were fixed with 2% PFA for 15min, washed five times with PBS and blocked with PBS containing 5% goat serum, 0.5% Triton-X100 overnight at 4°C. On the next day, spheroids were counterstained with 2.5µg/mL DAPI for 60 minutes at room temperature, and washed three times with PBS. For imaging, spheroids were transferred into µ-slide angiogenesis slides and mounted with ibidi mounting medium. 2 step z-stack of spheroids were taken with Leica SP8 confocal microscope using 20x objective. 3D images were analyzed with ImageJ and Imaris software.

Assay was performed by Kirsten Bruderek.

3.4. GENE SIGNATURE ANALYSIS

3.4.1. QPCR

10^6/mL tumor cells were stimulated with conditioned supernatants for 6h at 37°C, 5% CO_2. RNA was isolated from the tumor cells using NucleoSpin® RNA II kit, following manufacturer protocol. Up to 1µg of RNA was used for reverse transcription with SuperScript™ II Reverse Transcriptase, according to manufacturer protocol. RT-PCR was performed on diluted cDNA using Luna® Universal qPCR Master Mix and StepOnePLus Real-Time PCR System with StepOne software; all samples were standardized to untreated cells and house-keeping gene (β-actin).

3.4.2. BULK RNASEQ

Measurement was performed in Genomics & Transcriptomics Facility of University Hospital Essen. Dr. Bettina Budeus helped with Bioinformatics analysis of data.

10^6/mL tumor cells were stimulated with conditioned supernatants for 8h at 37°C, 5%CO2. RNA was isolated according to manufacturer's protocol using NucleoSpin® RNA II kit. Concentration and quality of RNA was measured with Qubit (Invitrogen, Waltham, MA, USA) and Agilent Bioanalyzer DNA HS (Agilent, Santa Clara, CA USA). Library preparation was performed with Lexogens QuantSeq 3' mRNA-Seq Library Prep Kit FWD and sequenced on a NextSeq500

(Illumina, San Diego, CA, USA). Sequences were cleaned with TrimGalore (v.0.6.0 DOI:10.14806/ej.17.1.200) and aligned with hisat2 (https://doi.org/10.1038/s41587-019-0201-4). Statistical analysis was performed with R (v. 4.2.0, R Core Team (2022). R: A language and environment for statistical computing. R Foundation for Statistical Computing, Vienna, Austria. URL https://www.R-project.org/.) using the R-packages DESeq2 (10.1186/s13059-014-0550-8), pheatmap (v 1.0.12; Kolde R (2019). pheatmap: Pretty Heatmaps), umap (v 0.2.8.0; Konopka T (2022). umap: Uniform Manifold Approximation and Projection), fgsea(10.1101/060012).

3.5. STAININGS

3.5.1. PAPPENHEIM STAINING

Bacteria in tumor sections were visualized by Pappenheim staining. In brief, slides were stained for 2 minutes with May-Grünwald solution, washed in distilled water followed by 10 minutes counterstaining with Giemsa solution and mounted with Roti Histo Kit II. Quantitation of bacteria was done by manual counting using Multiview Microscopy System.

3.5.2. IF STAINING OF TUMOR CELLS

For immunofluorescence staining of tumor cells, tumor cells were seeded on coverslip for stimulation with conditioned supernatants. Coverslips were fixed and permeabilized with BD Cytofix/Cytoperm for 30min. Samples were stained with primary antibodies overnight at 4°C followed by secondary antibodies for 45min at room temperature. DAPI was used for nuclei visualization. Samples were mounted with Fluoromount–G Mounting medium and analyzed with a Zeiss Axioscope 2 and Zeiss AxioObserver.Z1. Quantification of positive tumor cells was performed with the ImageJ software.

3.5.3. IF STAINING OF TUMOR TISSUE

Tumor biopsies from HNC patients were frozen in OCT-Compound and 5µm thick sections were prepared. Tissue sections and coverslips were fixed and permeabilized with BD Cytofix/Cytoperm for 15min. Samples were stained with primary antibodies overnight at 4°C followed by secondary antibodies for 45min at room temperature. DAPI was used for nuclei visualization. Samples were mounted with Fluoromount–G Mounting medium and analyzed with a Zeiss Axioscope 2 and Zeiss AxioObserver.Z1. Quantification of Vimentin expression and CD66b+ TAN frequency in tumor tissue was performed using Tissue Studio software.

3.5.4. FACS

$0.2x10^6$/mL tumor cells were stimulated with conditioned supernatants for 72h at 37°C, 5% CO_2. 50µL of $2x10^6$/mL cells were stained with fluorophore-conjugated antibodies for 30min at 4°C. Isotype control was used as a negative control. Cells were analyzed using BD FACSCanto II flow cytometer and BD FlowJo Software.

3.6. SUPERNATANT SCREENING

3.6.1. MASS SPECTROMETRY – PROTEOMICS

Measurement of proteome content in supernatants was performed by group of Prof. Aleksandra Skirycz at Max Planck Institute of Molecular Plant Physiology in Potsdam, Germany.

Protocol of LC-MS proteomics analysis was previously described by Veyel et.al., 2017.

3.6.2. NMR

Measurement was performed by Dr. Robert Knitsch at ISAS in Dortmund, Germany.

The metabolite concentrations for each individual sample have been obtained by lineshape deconvolution of the respective NMR spectrum, fitting well-known lineshapes of common metabolites to the observed NMR resonances. Normalization of data was avoided due to possible impairment of the results.

3.6.3. ETHANOL DETECTION ASSAY

Ethanol content in supernatants was determined with Ethanol Assay Kit. Ethanol concentration was determined by a coupled enzyme reaction, which results in a colorimetric product, proportional to the ethanol presence. Diluted or undiluted samples and standards were placed on 96 well plate, Master Reaction Mix containing Enzyme Mix was added and plate was incubated for 30min at 37°C. Afterwards absorbance was measured at 570nm and ethanol content was calculated using ethanol standard curve

3.6.4. ACETALDEHYDE DETECTION ASSAY

Acetaldehyde content in supernatants was determined with Acetaldehyde Assay Kit. Kit is based on the aldehyde dehydrogenase catalyzed oxidation of acetaldehyde with the reduction of NAD to NADH. Formed NADH reduces MTT, producing a colored formazan compound, which intensity can be measured at 565nm and is directly proportional to acetaldehyde concentration in the sample

(information coming from the Technical Bulletin of the kit). Diluted or undiluted samples and standards were placed on the 96 well plate. Working reagent, containing NAD/MTT Solution and enzymes was added to the samples and incubated for 30min at RT. Afterwards the optical density at 565nm was measured.

3.6.5. GLUCOSE DETECTION

Glucose was measured in undiluted samples in the Central Laboratory at University Hospital Essen.

3.7. ANIMAL EXPERIMENTS

3.7.1. MICE LN METASTASIS MODEL

Male, 6-10 weeks old NMRI-nude mice were injected with stimulated and unstimulated FaDu cells in the floor of the mouth (M. myelohyoideus). Orthotopic model has been previously described by Vahle et al., 2012. For NK depletion each mouse was intraperitoneally injected with rabbit anti-Mouse/Rat Asialo GM1 Polyclonal Antibody every 5 days until the end of the experiment. The first injection of asialo-GM1 was performed 2 days before initial tumor injection. Control group was injected with Normal Rabbit Serum. The mice were sacrificed at 19-22 days post-injection. The two pairs of superficial cervical lymph nodes were isolated and cut into 5µm sections. Every 6th section was stained with hematoxylin/eosin and analyzed for the presence of metastases by light microscopy. All experiments were approved by the local animal ethics committee. Experiments were performed by Dr. Claudia Dumitru and Sebastian Vollmer.

3.7.2. CHICK CHORIOALLANTOIC MEMBRANE (CAM) – IN OVO INVASION ASSAY

Fertilized eggs were kept at 38°C for 10 – 12 days. Subsequently, stimulated FaDu tumor cells were either inoculated ($0.15x10^6$ cells) onto the chorioallantoic membrane (CAM) or stimulated FaDu-eGFP cells ($0.075x10^6$cells) were injected into a CAM vein. At day 3 after the inoculation eggs were opened and samples of upper CAM and tumor were collected. Five days after injection, lower CAM samples were collected. Tumors size was measured. For angiogenesis and invasion studies photos of the punches from lower and upper CAM were taken and analysis was performed with ImageJ software. Experiments were performed by Lara-Jasmin Schroeder as part of her Master thesis project.

3.8. STATISTICS

Statistical analysis was performed with GraphPad Prism 8 software. Tests used in this study are indicated within the legends. Used tests include unpaired t-test and one-way ANOVA with Tukey's multiple comparisons test. Data are depicted as mean value with standard deviation (+/- SD).

4. RESULTS

4.1. IMPACT OF TME COMPONENTS ON THE TUMOR CELLS FEATURES

In the first set of experiments we stained 54 tumor tissues from HNC patients to evaluate overall bacterial colonization of cancers. We could detect bacteria in all analyzed tissues (Fig 5A); however, the level of colonization differed between patients. We also checked for specific localization pattern, but found out that the bacteria were evenly distributed between tumor islands and stroma. What we discovered, was a clear correlation between bacterial infection and PMN density in the tissues (Fig 5B). This correlation led us to investigate in more detail the interaction of bacteria, PMN and tumor cells as well as the impact of this interaction on the biology of tumor cells.

To mimic the interaction of tumor cells and PMN in the presence of bacterial stimulation in TME, we designed an unidirectional and a sequential stimulation system (Fig 5C). We co-cultured tumor cells together with bacteria and harvested the resulting supernatant. With this supernatant we stimulated PMN coming from healthy blood donors to gain the final supernatant, designated as SAFP (Fig 5C, right side). SAFP was supposed to mimic the environment in which tumor cells are growing. To show the importance of the bacterial presence in the system we produced an extra supernatant, which did not include bacterial co-cultivation of tumor cells (FP, Fig 5C, left side). To check effects of the acquired supernatants we stimulated tumor cells with them, for 72h. We observed changes in morphology of cells stimulated with SAFP, while control and FP stimulated cells kept their epithelial phenotype (Fig 5D). We could also see changes in EpCam and PDL-1 expression (Fig 5E), as well as in regulation of typical mesenchymal genes (Fig 5F). SAFP stimulated cells showed a downregulation of epithelial and upregulation of mesenchymal markers, which was in the agreement with the epithelial to mesenchymal morphology transition of those cells.

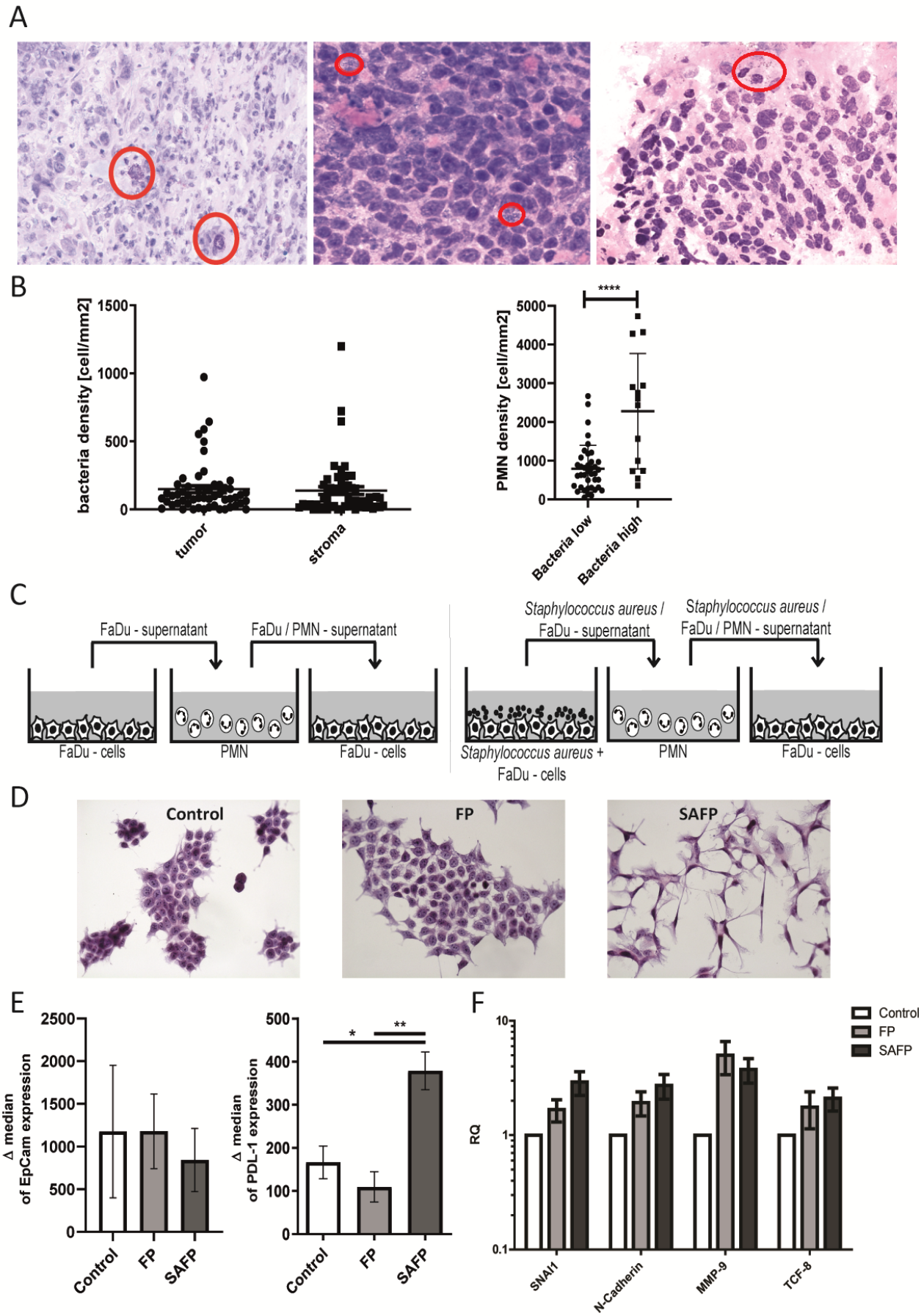
A
B
bacteria density [cell/mm2]
1500
1000
500
0
tumor
stroma
PMN density [cell/mm2]
****
5000
4000
3000
2000
1000
0
Bacteria low
Bacteria high
C
FaDu - supernatant
FaDu / PMN - supernatant
FaDu - cells
PMN
FaDu - cells
Staphylococcus aureus / FaDu - supernatant
Staphylococcus aureus / FaDu / PMN - supernatant
Staphylococcus aureus + FaDu - cells
PMN
FaDu - cells
D
Control
FP
SAFP
E
Δ median of EpCam expression
2500
2000
1500
1000
500
0
Control
FP
SAFP
Δ median of PDL-1 expression
500
400
300
200
100
0
*
**
Control
FP
SAFP
F
RQ
10
1
0.1
Control
FP
SAFP
SNAI1
N-Cadherin
MMP-9
TCF-8

FIGURE 5: BACTERIAL STIMULATION ENHANCES THE INDUCTION OF A MESENCHYMAL PHENOTYPE IN TUMOR CELLS

(A) Pappenheim staining of bacteria in tumor tissues. Representative photos with bigger bacterial colonies marked with red circle. **(B)** Quantification of bacteria and PMN density in tumor tissue. Cut off for high vs low bacteria was set on 200 cells/mm^2, n=54. **(C)** For FP production, PMN were stimulated with FaDu supernatant for 20h, supernatant was harvested and then used for further stimulation of FaDu 'responder´ cells. For SAFP production, tumor cells were first 'primed/stimulated' with *Staphylococcus aureus* for 12h; supernatant was harvested, filtered to remove bacteria, and then used for PMN stimulation. Supernatant obtained with this method was again used for further stimulation of FaDu ´responder´ cells. Supernatants description can be found in Table 1. **(D)** HE staining of FaDu cells after 72h of stimulation with the indicated supernatants. **(E)** FACS staining results of EpCam and PDL-1 expression in stimulated FaDu cells, n=3. **(F)** qPCR performed on FaDu cells after 6h stimulation with supernatants, results are normalized to β-actin and untreated cells as a reference sample (RQ=1); n=7. **(B, E-F)** n indicates number of independent experiments). Statistical analysis was performed with un-paired t-test **(B)** and one-way ANOVA test with Tukey's multiple comparisons test **(E)**: * $p<0.05$, ** $p<0.01$, **** $p\leq0.0001$. Data are displayed as mean +/- SD.

In the next series of experiments, we wanted to check the functional changes of stimulated tumor cells. Because of their altered morphology, we hypothesized that migratory abilities of cells will be affected. Indeed, tumor cells stimulated with SAFP were faster to close the gap in a wound healing assay (Fig 6A). In addition, those stimulated cells showed slower proliferation (Fig 6B).

Resistance to NK cytotoxicity is a feature that has been occasionally reported in the literature for metastatic tumor cells (Lopez-Soto et al., 2017, Teijeira et al., 2020). Therefore, we tested stimulated tumor cells in the *in vitro* NK cytotoxicity assay. Those cells showed certain resistance to NK cell cytotoxicity as compared to FP-stimulated and unstimulated tumor cells (Fig 6C).

We could also observe an increase of cells invasiveness in the *in ovo* CAM assay. Stimulated tumor cells were either inoculated on the CAM membrane of fertilized eggs or injected into main vein of the developing embryo. The first model allowed us to investigate the local progression, while the second model investigates distant migration and metastasis. Inoculation model revealed that SAFP stimulated cells formed bigger tumors with increased angiogenesis in the developing embryo (Fig 6D-E) as compared to control and FP-stimulated cells. The injection model also revealed certain changes between the groups of cells, pointing out invasiveness of SAFP-treated cells (Fig 6F).

Followed by observations from *in ovo* experiments, we studied proliferation of stimulated tumor cells over time using the xCelligence system (Fig 6G). We stimulated tumor cells with indicated supernatants for 72h and then either left them unchanged or we exchanged supernatant for culture medium. Tumor cells that were continuously cultured in SAFP/SAHP showed reduced proliferation in the agreement with Fig 6B. Tumor cells that were primed with SAFP / SAHP and then transferred to control culture medium showed enhanced proliferation compared to non-primed

tumor cells; confirming enhanced invasiveness and aggressiveness of these tumors in the assay shown in Fig 6D and 6F.

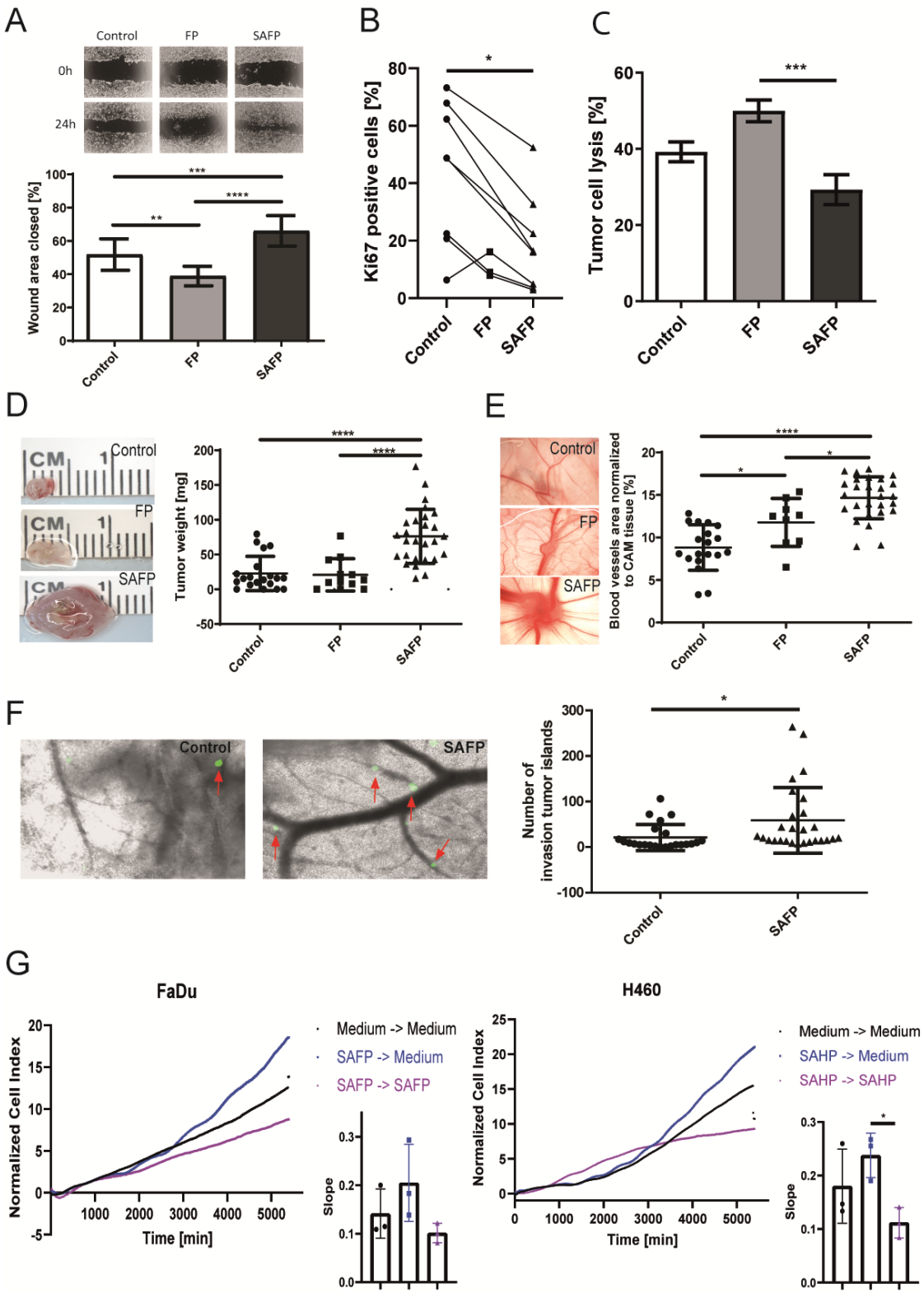

FIGURE 6: BACTERIAL STIMULATION ENHANCES MIGRATORY AND INVASIVE ABILITIES OF TUMOR CELLS

Supernatants description can be found in Table 1. **(A)** Control and stimulated FaDu cells were grown until confluence and the closure level of a scratch "wound" was recorded after 16h and quantified with ImageJ; n=11. **(B)** Expression of Ki67 in stimulated and unstimulated tumor cells, determined by immunofluorescence staining; (Control/SAFP n=8, FP n=3). **(C)** Tumor cells were stimulated with supernatants for 72h, IL-2 stimulated-NK cells were added for 24h and tumor cell death was determined via Annexin-7AAD flow cytometry assay (Control n=20, FP n= 14, SAFP n=22). **(D-F)** *In ovo* CAM assays. **(D-E)** Stimulated tumor cells were inoculated onto the upper CAM (Control n=20, FP n=12, SAFP n=27). Macro-morphology, tumor weight **(D)**, and angiogenesis **(E)** were recorded on day 3, after inoculation. **(F)** GFP-labeled, stimulated FaDu cells were injected into the main CAM vein of the developing chicken embryo. After 5 days fluorescent tumor cells (marked by arrows) in the punches obtained from lower CAM, were counted (Control n=23, SAFP n=27). **(G)** Tumor cells were cultured in the control medium or stimulated with SAHP or SAFP for 72h, supernatant was removed and cells reseeded as indicated. Increased cell growth after removal of the inducing supernatant was observed, n=3. **(A-B, G)** n indicates number of independent experiments, **(C)** n indicates number of NK cells donors **(D-F)** n indicates the number of eggs used in the experiment. **(A-G)** Statistical analysis was performed with one-way ANOVA test with Tukey's multiple comparisons test: *=$p<0.05$, ** $p<0.01$, *** $p<0,001$, **** $p\leq0.0001$. Data are displayed as mean +/- SD.

Summing up, tumor cells stimulated by TME mimicking supernatant underwent substantial changes, suggesting transition into pro-metastatic phenotype. Further investigating this exciting discovery, we wanted to study how universal this phenomenon is. We decided to check several HNC (Fig 7) and lung tumor (Fig 8) cell lines in combination with *Staphylococcus Aureus*, to compare the results. Out of 10 tested cell lines 2 showed comparable effect, while other were unchanged. Following these observations, we decided to extend our model to PCI1 and H460 and other bacterial strains. We chose: *Klebsiella Pneumoniae* and *Streptococcus Pneumoniae*, which are often found in lung and HNC tumors respectively. Upon stimulation with supernatants produced with those bacteria, we did not observe any changes in morphology of tumor cells (Fig 9A), also expression of EpCam (Fig 9B) and PDL-1 (Fig 9C) were not affected. No functional changes were detected (similar migration (Fig 9D) or resistance to NK cell cytotoxicity (Fig 9E)). The biggest difference between two groups was level of NE (Fig. 9F), which suggested differential PMN activation. Based on these results we divided the six supernatants into two groups: inducing ('responder') and non-inducing ('non-responder') response.

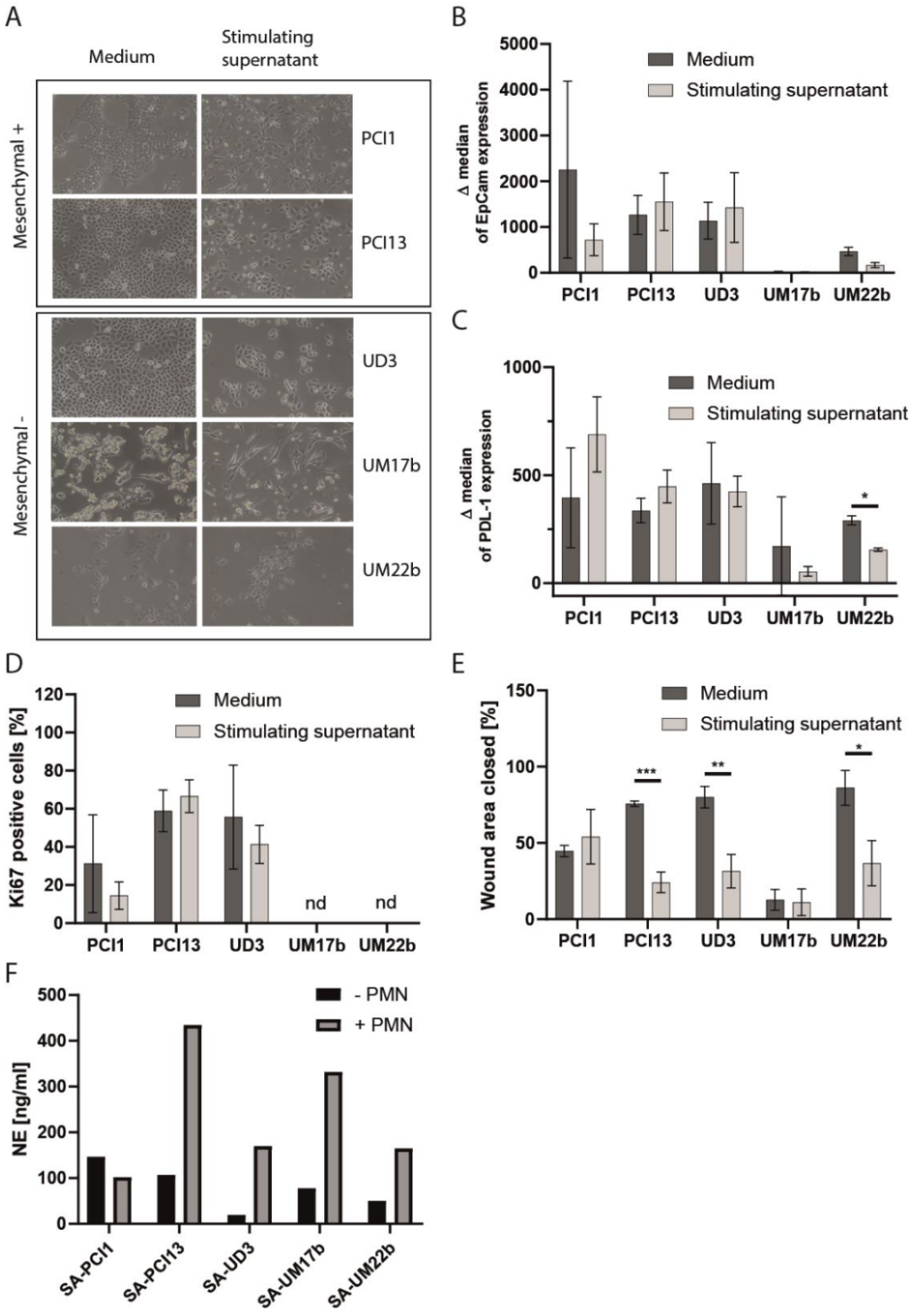

FIGURE 7: DIFFERENCES IN STIMULATION OF HNC CELL LINES WITH *STAPHYLOCOCCUS AUREUS*

(A) Microscopy imaging of cells stimulated with supernatants for 72h. **(B-C)** Tumor cells were stimulated with supernatants for 72h, EpCam **(B)** and PDL-1 **(C)** expression was measured with FACS, n=3. **(D)** Expression of Ki67 in stimulated and unstimulated tumor cells, determined by immunofluorescence staining, n=3. **(E)** Tumor cells treated with supernatants were grown until confluence and the closure of a scratch "wound" was recorded after 16h. Wound closure was quantified with ImageJ, n=3. **(F)** Concentration of NE was measured in supernatants with ELISA, n=1. **(B-F)** n indicates number of independent experiments. All statistical analyses were performed with un-paired t-test: *=p<0.05, ** p<0.01, *** p<0,001. Data are displayed as mean +/- SD.

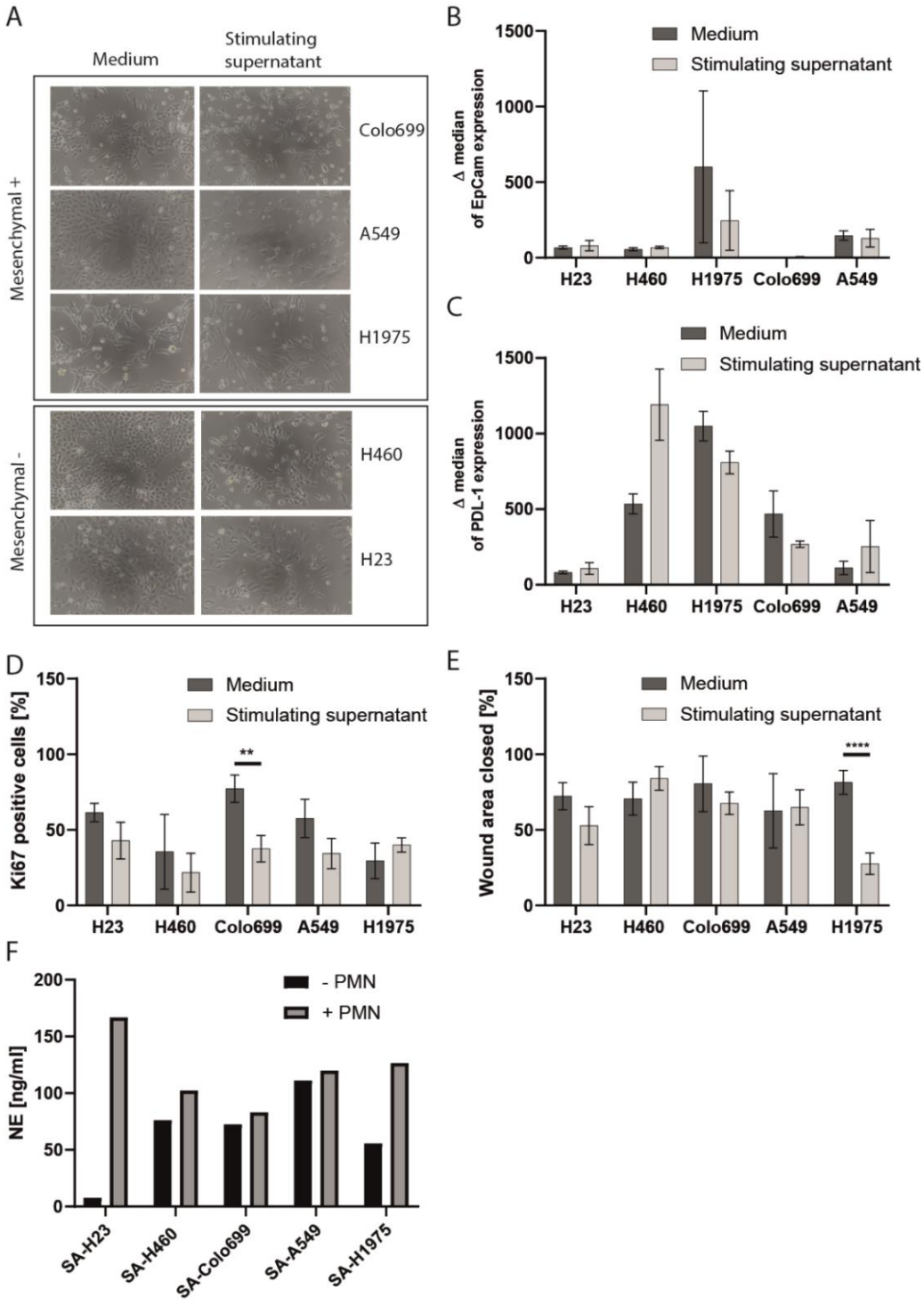

FIGURE 8: DIFFERENCES IN STIMULATION OF LUNG TUMOR CELL LINES WITH *STAPHYLOCOCCUS AUREUS*

(A) Microscopy imaging of cells stimulated with supernatants for 72h. **(B-C)** Tumor cells were stimulated with supernatants for 72h, EpCam **(B)** and PDL-1 **(C)** expression was measured with FACS, n=3. **(D)** Expression of Ki67 in stimulated and unstimulated tumor cells, determined by immunofluorescence staining, n=3. **(E)** Tumor cells treated with supernatants were grown until confluence and the closure of a scratch "wound" was recorded after 16h. Wound closure was quantified with ImageJ, n=3. **(F)** Concentration of NE was measured in supernatants with ELISA, n=1. **(B-F)** n indicates number of independent experiments. All statistical analyses were performed with un-paired t-test: ** $p<0.01$, **** $p\leq0.0001$. Data are displayed as mean +/- SD.

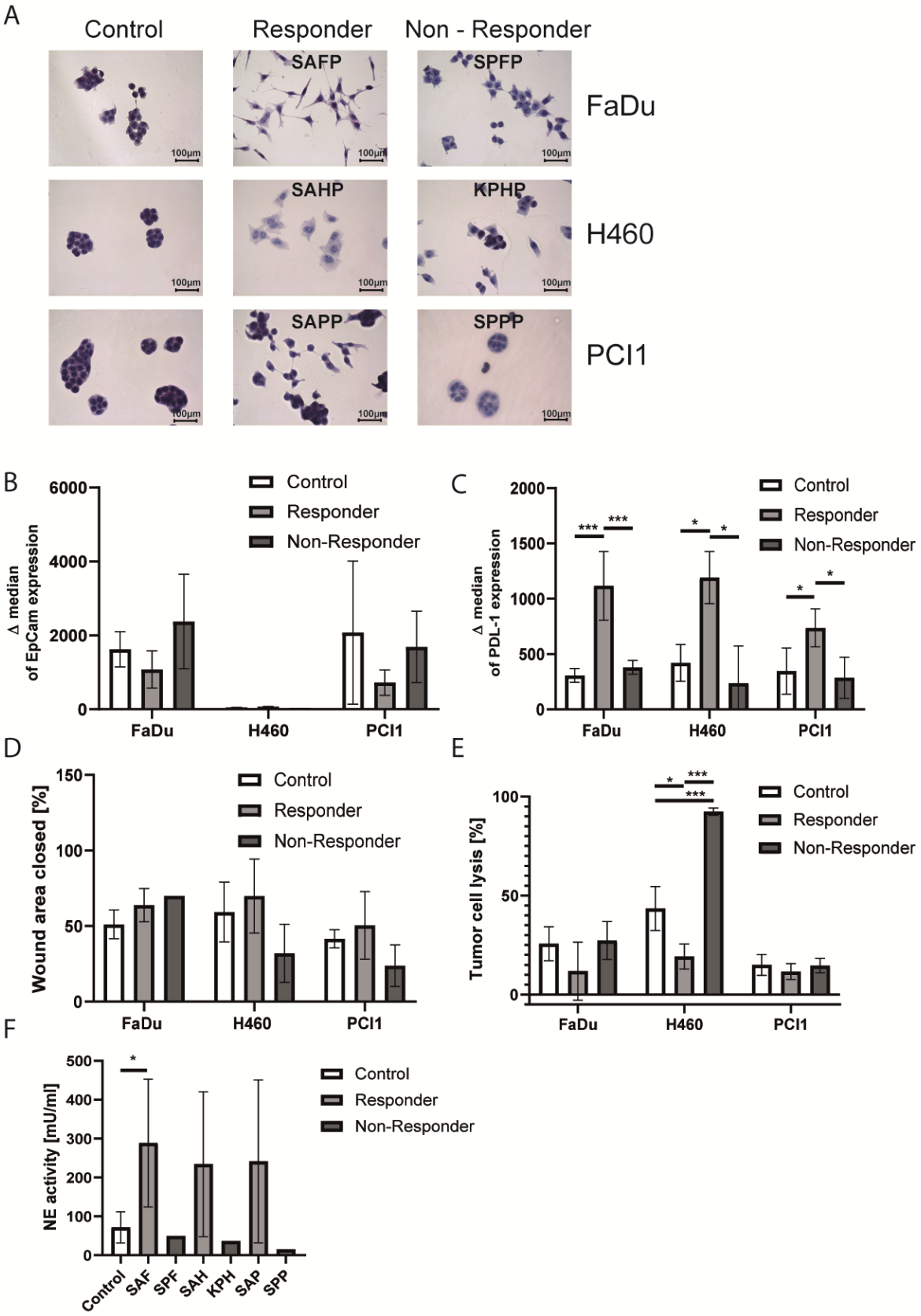

FIGURE 9: INDUCTION OF A MESENCHYMAL MORPHOTYPE IN HNC AND LUNG CANCER CELL LINES BY DIFFERENT BACTERIAL STRAINS

Supernatants description can be found in Table 1. **(A)** HE staining of tumor cells stimulated with supernatants for 72h (SA – *S. aureus*, SP – *S. pneumoniae*, KP – *K. pneumoniae*). **(B-C)** Tumor cells were stimulated with supernatants for 72h, EpCam **(B)** and PDL-1 **(C)** expression was measured with FACS, n=3. **(D)** Tumor cells treated with supernatants were grown until confluence and the closure of a scratch "wound" was recorded after 16h. Wound closure was quantified with ImageJ, n=3. **(E)** Tumor cells were stimulated with supernatants for 72h, IL-2 stimulated-NK cells were added for 24 h and tumor cell death was determined via Annexin-7AAD flow cytometry assay, n=3. **(F)** Concentration of NE was measured in supernatants with ELISA, n=1-6. **(B-D)** n indicates number of independent experiments **(E)** n indicates number of NK cells donors **(F)** n indicates number of technical replicates. Statistical analysis was performed with one-way ANOVA test with Tukey's multiple comparisons test **(B-E)** and un-paired t-test **(F)**: *=p<0.05, *** p<0,001. Data are displayed as mean +/- SD.

Next, we decided to take a closer look on gene signature of differentially stimulated cells and run bulk RNAseq analysis. As a 'responder' group, we used FaDu cells stimulated with SAFP and H460 cells stimulated with SAHP, as a 'non-responder' group FaDu cells stimulated with SPFP and H460 cells with KPHP. Unstimulated tumor cells were used as a control group. First, when we compared all 3 groups together we observed that 2 cell lines: FaDu and H460 significantly different from each other on the base gene expression level (Fig 10A-B). However, we decided to look for the similarities and constructed a volcano plot analysis of expressed genes on both cell lines combined, to search for overarching mechanisms operative in both models (Fig 10C).

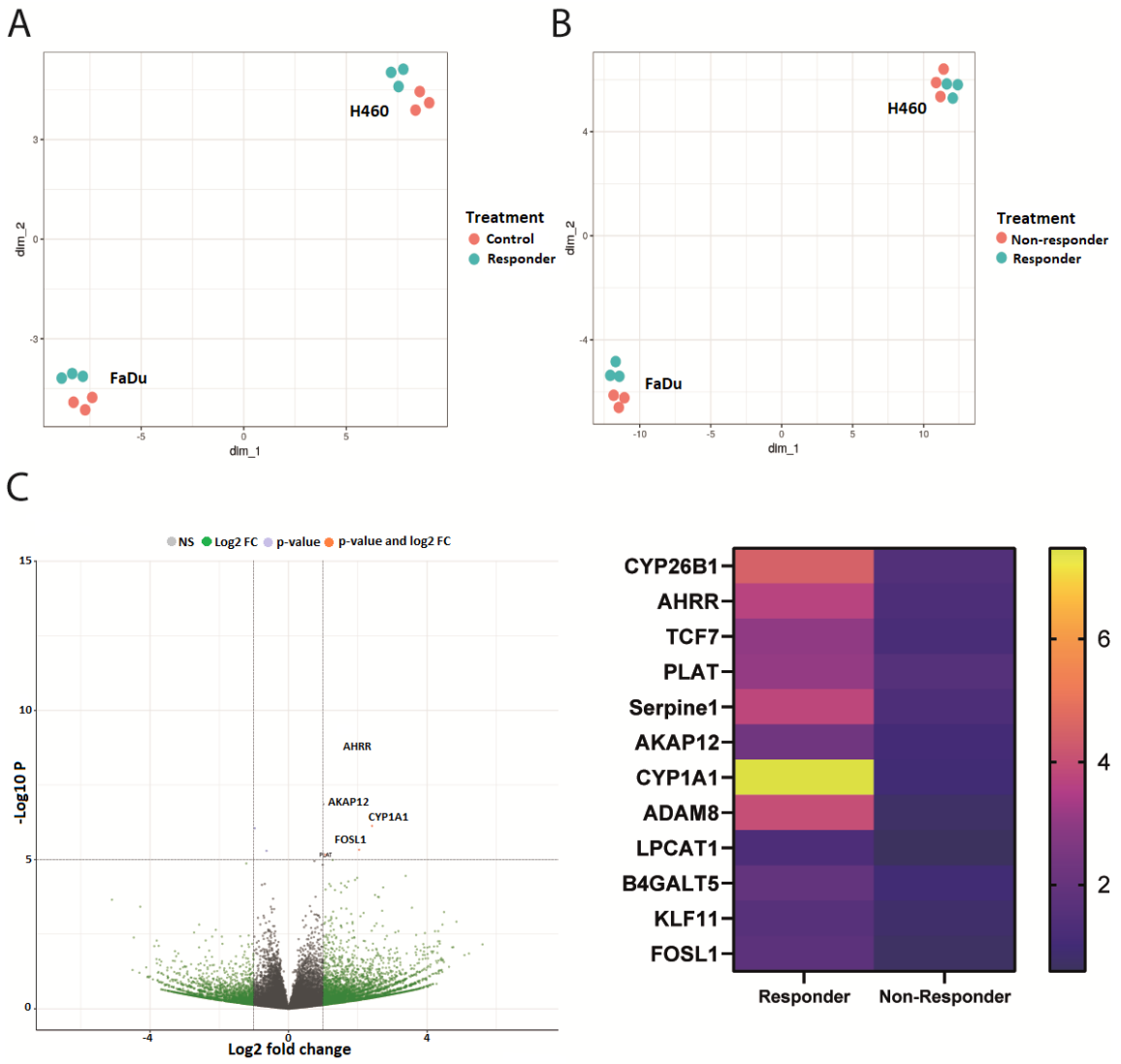

FIGURE 10: DIFFERENCES IN GENE EXPRESSION PATTERNS BETWEEN CELL LINES AND STIMULATION CONDITIONS

(A-B) UMAP analysis of all expressed genes in both cell lines. Color discriminates the response type/treatment and it´s indicated in the legend. **(C)** Volcano plot of 'responder' vs 'non-responder' cells (FaDu + H460 cell lines combined). Heatmap focuses on genes significantly different between those groups.

This analysis revealed a small number of genes, which significantly differed between 'responder' and 'non-responder group'. Most of these genes are connected with metastatic behavior of tumor cells. With this knowledge, we performed a literature search to identify other well-known metastasis linked genes and evaluated their expression in our group of cells. We observed significant differences in metastasis-linked gene expression between all three groups: control, 'responder' and 'non-responder' in both cell lines (Fig 11A). Therefore, we run a clustering analysis, which also showed certain differences in the gene expression pattern between the groups inside the cell line suggesting that cells from 'responder' group have pro-metastatic features (Fig 11B).

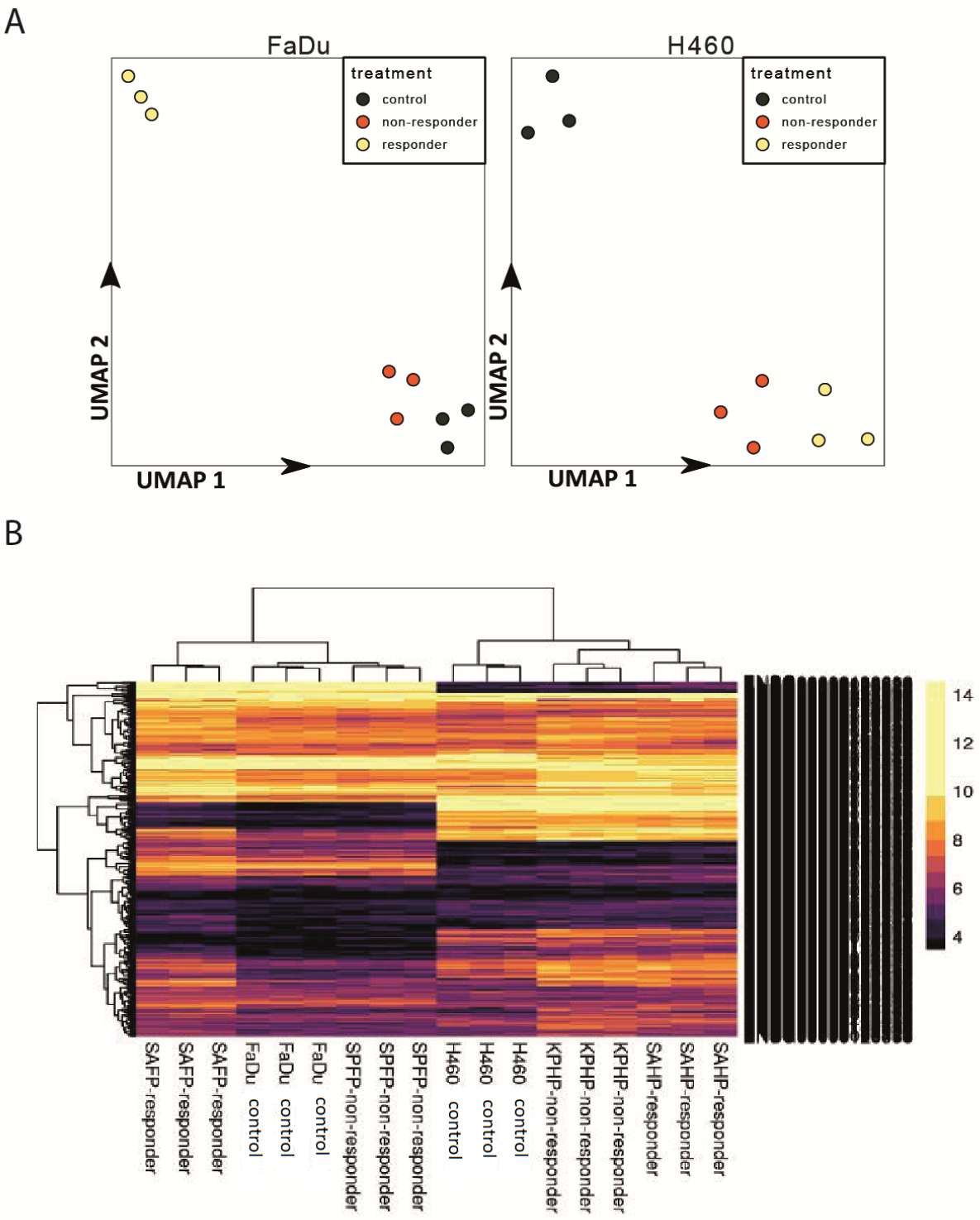

FIGURE 11: PRO-METASTATIC GENE SIGNATURE IN 'RESPONDER' STIMULATED TUMOR CELLS

(A) UMAP analysis of metastasis-linked genes separated for the two cell lines (left panel = FaDu, right panel = H460) and colored by response type/treatment (black = control, red = 'non-responder', yellow = 'responder'). **(B)** Heatmap showing results of HCA with pre-selected 387 metastasis-connected genes. Heatmap was generated with the R-package pheatmap (standard settings with clustering of genes and samples enabled).

4.2. WHAT IS BACTERIAL IMPACT ON TME

In the last chapter we showed how important the bacterial strain is for the stimulation of tumor cells, now we would like to focus on the potential mechanism of this stimulation.

First, we asked whether living bacteria are required to trigger the observed morphological and functional changes. To do so, we used non-viable Staphylococcus aureus (inactivated by either ethanol or heat treatment) to produce the stimulating supernatants – modified SAFP (Fig 12A). When FaDu cells were stimulated with those supernatants, we did not observe any changes in their morphology (Fig 12B), expression of EpCam and PDL-1 (Fig 12C-D), proliferation (Fig 12E) or resistance to NK cytotoxicity (Fig 12F). We could also observe that level of NE in those supernatants was decreased compared to SAFP (Fig 12G). These results suggest that stimulation with living bacteria is crucial to influence the tumor cells.

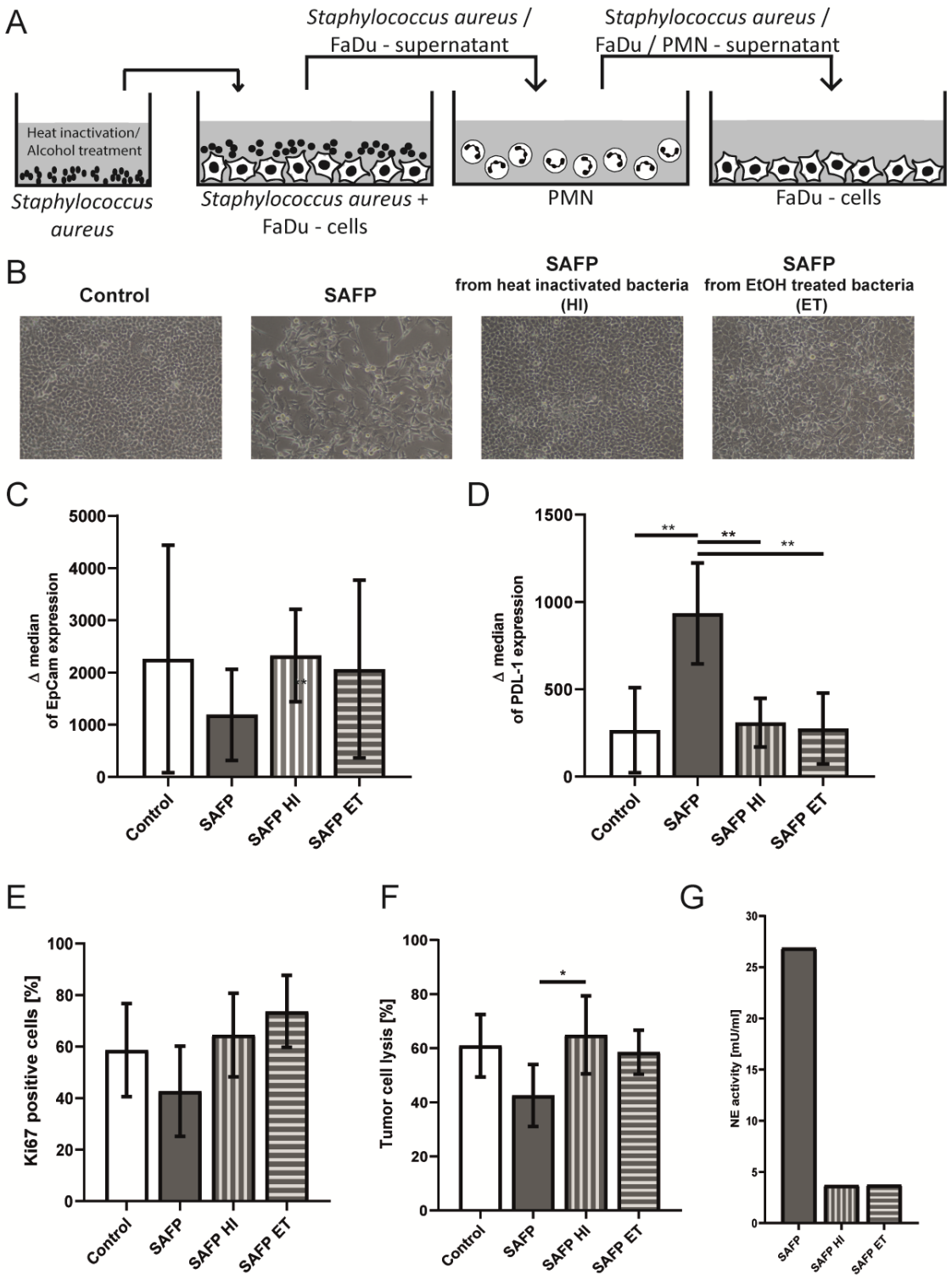

FIGURE 12: SUPERNATANT FROM INACTIVATED BACTERIA DID NOT CAUSE CHANGES IN STIMULATED TUMOR CELLS

(A) A scheme of the supernatant production - bacteria were inactivated with either heat or alcohol treatment followed by the co-cultivation with tumor cells. **(B)** Microscopy photos of cells stimulated for 72h with indicated supernatants. **(C-D)** Tumor cells were stimulated with supernatants for 72h, EpCam **(C)** and PDL-1 **(D)** expression was measured with FACS, n=3. **(E)** Expression of Ki67 in stimulated and unstimulated tumor cells, determined by immunofluorescence staining, n=3. **(F)** Tumor cells were stimulated with supernatants for 72h, IL-2 stimulated-NK

cells were added for 24 h and tumor cell death was determined via Annexin-7AAD flow cytometry assay, n=3. **(G)** NE activity was measured with a commercial activity assay. **(C-E)** n indicates the number of independent experiments. **(F)** n indicates number of NK cells donors. **(C-F)** Statistical analysis was performed with one-way ANOVA test with Tukey's multiple comparisons test: *=p<0.05, ** p<0.01. Data are displayed as mean +/- SD.

Additionally, analysis of the metabolite composition of the supernatants (Fig 13A) revealed the presence of plethora of bacterial metabolites, which levels varied significantly between different supernatants. For SAFP, highest amount of ethanol, acetaldehyde and glucose was observed (Fig 13B-D). All these compounds are important parts of the bacterial metabolism, playing a role in the glycolysis and fermentation processes. Surprisingly, we did not observe a clear correlation between the level of metabolites and the division of supernatants into 'responder' and 'non-responder' groups.

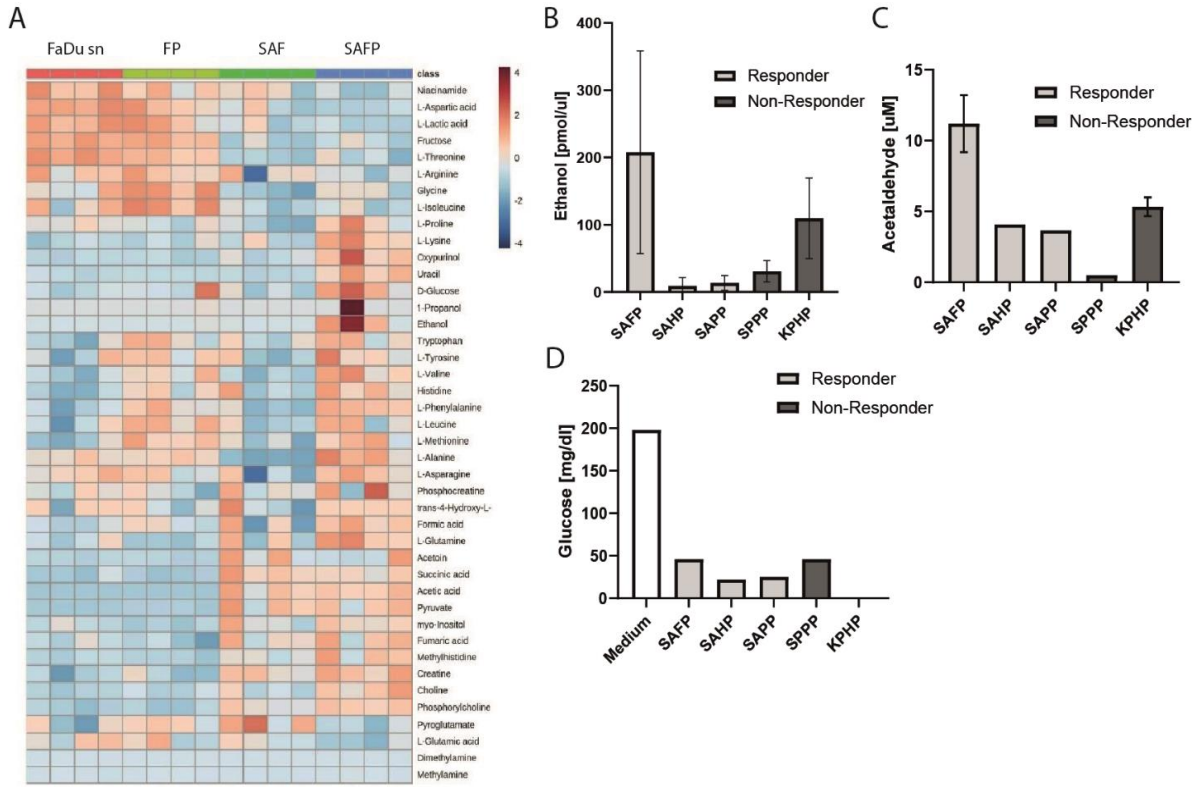

FIGURE 13: SELECTED METABOLIC CONTENT ANALYSIS OF SUPERNATANTS

(A) NMR measurement results of selected supernatants. Each supernatant was measured in 4 replicates. **(B)** The ethanol content of supernatants measured by a commercial Ethanol Detection Assay. **(C)** The acetaldehyde content of supernatants measured by commercial Acetaldehyde Detection Assay **(D)** The glucose measurement in supernatants. **(B-D)** Statistical analysis was performed with one-way ANOVA test with Tukey's multiple comparisons test.

While screening the supernatants we also investigated the protein content (Fig 14A). We selected a few proteins which level was significantly higher in SAFP compared to the control and FP to

confirm their presence in the supernatant using Western Blot (Fig 14B). Myosin-9 (chosen after literature research) was a potential candidate, whose importance in the system was then tested with its inhibitor – Blebbistatin; however, in the performed assays there were not any observable effects of blocking the protein (Fig 14C). Those results suggest no clear correlation between bacterial compounds present in supernatants and changes in behavior of stimulated tumor cells.

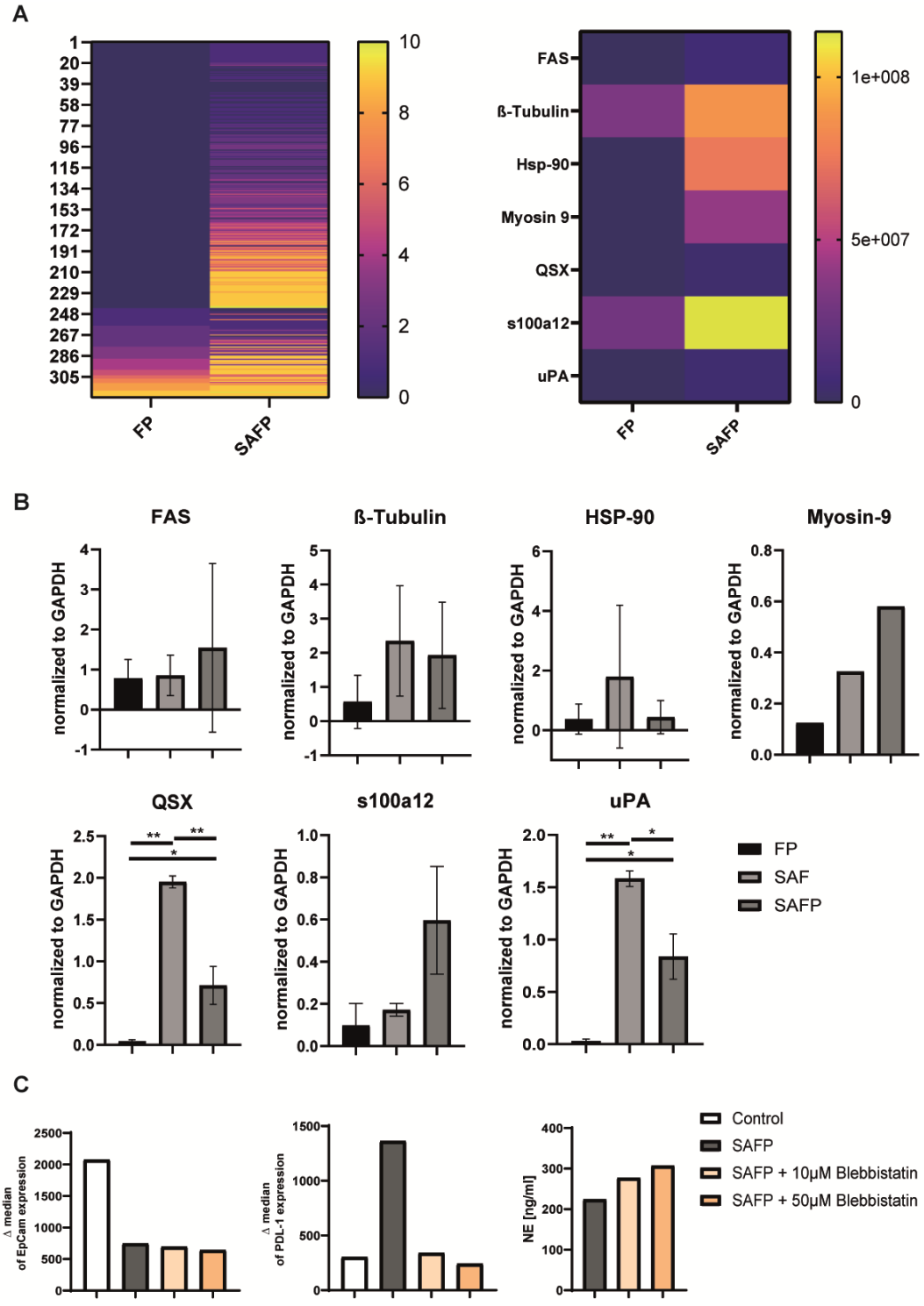

FIGURE 14: THE PROTEIN CONTENT ANALYSIS OF SUPERNATANTS

(A) Heatmap of selected proteins content, detected in a MS proteomic analysis, in FP and SAFP supernatants (left panel). Heatmap of proteins, which significantly differed between supernatants (right panel). Values in both panels were normalized to the control. **(B)** Confirmation of the presence of selected proteins in the supernatants with the Western Blot analysis, n=2. **(C)** Importance of Myosin-9 in the system was tested with its inhibitor – Blebbistatin. (From the left) Cells were stimulated with supernatants with or without inhibitor for 72h and expression of EpCam and PDL-1 was measured with FACS. The level of NE was measured in supernatants with ELISA, n=1. **(B-C)** n indicates number of independent experiments. Statistical analysis was performed with one-way ANOVA test with Tukey's multiple comparisons test: *=p<0.05, ** p<0.01. Data are displayed as mean +/- SD.

In the next series of experiments, we tested the role of Lipoteichoic acid (LTA) which was hypothesized to be an important effector. LTA has already been investigated by other researchers and was shown to stimulate EMT in tumor cells (Kim et al., 2017). We observed that LTA spiked the culture medium did not affect cells morphology, but when we combined FaDu supernatant with LTA, then the change was similar to the one caused by SAF stimulation (Fig 15A). Similar dependency was visible with the EpCam expression by stimulated cells (Fig 15B). However, PDL-1 level was not affected in any of the conditions, besides SAFP (Fig 15C). This data suggested that the stimulation of tumor cells with just LTA was not enough to induce changes in tumor cells. Co-cultivation of bacteria with tumor cells was needed to achieve the effect.

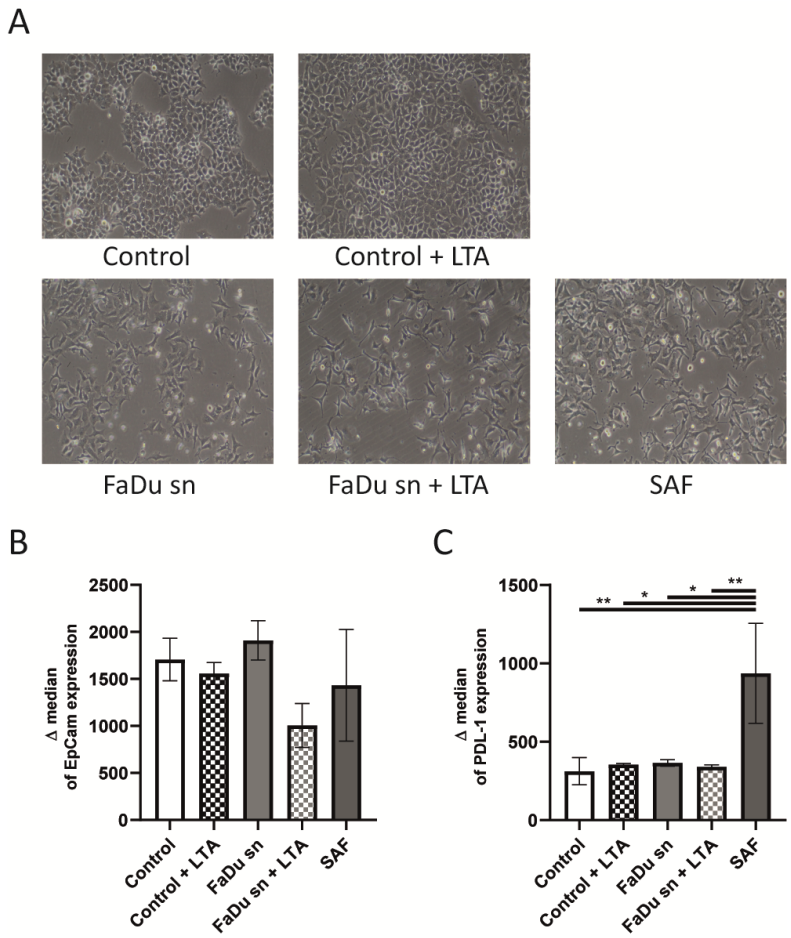

FIGURE 15: LTA ALONE IS NOT RESPONSIBLE FOR THE PHENOTYPE CHANGES IN STIMULATED CELLS

(A-C) Tumor cells were stimulated as indicated for 72h (LTA was added in the concentration of 10µg/mL), afterwards microscopy photos were taken **(A)** and expression levels of EpCam **(B)** and PDL-1 **(C)** were determined with FACS, n=3. **(B-C)** n indicates number of independent experiments. Statistical analysis was performed with one-way ANOVA test with Tukey's multiple comparisons test: *=p<0.05, ** p<0.01. Data are displayed as mean +/- SD.

4.3. STIMULATED PMN AS THE MAIN DRIVER OF FUNCTIONAL CHANGES OF TUMOR CELLS.

So far we have identified distinct (viable) bacteria that enhanced the pro-metastatic cross-talk of tumor cells and PMN.

In the second part of the project, we focused on elucidation of the molecular mechanism and potential mediators secreted by PMN that were required for the phenotype change of tumor cells.

To this end, we first investigated cell biological changes in differentially stimulated PMN. To do so, we stimulated PMN with supernatants coming from FaDu cells as well as one from tumor cells co-cultivated with bacteria (SAF). We observed significant differences in the level of MIF and IL-8 (Fig 16A-B) and activity of MMP-9 (Fig 16C) upon the stimulation, suggesting that SAF is a stronger activator of PMN. In addition, we established that SAF significantly increased ROS production in PMN (Fig 16D) as well as PMN death (Fig 16E). We observed no differences in the chemotaxis index between both supernatants however; it can be caused by high cytotoxicity of SAF and low number of PMN surviving after migration (Fig 16F). Next we used previously established ‘responder’ and ‘non-responder’ supernatants and tested their efficacy to induce NE in PMN. Firstly, we found that level and activity of NE between those two groups varied, and ‘responder’ supernatants have a positive stimulation effect (Fig 16G-H). NE is one of the proteins, released by PMN during NETosis process, so in our next step we checked the potential of the supernatants to induce NETs production. The analysis showed that stimulation of PMN with ‘responder’ supernatants let to significantly higher NETosis than with ‘non-responder’ supernatants (Fig 16I).

Because NETs are known for promoting tumor growth (Masucci et al., 2020), in the next experiment we decided to check if differentially stimulated PMN have different impact on the survival of tumor cells. We stimulated PMN with supernatants from both groups and with PMA as a positive control for NETs induction. After 30 min the stimulated PMN were harvested and co-cultured with tumor cells for up to 3 days. Interestingly, tumor cells exposed to NET forming PMN

showed increased proliferation. This was in stark contrast to the effects of non-NET forming PMN, which arrested or even reduced tumor cell numbers in the 24h and 72h time window (Fig 16J).

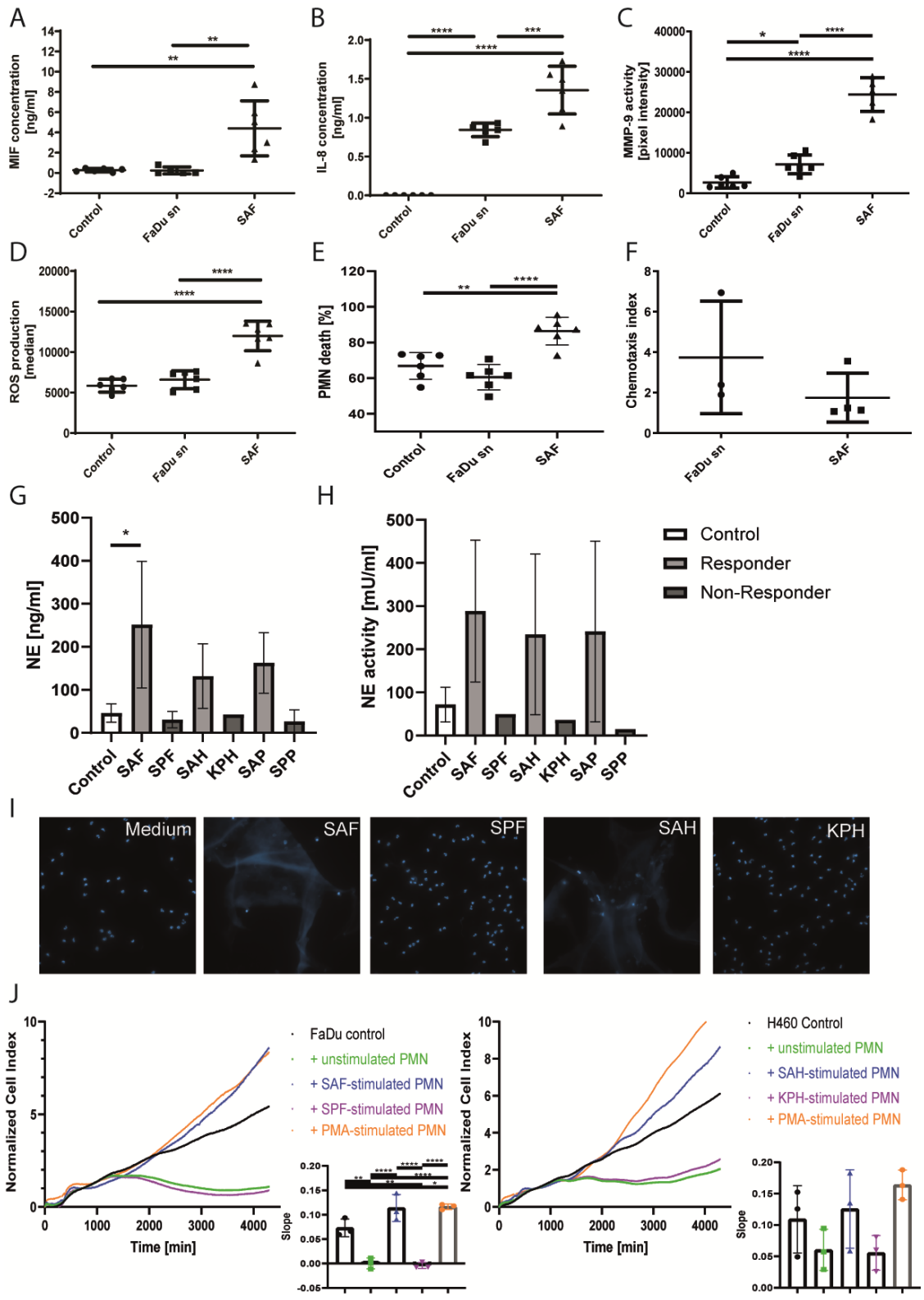

FIGURE 16: BACTERIAL STIMULATION OF TUMOR CELLS INDUCES THE PMN ACTIVATION

Supernatants description can be found in Table 1. **(A-C)** Supernatants from 24h stimulated PMN (10^6cells/mL) were harvested and concentration of MIF **(A)** and IL-8 **(B)** was determined with ELISA; activity of MMP-9 was determined with zymography **(C)**, n=6. **(D)** PMN (10^6cells/mL) were stimulated for 3h and ROS production was determined with Dihydrorhodamine 123 by flow cytometry, n=6. **(E)** PMN (10^6cells/mL) were stimulated for 24h and the amount of dead cells was determined by Annexin/7AAD flow cytometry, n=6. **(F)** PMN were placed into 3µm inserts and let for 3h to migrate into different supernatants, n=4. **(G-H)** Supernatants from PMN (10^6cells/mL) stimulated for 20h were harvested and concentration **(G)** and activity **(H)** of NE were determined, n=1-6. **(I)** NET formation by PMN, stimulated for 30min with different supernatants. **(J)** PMN were stimulated with designated supernatants for 30min, afterwards they were added to tumor cells on the E-plate. Proliferation of tumor cells was tracked with xCelligence for 72h n=3. **(A-F)** n indicates number of PMN donors **(G-H)** n indicates number of technical replicates **(J)** n indicates number of independent experiments and PMN donors. Statistical analysis was performed with one-way ANOVA test with Tukey's multiple comparisons test **(A-E, G-H, J)** and un-paired t-test **(F)**: *=p<0.05, ** p<0.01, *** p<0,001, **** p≤0.0001. Data are displayed as mean +/- SD.

Additionally, we compared effects of PMN stimulation by 'responder' supernatants with the effects of already established ways of PMN activation. We stimulated PMN with TLR activators: LPS, fMLP, ionomycin and LTA or we co-cultivated them directly with *Staphylococcus aureus*. In most of the cases, we could observe an increase in the release level of NE, MIP1b and MMP-9 (Fig 17) as expected in the dose dependent manner.

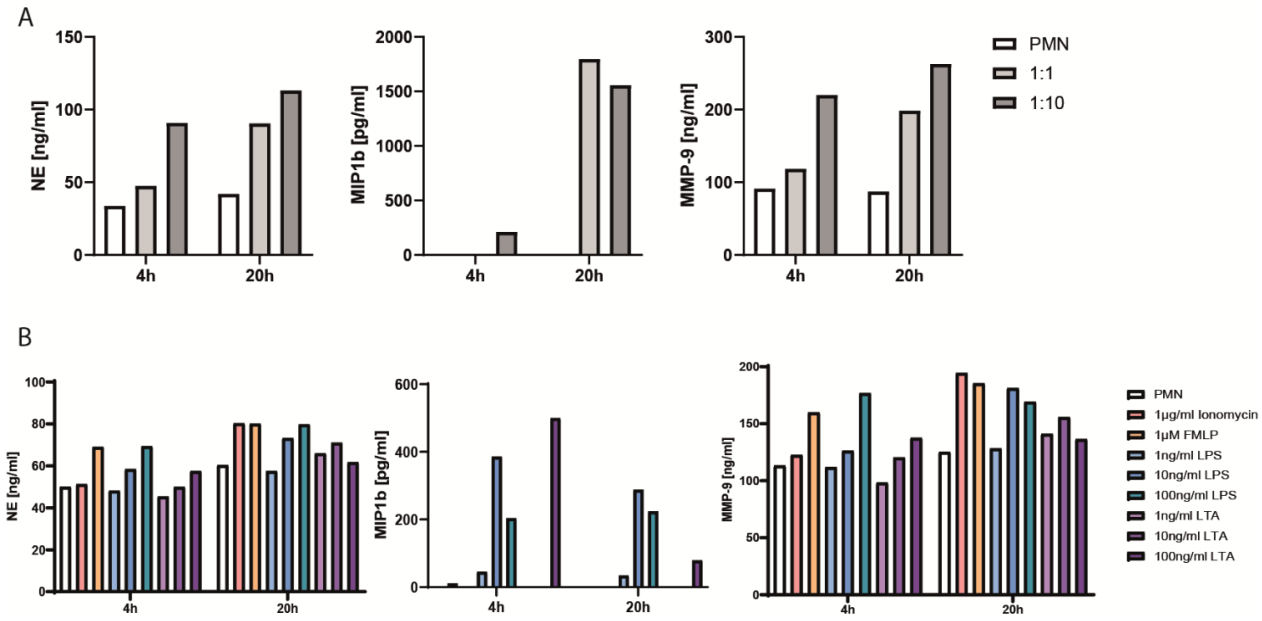

FIGURE 17: CLASSICAL ACTIVATION OF PMN

(A) PMN were co-cultured with living bacteria (in different ratio) for 4h and 20h, supernatants were harvested. The levels of NE, MIP1b and MMP-9 were measured with ELISA. **(B)** PMN were stimulated with TLR ligands for 4h and 20h, supernatants were harvested. Levels of NE, MIP1b and MMP-9 were measured with ELISA.

However, when we stimulated tumor cells with such supernatants we did not reproduce the effects observed with SAFP stimulation (Fig 18). This confirmed that effects, which we see in our system, cannot be induced by classical direct activation of PMN.

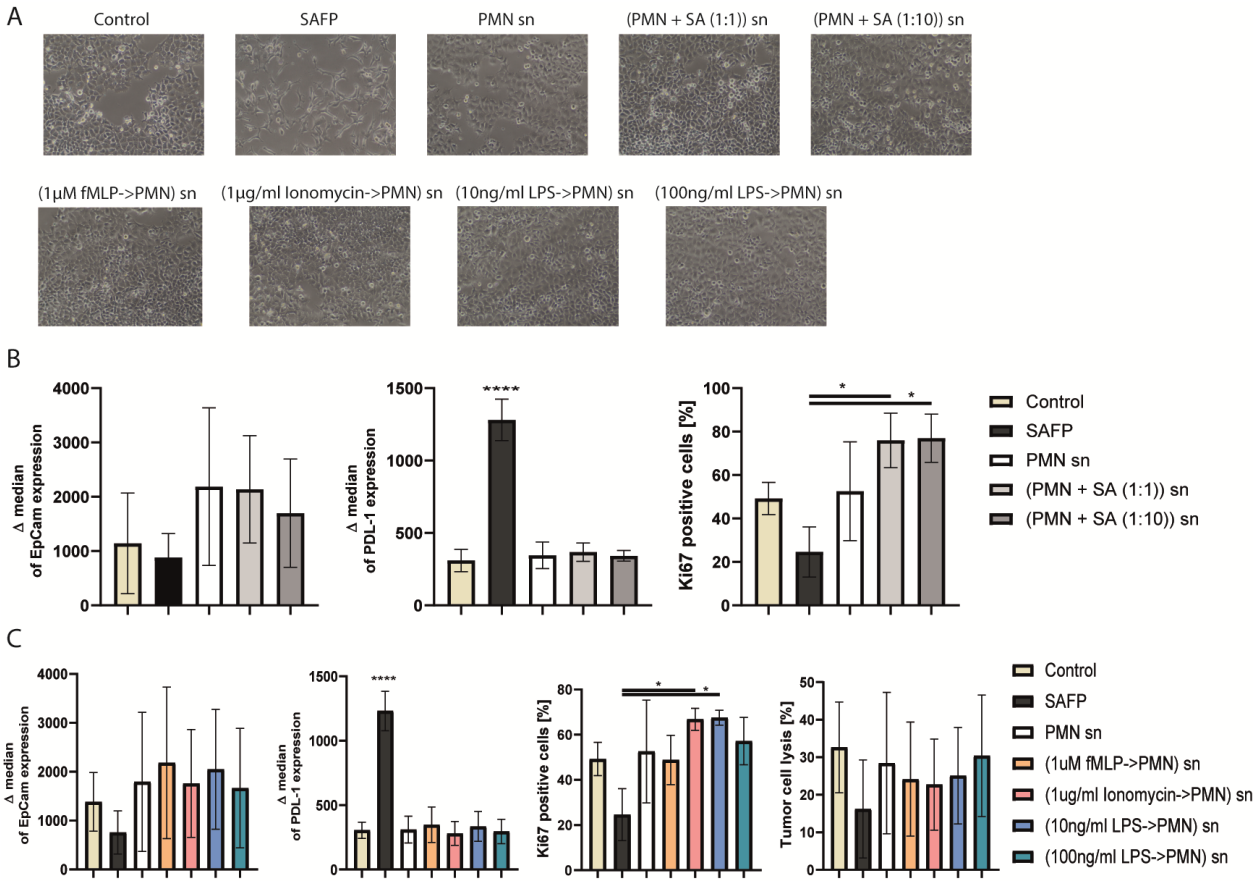

FIGURE 18: CLASSICALLY ACTIVATED PMN DO NOT STIMULATE TUMOR CELLS IN THE SAME WAY AS 'RESPONDER' SUPERNATANTS

(A) Microscopy photos of tumor cells stimulated with indicated supernatants for 72h. **(B)** Tumor cells were stimulated with indicated supernatants for 72h, (from the left) expression of EpCam and PDL-1 was measured with FACS and expression of Ki67 was determined with IF staining, n=3. **(C)** Tumor cells were stimulated with indicated supernatants for 72 h, (from the left) expression of EpCam, PDL-1 was measured with FACS and expression of Ki67 was determined with IF staining. For determining tumor lysis by NK cells, IL-2 stimulated-NK cells were added for 24 h and tumor cell death was determined via Annexin-7AAD flow cytometry assay, n=3. **(B-C)** n indicates number of independent experiments. Statistical analysis was performed with one-way ANOVA test with Tukey's multiple comparisons test: *=$p<0.05$, **** $p\leq0.0001$. Data are displayed as mean +/- SD.

In the next series of experiments, we focused on two proteins, which release was significantly increased in PMN stimulated with supernatants from 'responder' group: NE and MMP-9. Both of them are also main components of PMN's released NETs.

To determine their function we decided to use inhibitors: Sivelestat (NE inhibitor) and GM6001 (MMP inhibitor) during the stimulation of PMN with SAF (Fig 19A, 20A).

The addition of Sivelestat expectedly decreased activity of NE in the supernatant (Fig 19B). This supernatant was then used for the tumor cells stimulation, which effected in reversing the

expression levels of EpCam and PDL-1 close to their control levels (Fig 19C-E). No changes in Ki67 expression and migration abilities of cells were observed (Fig 19F-G). The characteristic formation of bigger tumor and the induction of angiogenesis visible in the *in ovo* assay, was not visible anymore after usage of supernatant with Sivelestat (Fig 19H-I).

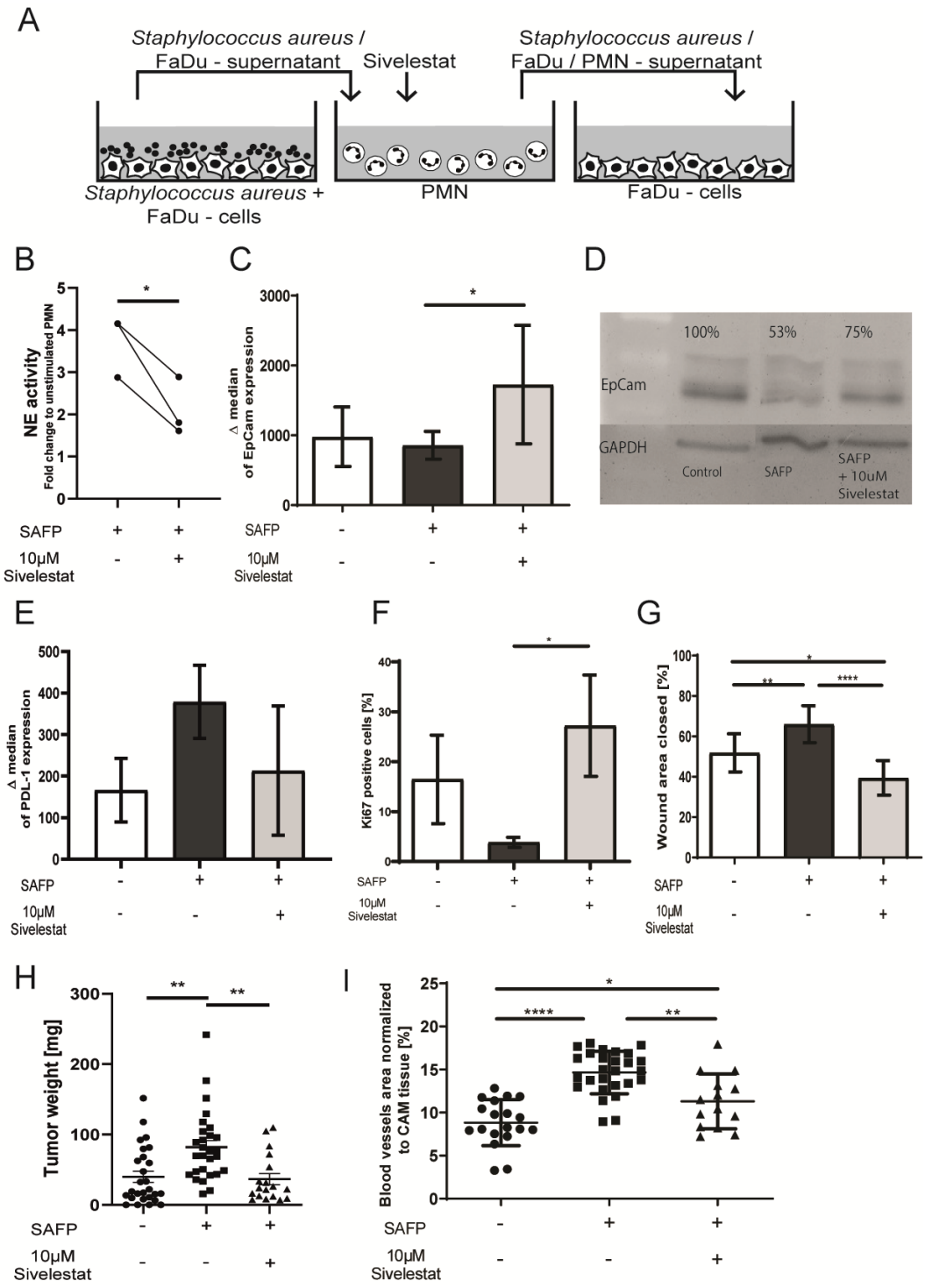

FIGURE 19: THE ROLE OF NEUTROPHIL ELASTASE IN THE TUMOR CELL STIMULATION

Sivelestat (NE inhibitor, 10µM) was added during the production of SAFP supernatant as indicated in the panel **A**. **(B)** The activity of NE was determined in the supernatant, in the presence or the absence of Sivelestat, using NE activity assay, n=3. **(C-D)** After 72h of stimulation the expression of EpCAM was determined by flow cytometry, n=3 **(C)**, and Western Blot, shown one representative experiment out of 3 **(D)** on the tumor cells in the presence or absence of Sivelestat. **(E)** After 72h of stimulation the expression of PDL-1 was determined by flow cytometry in the presence or the absence of Sivelestat, n=3. **(F)** Expression of Ki67 on tumor cells in the presence or the absence of Sivelestat, obtained with the immunofluorescence staining; n=3. **(G)** The effect of Sivelestat on the scratch closure was determined in the wound healing assay, n=7. **(H-I)** Effects of Sivelestat were also checked in *in ovo* CAM assay: effect on the tumor weight **(H)** and angiogenesis in the upper CAM **(I)** (Control n=20, SAFP n=27, SAFP+Sivelestat n=15) is displayed. **(B)** n indicates number of independently acquired supernatants **(C,E-G)** n indicates number of individual experiments **(H-I)** n indicates number of eggs used for the experiment. Statistical analysis was performed with an un-paired t-test **(B)** and one-way ANOVA test with Tukey's multiple comparisons test **(C, E-I)**: *=$p<0.05$, ** $p<0.01$, **** $p\leq0.0001$. Data are displayed as mean +/- SD.

We observed similar effects with the addition of GM6001, MMP-9 activity was reduced (Fig 20B), expression of EpCam and PDL-1 was not significantly different from the control level (Fig 20C-D). In addition, we could not detect any more effects caused by SAFP in the migration assay (Fig 20E) and *in ovo* (Fig 20F-G).

This data suggested that NE and MMP-9 coming from stimulated PMN could drive changes caused by ‘responder’ supernatants in tumor cells.

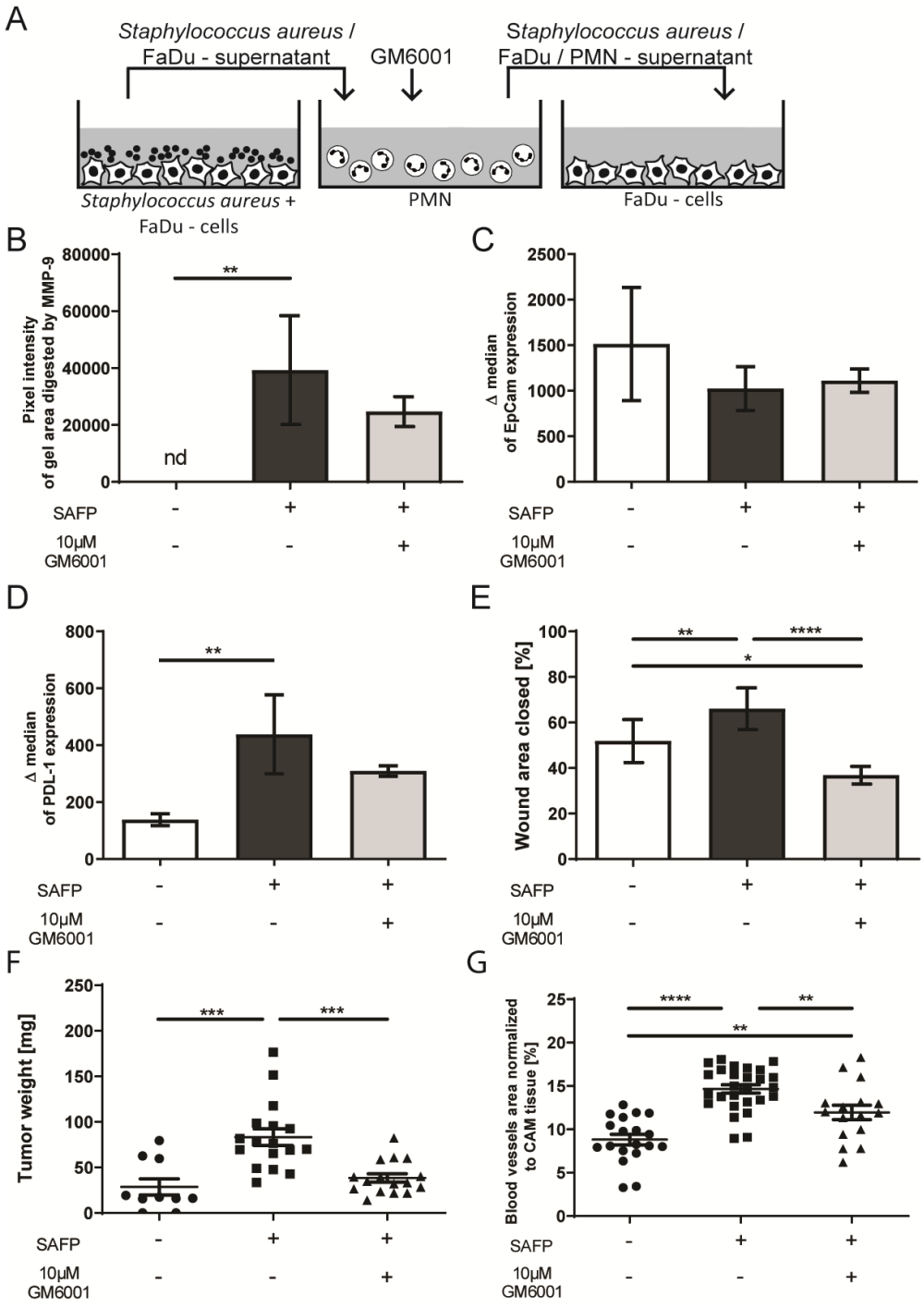

FIGURE 20: THE ROLE OF MMP-9 IN THE TUMOR CELL STIMULATION

GM6001 (MMP-9 inhibitor, 10μM) was added during the production of SAFP supernatant as indicated in panel **A**. **(B)** Levels of active MMP-9 in PMN supernatants were determined by zymography, n=3. **(C-D)** After 72h of stimulation the expression of EpCam **(C)** and PDL-1 **(D)** was determined by flow cytometry in the presence or absence of GM6001, n=3. **(E-G)** Effects of GM6001 on scratch closure (**E**; n=4); tumor growth (**F**, Control n=10, SAFP n=17, SAFP+GM6001 n=16) and angiogenesis in the upper CAM (**G**, Control n=19, SAFP n=27, SAFP+GM6001 n=16) were determined. **(B)** n indicates number of independently acquired supernatants, **(C-E)** n indicates number of independent experiments, **(F-G)** n indicates number of eggs used in the experiment. Statistical analysis was performed with one-way ANOVA test with Tukey's multiple comparisons test: *=p<0.05, ** p<0.01, *** p<0,001, **** p≤0.0001. Data are displayed as mean +/- SD.

4.4. INNATE IMMUNE ESCAPE CONTRIBUTES TO ENHANCED METASTASIS

After demonstrating enhanced invasion and migration *in vitro* we next probed the metastatic features of tumor cells in *in vivo* models.

Firstly, to confirm the pro-metastatic function of cells we decided to use the orthotopic mice model (experiment performed by Dr Claudia Dumitru and Sebastian Vollmer) and administered stimulated tumor cells. Indeed, we observed that cells stimulated with SAFP formed significantly more lymph node metastasis as compared to the untreated cells (Fig 21A, left two bars). Interestingly, when we depleted NK cells with Asialo antibody, metastasis in the unstimulated tumor control group had increased to the levels of metastasis in the SAFP group (Fig 21A, right two bars). This observation suggests that lymph node metastasis in this model is under control of NK cells and that SAFP treated cells are able to escape from NK cells cytotoxicity, in line with data observed in *in vitro* killing assays (Fig 21B). In the next series of experiments, we investigated the cause of increased resistance against NK cells cytotoxicity of stimulated tumor cells. We have not observed any differences in the expression of NKG2D ligands between cells (Fig 21C), but we noticed a significant reduction in the conjugates formation between stimulated tumor cells and NK cells (Fig 21D). We hypothesized that such reduction in conjugate formation could stem from a physical barrier that prevents interaction of tumor target cells and NK cells. One of the examples of such a barrier can be NETs, which are an important component in our supernatant. To confirm this hypothesis we added DNAse to the supernatant during cells stimulation, which should digest parts of DNA sticking to the cells. This treatment caused a significant decrease in tumor cells resistance (Fig 21E), which showed that NETs formed by activated PMN were the main cause of this phenomenon.

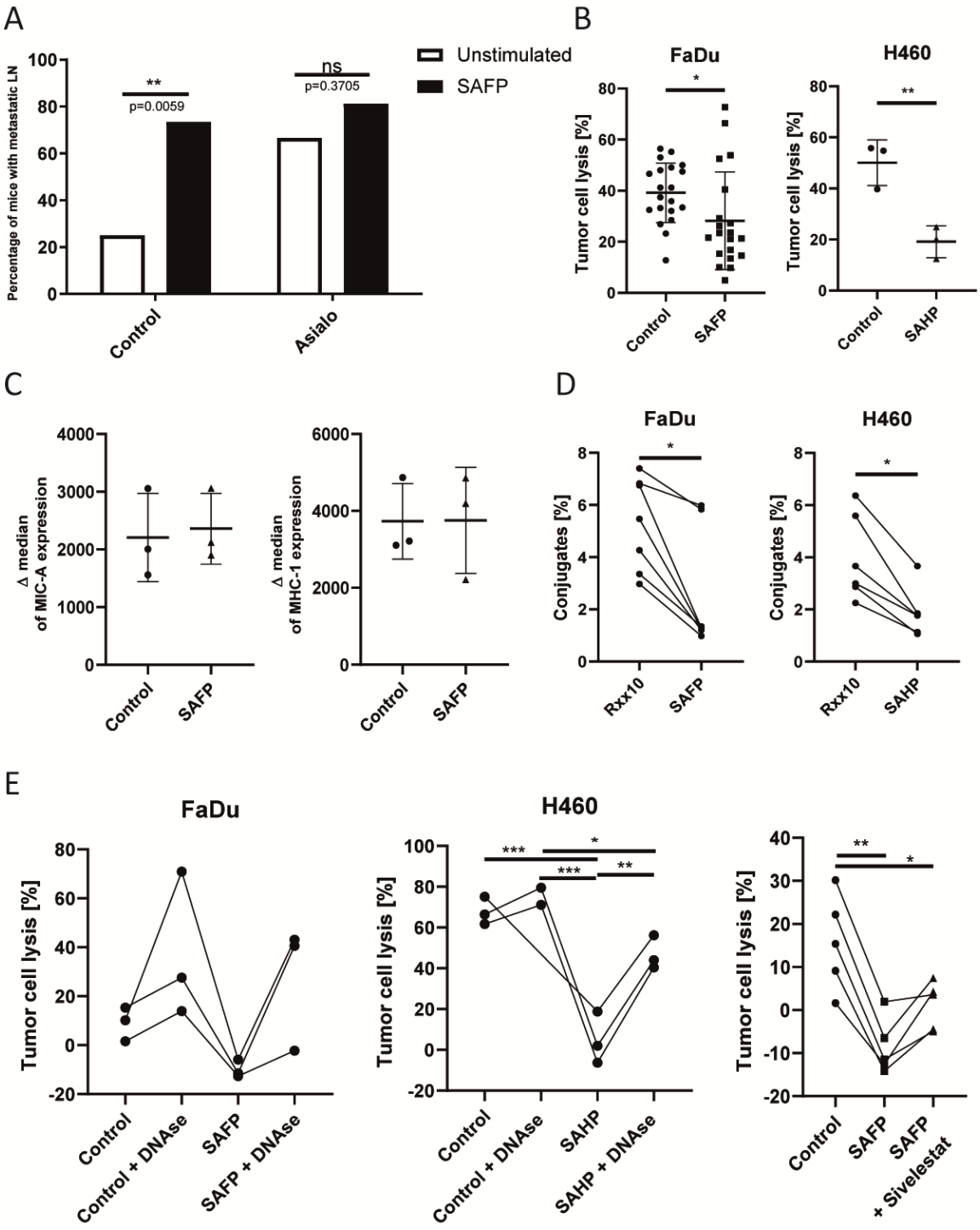

FIGURE 21: SAFP-STIMULATED MESENCHYMAL TUMOR MORPHOTYPES ARE RESISTANT TO NK CYTOTOXICITY

Supernatants description can be found in Table 1. **(A)** Unstimulated tumor cells (control) or tumor cells stimulated with SAFP supernatant were injected into the floor of the mouth of nude mice. After 20 days mice were sacrificed and the frequency of lymph node metastases was determined. Anti-asialo GM1 antibody was injected for depletion of NK cells. **(B)** Tumor cells were stimulated with supernatants for 72h, IL-2 stimulated-NK cells were added for 24h and tumor cell death was determined via Annexin-7AAD flow cytometry assay (FaDu: Control n=20, SAFP n=22, H460: n=3). **(C)** Tumor cells were stimulated with indicated supernatants for 72h and expression of MIC-A and MHC-1 were measured on FACS, n=3. **(D)** Tumor cells were stimulated with supernatants for 72h, NK cells were stimulated with

IL-2 for 48h. Afterwards both cell types were fluorescently labelled and placed together to form conjugates, which could be tracked with flow cytometry, (FaDu n=7, H460 n=6). **(E)** Tumor cells were stimulated with supernatants for 72h (DNAse – addition of 0.5U/mL DNAse1, Sivelestat – addition of 10µM Sivelestat during supernatant production), IL-2 stimulated-NK cells were added for 24 h and tumor cell death was determined via Annexin-7AAD flow cytometry assay (DNAse experiments n=3, Sivelestat experiment n=5). **(A)** n indicates number of mice, **(B, D-E)** n indicates number of NK cells donors, **(C)** n indicates number of independent experiments. Statistical analysis was performed with an un-paired t-test **(A-D)** and one-way ANOVA test with Tukey's multiple comparisons test **(E)**: *=p<0.05, ** p<0.01, *** p<0,001. Data are displayed as mean +/- SD.

To confirm the constant activation of PMN in our tumor microenvironment model, we utilized spheroids, a 3D model of TME. We placed spheroids formed from FaDu cells into different supernatants together with the isolated PMN. We observed that PMN placed in SAFP clustered together, which is a sign for their activation (Fig 22A). In addition, we could observe that PMN in this condition are heavily migrating inside the spheroid (Fig 22B); however, the distance of migration into spheroid was not varied between different conditions (Fig 22C). This and previous experiments showed that TME can highly PMN, induce their NETs production and by that trigger the immune escape of tumor cells.

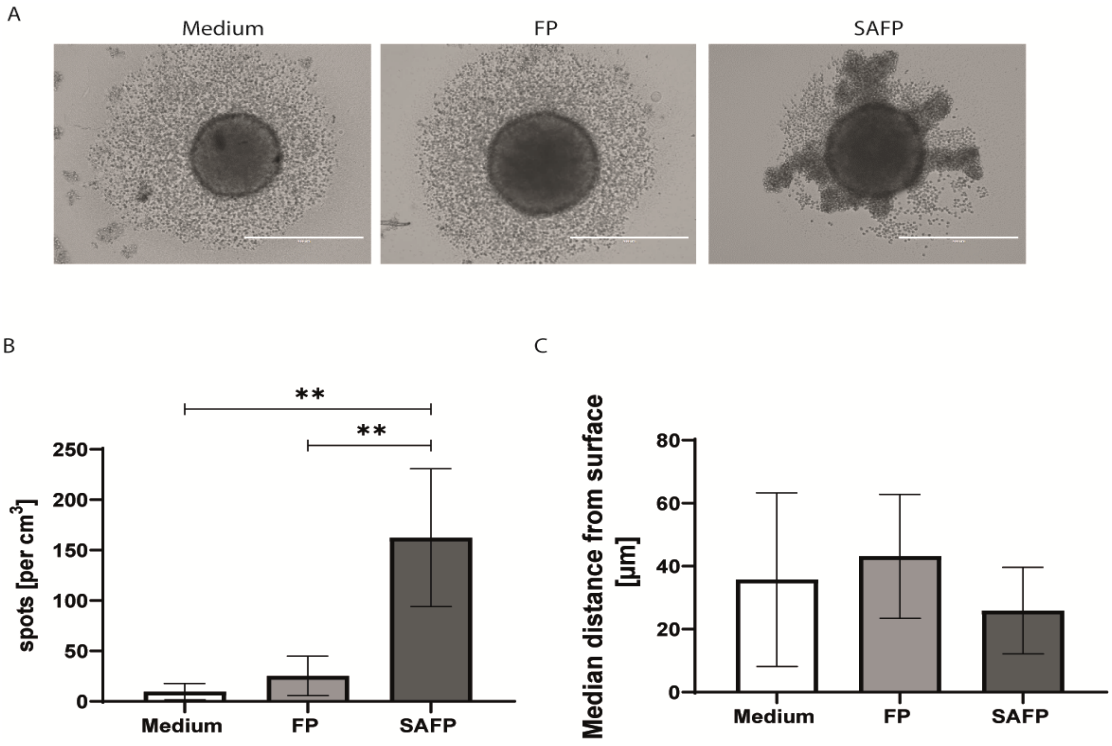

FIGURE 22: PMN IN SAFP ARE HIGHLY ACTIVATED AND HAD INCREASED MIGRATION INTO 3D SPHEROID TUMOR MODEL.

(A) Representative microscopy image of PMN state in the spheroid model and indicated supernatants. **(B)** Quantification of PMN migrated into tumor spheroids, n=4. **(C)** Calculated depth of the PMN migration into spheroid, n=4. **(B-C)** n indicates number of independent experiments. Statistical analysis for all experiments was performed with one-way ANOVA test with Tukey's multiple comparisons test: ** p<0.01. Data are displayed as mean +/- SD.0

4.5. THE ROLE OF STROMA IN TUMOR MICROENVIRONMENT

In the first part of the study we observed that both, tumor core areas and mesenchymal stromal parts of the TME are colonized by bacteria. The stromal parts of the TME are also strongly infiltrated by PMN in many patients (Fig 23A). Thus, in the final part of the study we tested the effects of tumor-stromal cross-talk on PMN recruitment and probed whether bacterial stimulation of mesenchymal stromal cells could also induce phenotype switching in tumor cells via PMN activation.

To this end, we produced different supernatants, which were supposed to imitate the tumor, stromal and primed stroma (stromal cells stimulated with tumor supernatant) compartments of the TME (Fig 23B). Afterwards they were used as chemoattractants in the chemotaxis and TEM (trans-endothelial migration assay) assays; we could observe that primed stroma was the most attractive for PMN to migrate into (Fig 23C). To better mimic the conditions in TME we exposed PMN for both tumor and stromal cells at the same time and observed their behavior. For this purpose, we utilized again 3D spheroid model, this time with forming mixed spheroids, containing both tumor and stromal cells. When given a choice PMN clearly migrated more into stromal parts of spheroid, confirming our observations from patient data (Fig 23D).

It is not clear how exactly PMN move into TME. We wanted to elucidate the order they travel through compartments and whether the increased abundance in stroma was a sign of PMN being trapped there. To answer this question we performed a non-classical trans-well migration assay. We placed PMN suspension (PMN in different supernatants, mimicking TME compartments) in the trans-wells, which then were placed in the well containing the same or different supernatant. With this approach, we could observe if PMN placed in certain environment are willing to change it for another one. Data show that primed stroma has strongest recruitment capacity in this system, with tumor to primed stroma showing the strongest directed migration. However, we also observed migration from primed stroma into tumor supernatant, suggesting that PMN may not be finally trapped in certain compartments, but are rather able to bidirectionally move between them. (Fig 23E).

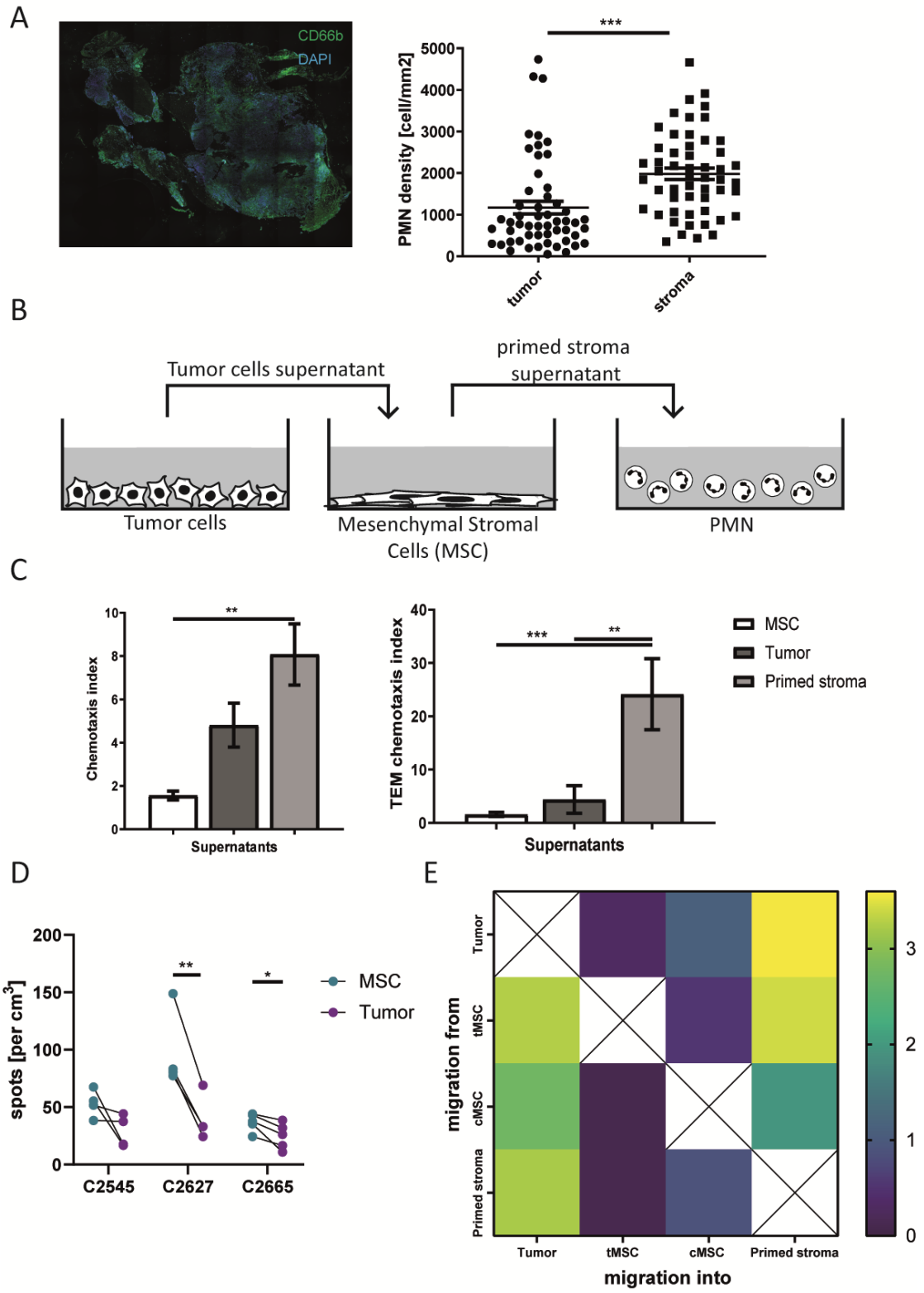

FIGURE 23: THE IMPORTANCE OF STROMAL CELLS IN TME

(A) A representative photograph of CD66b staining in the tumor tissue (left panel), the quantification of PMN density in the tumor vs stromal regions of HNC tumor tissue (right panel), n=54. **(B)** Supernatant from tumor cells was used to prime mesenchymal stromal cells, afterwards supernatants were harvested and used for the further stimulation of PMN. **(C)** Chemotaxis (left panel) and trans-endothelial migration assay (right panel) were run for 3h, PMN were

placed in 3µm inserts and allowed to migrate into supernatants below, n=3. **(D)** Mixed spheroids were formed from tumor and MSC cells, PMN were allowed to migrate into them and afterwards were counted in both regions, n=3-5. **(E)** A heatmap presenting bidirectional migration of PMN, from one supernatant inside the trans-well to another in the bottom well, n=3. **(A)** n indicates number of patients **(C-E)** n indicates number of PMN donors. Statistical analysis was performed with an un-paired t-test **(A, D)** and one-way ANOVA test with Tukey's multiple comparisons test **(C):** *=p<0.05, ** p<0.01, *** p<0,001. Data are displayed as mean +/- SD.

To have a full overview of the role of bacteria in TME, we turned to our *in vitro* system of stimulating supernatants, and additionally included in it stromal cells. Supernatants were produced according to the general protocol, with mesenchymal stromal cells replacing tumor cells. Firstly, we assessed similarities in the PMN activation with supernatants originating from tumor and stromal cells (either from the tumor (tMSC) or mucosa (cMSC)) challenged with bacteria. We observed that the increase in MIF, IL-8, MMP-9 and NE levels was similar between PMN stimulated with all types of supernatants (Fig 24A-D). We noticed a difference in the ROS production - increase just upon SAFP stimulation (Fig 24E). Additionally, similarities were visible in a decrease in the PMN survival upon the stimulation of supernatants (Fig 24F) and in increased potential to attract PMN during chemotaxis assay (Fig 24G). These results showed that the bacterial co-cultivation with either tumor or stromal cells had a similar effect on the PMN activation.

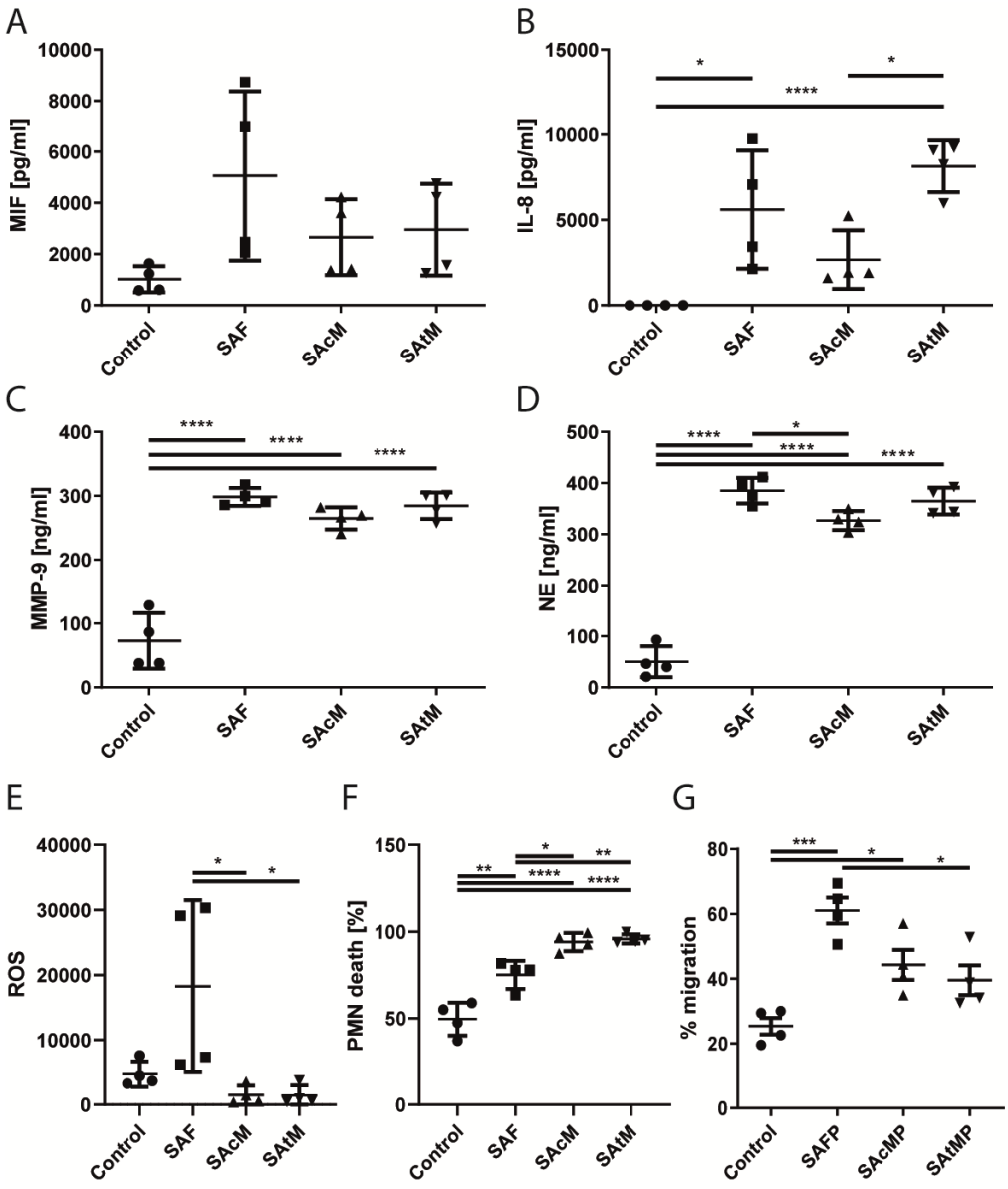

FIGURE 24: SUPERNATANT FROM STROMAL CELLS CO-CULTIVATED WITH BACTERIA ACTIVATED PMN IN THE SAME WAY AS SAF

(A-D) PMN (10^6cells/mL) were stimulated with indicated supernatants for 20h, supernatants were harvested and the level of MIF **(A)**, IL-8 **(B)**, MMP-9 **(C)** and NE **(D)** were determined with ELISA, n=4. **(E)** PMN (10^6cells/mL) were stimulated for 3h and the ROS production was determined with Dihydrorhodamine 123 by flow cytometry, n=4. **(F)** PMN (10^6cells/mL) were stimulated for 24h and the amount of dead cells was determined by Annexin/7AAD flow cytometry assay, n=4. **(G)** PMN were placed into 3µm inserts and let for 3h to migrate into different supernatants, n=4. **(A-G)** n indicates number of the PMN donors. All statistical analyses were performed with one-way ANOVA test with Tukey's multiple comparisons test: *=p<0.05, ** p<0.01, *** p<0,001, **** p≤0.0001. Data are displayed as mean +/- SD.

In next series of experiments, we stimulated tumor cells with SAcMP (*S. aureus* + cMSC + PMN) or SAtMP (*S. aureus* + tMSC + PMN) supernatants and compared them to the cells stimulated with SAFP. We observed similar changes in stimulated cells in all the standard readouts (Fig 25), which

showed that the PMN activation was mainly dependent on the bacterial presence and independent of the cell types they interacted with. Those results showed that changes in both, tumor and stromal compartments could equally influence tumor pro-metastatic features.

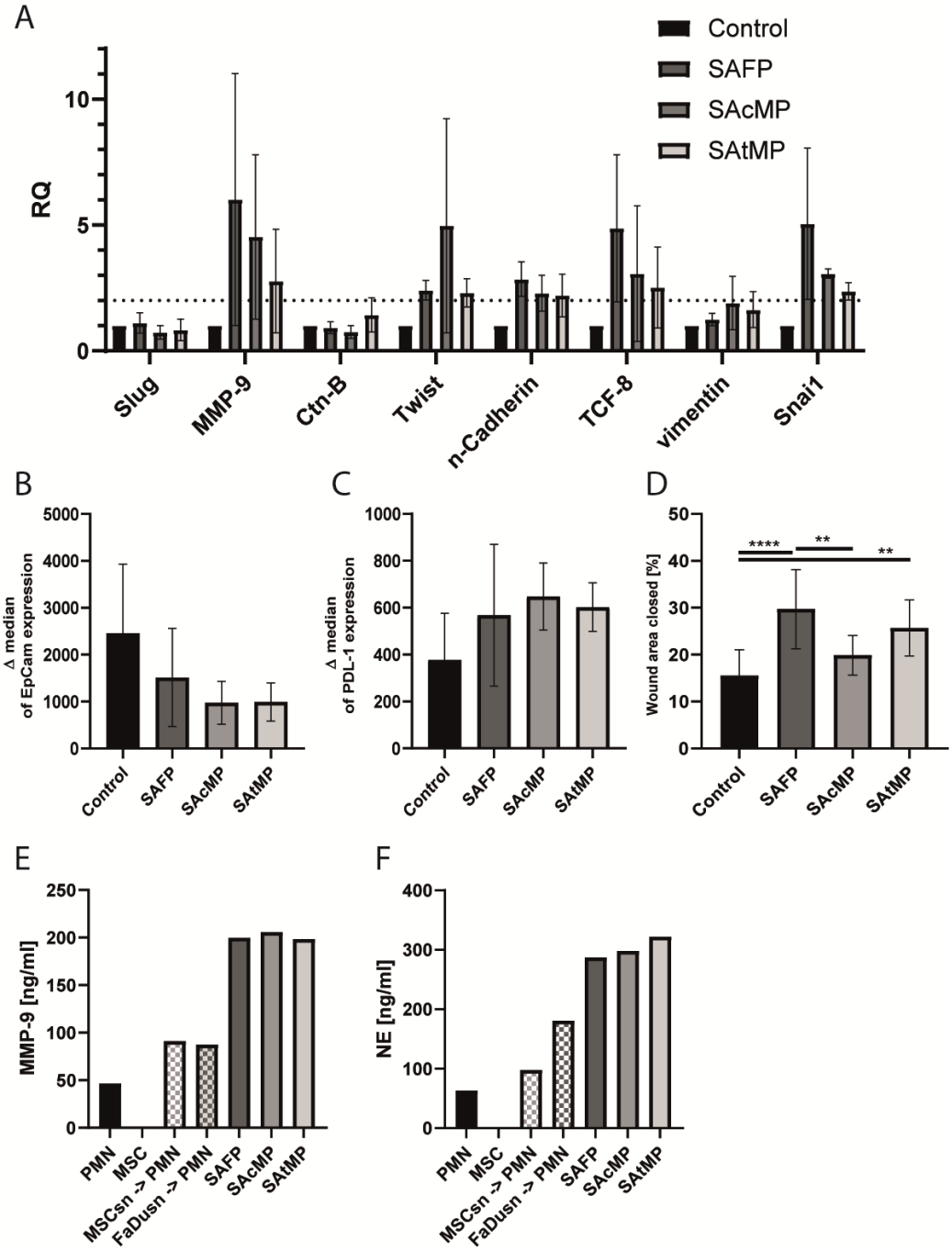

FIGURE 25: SACMP AND SATMP CAUSED SIMILAR CHANGES IN TUMOR CELLS AS SAFP

(A) qPCR performed on FaDu cells after a 6h stimulation with supernatants. The results are normalized to β-actin and untreated cells as a reference sample (RQ=1), n=3. **(B-C)** Tumor cells were stimulated with supernatants for 72h, EpCam **(B)** and PDL-1 **(C)** expression was measured with FACS, n=3. **(D)** Tumor cells treated with supernatants were grown until confluence and the closure of a scratch "wound" was quantified with ImageJ after 16h, n=3. **(E-F)**

Concentration of MMP-9 **(E)** and NE **(F)** in the supernatants was measured with ELISA, n=1. **(A-D)** n indicates number of independent experiments **(E-F)** n indicates number of pooled supernatants (each sample consisted of 3 separately produced supernatants). **(B-D)** Statistical analysis was performed with one-way ANOVA test with Tukey's multiple comparisons test: ** p<0.01, **** p≤0.0001. Data are displayed as mean +/- SD.

In the final experiment, we wanted to correlate the results from *in vitro* experiments with patient tissue data. We stained patient tumor tissues for EpCam (epithelial marker) and Vimentin (mesenchymal marker) to look for potential EMT changes, which we observed in the supernatant-stimulated cells. We also stained for PMN and bacteria, which played an important role in our *in vitro* system (Fig 26A). We observed a significant association of high PMN density, high bacteria density and strong Vimentin staining intensity (Fig 26B).

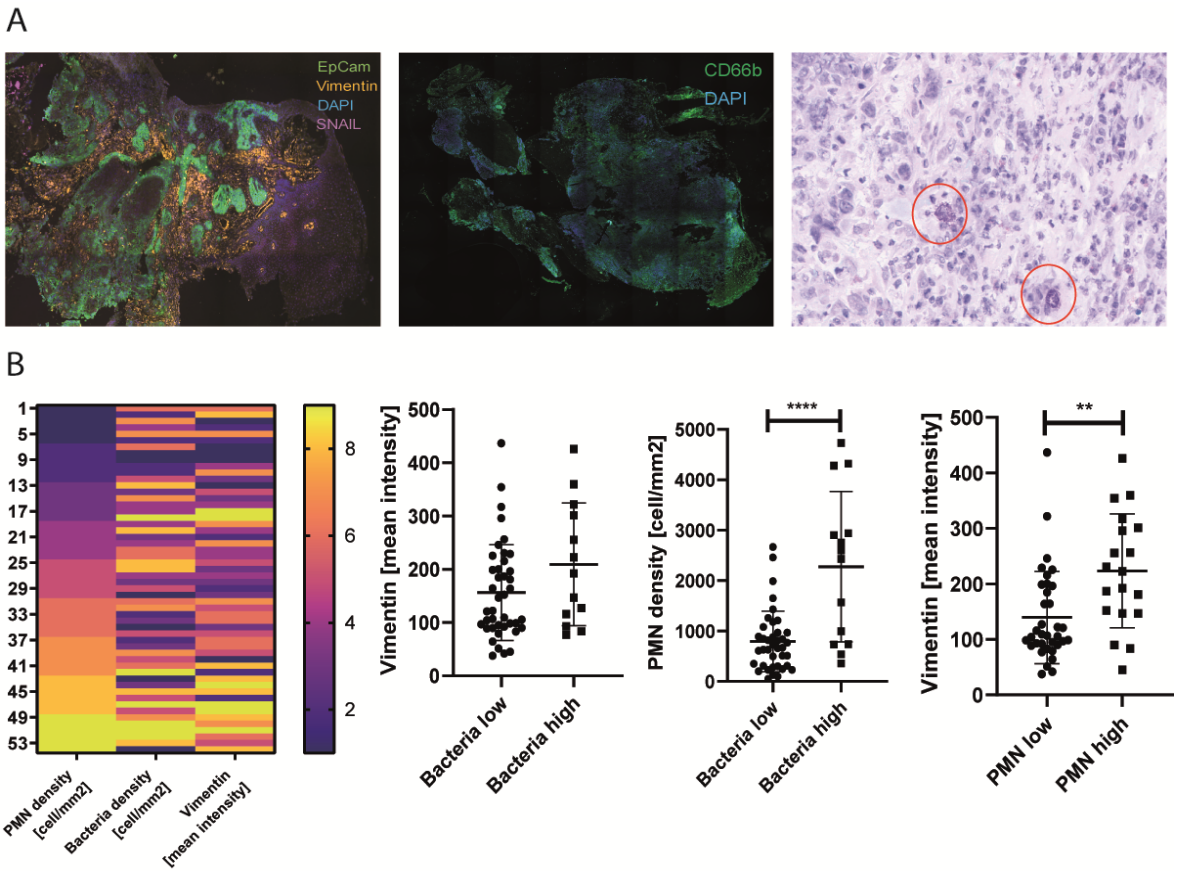

FIGURE 26: STAINING OF PATIENT'S TUMOR TISSUES CONFIRMED *IN VITRO* OBSERVATIONS

(A-B) Tumor tissues from 54 HNC patients were stained with fluorescent antibodies for CD66b (PMN marker) and Vimentin (mesenchymal marker). Bacteria were visualized with Pappenheim staining. Quantification **(B)** was performed with Tissue Studio. All statistical analyses were performed with un-paired t-test: ** p<0,01, **** p≤0.0001. Data are displayed as mean +/- SD.

In sum, these data suggest that PMN preferentially infiltrate regions of high bacterial colonization. In these regions tumor cells are exposed to bacterial stimulation, which leads to PMN activation and in turn to the induction of an aggressive tumor cell phenotype. This cascade may take place in tumor core areas, but also at the (primed) tumor-stroma interface.

5. DISCUSSION

5.1. TME-DRIVEN EMT

In the oncology research space it is now generally accepted that the progression of a tumor and its response to therapy not only depend on intrinsic characteristics of the tumor cells, but also on tumor microenvironmental factors. Thus, in addition to studying the tumor cells themselves, scientists are now also investigating the interaction between tumor cells and other cells, such as immune cells or stromal cells. Head and neck tumors (HNC) are among the most bacteria-colonized tumors. This is due to their location in the bacteria-exposed oral and pharyngeal cavity together with the associated risk factors alcohol and smoking, both making the oral mucosa, more susceptible to bacterial infection. Studies have shown that bacterial infections, in particular from *Staphylococcus aureus*, can influence recovery rate of patients after tumor removal (Helmink et al., 2019, Schwabe et al., 2013, Shiomori et al., 2007).

Despite the importance of understanding the impact of bacteria on the tumor-immune cross-talk, most of the existing literature focuses on post-surgery infections (Durand et al., 2015). Our study aimed to fill this gap by investigating the presence of bacteria within tumor tissues. By staining 54 tumor tissues for bacteria presence, we were able to confirm that bacteria are present inside the tumor, potentially supporting tumor inflammation. Additionally, we found no significant quantitative differences in bacteria distribution between tumor and stroma compartments and observed a clear correlation of bacterial density with PMN density.

PMN are well-known for their role in tumor progression and development. They are particularly interesting for studies due to their dual function, as they can either promote or inhibit tumor growth. However, the reasons behind this diversity are not yet fully understood (Coffelt et al., 2016). PMN can influence the TME by releasing various cytokines and enzymes from their granules, either directly or indirectly. Additionally, previous research has shown that patients with HNC and high NLR (neutrophil-lymphocyte ratio) tend to have poor prognosis and low recovery rate (Si et al., 2019, Trellakis et al., 2011). In this project, we found that PMN were contributing to tumor progression and metastasis. Our study also revealed that PMN were accumulating more in stromal regions than in the tumor, further highlighting the importance of the stromal components of the TME.

In our *in vitro* system, we created a supernatant, containing compounds released by bacterially stimulated tumor cells and PMN, mimicking important elements of the TME. When treating tumor cells with this supernatant, we observed direct changes in cell morphology, from an epithelial phenotype to a mesenchymal phenotype. This process, known as Epithelial-Mesenchymal Transition (EMT), can be triggered by microenvironmental signals, such as bacteria, and is driven by various transcription factors. The SNAIL, SLUG and TWIST families of transcription factors play a major role in the classical EMT, and cells that undergo EMT gain migratory and invasive abilities, becoming pro-metastatic. Importantly, the whole process is reversible, and tumor cells can revert back to an epithelial state once they reach the metastasis site, a process known as MET. Recently, the EMT concept was partially refined, as in many cases only some of the EMT features are present and these cases are now referred to as partial EMT (Bakir et al., 2020, Dominguez et al., 2017). In line with these observations, also in our study we did not observe the full classical EMT. We found that cells were clearly changing their phenotype to mesenchymal, and they were also gaining migratory and invasive abilities, as shown in wound healing and *in ovo* CAM assays. However, we did not see clear changes in the expression of previously mentioned transcription factors. Therefore, in our project, other transcription factors may be driving these changes. We did not identify a potential candidate, but we did find a clear pattern of differences in gene expression when looking at metastasis-related genes. Additionally, we observed that when cells were no longer exposed to the supernatant, they started to proliferate more, further emphasizing their pro-metastatic phenotype.

5.2. ROLE OF BACTERIA IN TME

Over the past several years, the field of microbiome research has grown in importance, highlighting the role of bacteria in the tumor microenvironment. It has been known that certain bacteria can cause cancer, such as the well-known link between Helicobacter pylori and stomach cancer. However, more recent research has focused on the impact of the tumor microbiome on tumor progression and development (Schwabe et al., 2013, Zella et al., 2021). The first cancer to be studied in this context was colon cancer, due to the well-established knowledge of the presence and importance of bacterial flora in the colon (Sepich-Poore et al., 2021). Subsequent research involved full sequencing of several different solid tumors, in order to identify other candidates in which bacteria could play a role (Nejman et al, 2020). Among the tumors colonized by bacteria are lung and head & neck cancers, the two tumor types studied in this project.

As previously mentioned, the diverse ways in which bacteria can influence tumor cells is a crucial aspect of tumor research, and was the focus of this thesis. In the course of our project, we tested 9 different strains of bacteria, all connected to the head and neck or lung environment (*S. aureus, K. pneumoniae, S. pneumoniae, P. aeruginosa, S. epidermidis, S. oralis, S. salivarius, F. nucleatum* and *P. gingivalis*). We created stimulating supernatants with each of these strains and divided them into three groups, based on the effects they had on tumor cells. The first group, referred to as 'responders', contained S. aureus, which caused EMT changes in certain cell lines when used in our system. The 'non-responder' group consisted of *K. pneumoniae, S. pneumoniae, S. epidermidis, S. oralis, F. nucleatum* and *P. gingivalis*, which did not cause any visible changes in the stimulated cells. The last group consisted of P. aeruginosa and S. salivarius, whose supernatants were extremely toxic to tumor cells. This illustrates the diversity of effects among different strains. For the final experiments featured in this thesis, we selected 6 different supernatants, 3 from the 'responder' group (SAFP, SAHP, SAPP) and 3 from the 'non-responder' group (SPFP, KPHP, SPPP). S. aureus was present in all 'responder' supernatants, and for 'non-responder' group we selected *K. pneumoniae* for the lung cell line and *S. pneumoniae* for HNC, as these bacteria are commonly found in those environments. Stimulating cells with different supernatants showed that the 'responder' group had a morphology typical of cells undergoing EMT, while the 'non-responder' group remained epithelial. We also observed significant differences in the gene signature of the cells, particularly in genes related to metastasis. Finally, in functional assays, we found that cells stimulated with 'responder' supernatants gained migratory and invasive properties. These observations highlight the importance of further screening of bacteria in the TME and identifying patterns of 'good' and 'bad' bacteria that can be used to improve tumor therapy.

As previously mentioned, cell supernatants that were generated by *S. aureus* stimulation, caused EMT-like changes in tumor cells. A related phenomenon has been observed by Kim et al (2017), where LTA was used to directly stimulate tumor cells and caused the transition, without involvement of immune compounds. However, in our study, stimulation with LTA alone was not sufficient, but when combined with a tumor supernatant, slight changes in cell morphology were observed, suggesting that the compound responsible for the changes is derived from the co-stimulation of tumor and bacteria released compounds. More significant morphological changes were observed when we used live bacteria for co-cultivation with tumor cells. This suggests that the products of bacterial metabolism may play an important role in the stimulation of tumor cells. We analyzed the metabolite content of the supernatants and found that they contained significantly

higher amounts of ethanol and acetaldehyde compared to supernatants without bacteria. These metabolites are closely connected and can lead to the alcohol-mediated carcinogenesis (Rumgay et al., 2021). In this study, we did not see clear differences in the level of metabolites between the 'responder' and 'non-responder' groups; high ethanol content seems to be specific for the SAFP supernatant. However, as the field of tumor metabolism has already shown its importance (Bader et al., 2020), we should not rule out the possibility of further investigation of the metabolism of both tumor cells and bacteria and how it changes during co-cultivation in the future.

5.3. How PMN are involved in promoting immune escape of tumor cells?

As discussed in the previous chapter, bacteria play an important and diverse role in the TME, and this was reflected in our experimental system. However, as our experiments showed, supernatants produced from co-cultivation of bacteria and tumor cells alone caused only morphological changes in the stimulated cells. Only when PMN were added to the system, the sequential stimulation of inducer tumor cells and PMN led to functional changes in responder tumor cells.

PMN are a key component in the initial response of the body to distress situations. Due to their short lifespan, they are able to react quickly, which makes them easily activated, which is beneficial during infections but not necessarily advantageous during prolonged inflammation such as in cancer (Hedrick et al., 2022). In the TME, PMN can be activated by various factors from tumor cells, bacteria, or other immune cells. The most commonly known and used activators in *in vitro* stimulation are LPS (from gram-negative bacteria) and LTA (from gram-positive bacteria), known as PAMPs, which are recognized by TLR on the PMN surface. Other commonly used activators in *in vitro* studies are PMA, Ionomycin, and fMLP (Broz et al., 2011); however, in our project, we found that these PMN-activating compounds were not sufficient to cause changes in tumor cells during supernatant stimulation. Once activated, PMN have a tendency to burst and release ROS (reactive oxygen species), NETs (neutrophil extracellular traps), and various enzymes stored in their granules. Two of them, MMP-9 and NE, have already been well-documented in terms of tumor progression and EMT (Coffelt et al., 2016). As gelatinase and elastase, they can both degrade cell membranes, as well as other structures in the TME, and aid tumor cells in changing shape and more easily escaping from the solid mass to the metastasis site (Chang et al., 2001, Gong et al., 2013). In addition to working separately, they are known to support each other, particularly when found in close proximity (Lerman et al., 2018). This is especially visible in PMN-formed NETs, which can serve as a net that holds different compounds in one place (Albrengues et al., 2018).

NETs are primarily released to trap pathogens in the body. However, they can also be produced in response to other types of stimulation in the tumor microenvironment (TME) and instead of trapping pathogens, they can cover and protect nearby tumor cells. This mechanical barrier can enable tumor cells to escape the cytotoxic activity of some immune cells, leading to immune evasion (Teijeira et al., 2020).

In our project, we demonstrated the effects of PMN stimulation, which can occur in the real tumor microenvironment (TME) and are caused by a combination of bacteria and tumor cells. We observed that different types of bacteria had different impact on PMN. PMN treated with ‘responder’ supernatants, on the contrary to ‘non-responder’, were able to form NETs and produce higher amounts of active NE. Additionally, these ‘responder’ PMN had impaired abilities to kill tumor cells and even promoted tumor cell proliferation, which was a pro-metastatic, NETs-dependent effect. As previously mentioned, NETs can also serve as a mechanical barrier around cells, which we observed in our stimulated tumor cells. When these EMT-like tumor cells were administered into mice, we noted a higher rate of metastasis compared to the control group, and this effect was not changed by depleting NK cells. This suggests that the metastatic potential of stimulated tumor cells is connected to resistance to NK cell cytotoxicity, which we confirmed in *in vitro* studies. These results highlight that stimulated tumor cells have a ‘protection’ barrier made of NETs, which allows them to evade the natural cytotoxicity of NK cells.

Another feature of cells treated with supernatants from 'responder' group is the presence of higher amounts of active NE and MMP-9, which is likely a result of NETs-producing PMN. Using inhibitors, we were able to demonstrate that these compounds play a significant role in the pro-metastatic changes observed in tumor cells upon stimulation with 'responder' supernatants. Additionally, we observed that the morphology of stimulated cells was not affected by inhibitor treatment, further supporting the conclusion that morphological changes are caused by components released prior to PMN entering the system, originating from bacteria-tumor co-cultivation.

5.4. DYNAMIC CHANGES INSIDE TME

The importance of the stromal and tumor components of the tumor microenvironment has been previously discussed. I would now like to focus on the interactions between these components and the impact they have on other parts of the TME. When analyzing patient tumor tissue samples, we observed a correlation between the density of bacteria, PMN, and the intensity of Vimentin, which is a marker of cells undergoing an epithelial-mesenchymal transition (EMT). These findings

support the choice of players used in our in vitro supernatant system and the importance of studying the interactions between the stromal and tumor components of the TME. As previously mentioned, we were able to determine the number of bacteria and PMN in both compartments of the TME. While bacteria were evenly distributed between the tumor and stroma, PMN had a much higher abundance in the stromal compartment. This observation is in line with previous research in the field (Si et al., 2019) and raises questions about recruitment mechanisms of PMN into the TME as well as potential bi-directional migration of PMN between tumor core and stromal tumor compartments. Understanding how PMN enter the tumor area and their movement within the TME is a longstanding interest in the field and could have important implications for therapy (SenGupta et al., 2021). With our *in vitro* model, we were not able to fully answer the question of how PMN enter the tumor area, but we were able to gain insights into the patterns of PMN movement within the TME. We found that stromal supernatant alone was not as attractive for PMN as supernatant from stromal cells stimulated with tumor cells (primed stroma). This suggests that the ability of stromal cells to attract immune cells is greatly influenced by their proximity to tumor cells. This finding correlated with what we observed in patient data, as primed stroma is thought to mimic the stromal component of analyzed tumors. Additionally, using our 'supernatant stimulation system', we showed that the interaction between stromal cells and bacteria can also lead to pro-metastatic changes in tumor cells, similar to what we observed with the bacteria-tumor co-cultivation.

The finding that bacterially primed stroma is able to induce a metastatic phenotype in tumor cells via PMN activation is particularly important, as it highlights the potential for pro-metastatic signals to originate from all parts of the TME. The results of our bidirectional migration experiments also indicate that once PMN enter the TME, there is a free flow of them between its compartments, with PMN able to move from the primed stroma to the tumor islands as needed, despite the higher number of PMN in the primed stroma.

All of these experiments demonstrate the dynamic and responsive nature of the tumor microenvironment. Additionally, we showed through the use of spheroids, that these changes have a snowball effect, forming a vicious cycle that significantly accelerates the pro-metastatic changes in tumor cells. PMN are already known for their pro-tumor properties and this project further illustrates how their abilities, which are beneficial during infection, can become pro-metastatic tools in the context of chronic inflammation.

5.5. CONCLUSIONS

In conclusion, this project highlights the importance of several components of the TME in promoting tumor progression and increasing the likelihood of metastatic changes. We observed that compounds released during tumor-bacteria co-cultivation can initiate morphological changes in stimulated tumor cells, transforming them from an epithelial to a more mesenchymal morphotype. For these morphological changes, PMN were not required. Importantly, not all bacteria caused this effect, highlighting the need for further research on the microbiomes of head and neck and lung tumors. While bacteria were responsible for morphological changes, stimulated PMN were required for functional changes in tumor cells. Upon stimulation with supernatants from certain bacteria-tumor combinations, PMN released NETs which covered tumor cells and provided a mechanical shield, protecting them from the cytotoxicity of immune cells such as NK cells, leading to immune evasion of the tumor. We also confirmed that NE and MMP-9 molecules, which were released by PMN along with NETs, played a key role in transforming tumor cells into more invasive, migratory and pro-metastatic cells. In terms of metastasis, using bulk RNAseq, we were able to identify a clear pro-metastatic gene signature in cells stimulated with supernatants from 'responder' groups, which was not present in 'non-responder' groups. Further analysis and testing of these results could lead to the discovery of specific molecules that drive these changes and have great potential for use in future tumor therapies.

6. SUMMARY

Head and neck carcinomas (HNC) are often associated with dysbiosis and bacterial superinfection, high frequency of neutrophils in the tissue and increased metastasis. All these factors are associated with poor prognosis of patients. This study has functionally interconnected those three important factors and explored potential mechanism of actions.

To achieve this goal we designed an *in vitro* system that mimics the cross-talk of tumor cells and neutrophils in the presence of bacterial stimulation.

We found that such a stimulation enhanced the generation of an invasive and metastatic tumor cell phenotype via the neutrophil activation.
Metastatic tumor cells displayed strong mesenchymal phenotype, pro-metastatic gene signature and enhanced migratory and metastatic abilities. Morphological changes of tumor cells were directly induced by bacterial compounds, while functional modulation of cancer cells were indirectly induced by secretion of NE and MMP-9 from activated PMN. The main elucidated metastatic mechanism was the resistance of tumor cells to NK cells cytotoxicity, which led to the immune escape of tumor cells. This resistance was an effect of NETs forming a protective shield around the tumor cells. The bacterial modulation turned out not to be limited to tumor cells, as we also found that activation of stromal cells also promoted changes in the neighboring cancer cells.

Our data suggests that bacteria modulate the cross-talk of tumor cells/stromal cells and PMN thereby enhancing the tumor progression and metastasis via promoting innate immune escape mechanism.

7. ZUSAMMENFASSUNG

Kopf- und Halskarzinome sind häufig mit Dysbiose und bakterieller Superinfektion, einer hohen Anzahl von Neutrophilen im Gewebe und einer verstärkten Metastasierung verbunden. All diese Faktoren sind mit einer schlechten Prognose für die Patienten verbunden. In dieser Studie wurden diese drei wichtigen Faktoren funktionell miteinander verknüpft und mögliche Wirkmechanismen untersucht.

Um dieses Ziel zu erreichen, haben wir ein In-vitro-System entwickelt, welches es ermöglicht, die Interaktion und Kommunikation zwischen Tumorzellen und Neutrophilen in Gegenwart einer bakteriellen Infektion zu untersuchen.

Wir fanden heraus, dass eine solche Stimulation die Entstehung eines invasiven und metastatischen Tumorzellphänotyps durch die Aktivierung von Neutrophilen fördert. Metastatische Tumorzellen wiesen einen ausgeprägten mesenchymalen Phänotyp, eine pro-metastatische Gensignatur und erhöhte Migrations- und Metastasierungsfähigkeiten auf. Die morphologischen Veränderungen der Tumorzellen wurden direkt durch bakterielle Komponenten induziert, während die funktionelle Modulation der Krebszellen indirekt durch die Sekretion von Neutrophiler Elastase und Matrix-Metalloproteinase 9 durch aktivierte polymorphkernige neutrophile Leukozyten ausgelöst wurde. Der wichtigste metastatische Mechanismus, den wir aufklären konnten, war die Resistenz der Tumorzellen gegen die Zytotoxizität durch NK-Zellen, die zu einer Immunflucht der Tumorzellen führte. Diese Resistenz war ein Effekt der NETs (neutrophil extracellular traps), die einen Schutzschild um die Tumorzellen ausbildeten. Es stellte sich heraus, dass die bakterielle Modulation nicht allein auf die Tumorzellen beschränkt war, sondern dass auch die Aktivierung von Stromazellen Veränderungen in benachbarten Krebszellen förderte.

Unsere Daten deuten darauf hin, dass Bakterien die Interaktion und Kommunikation, zwischen Tumorzellen/Stromazellen und neutrophilen Granulozyten modulieren. Sie begünstigen Tumorprogression und Metastasierung durch die Immunflucht vor dem angeborenen Immunsystem.

8. REFERENCES

Albini, A., Mirisola, V., and Pfeffer, U. (2008). Metastasis signatures: genes regulating tumor-microenvironment interactions predict metastatic behavior. Cancer Metastasis Rev *27*, 75-83.

Albrengues, J., Shields, M. A., Ng, D., Park, C. G., Ambrico, A., Poindexter, M. E., Upadhyay, P., Uyeminami, D. L., Pommier, A., Küttner, V., *et al.* (2018). Neutrophil extracellular traps produced during inflammation awaken dormant cancer cells in mice. Science *361*.

Al-Hilu, S. A., and Al-Shujairi, W. H. (2020). Dual Role of Bacteria in Carcinoma: Stimulation and Inhibition. Int J Microbiol *2020*.

Azevedo, M. M., Pina-Vaz, C., and Baltazar, F. (2020). Microbes and Cancer: Friends or Faux? Int J Mol Sci *21*.

Bader, J. E., Voss, K., and Rathmell, J. C. (2020). Targeting Metabolism to Improve the Tumor Microenvironment for Cancer Immunotherapy. Mol Cell *78*, 1019-1033.

Bakir, B., Chiarella, A. M., Pitarresi, J. R., and Rustgi, A. K. (2020). EMT, MET, Plasticity, and Tumor Metastasis. Trends Cell Biol *30*, 764-776.

Bhat, A. A., Yousuf, P., Wani, N. A., Rizwan, A., Chauhan, S. S., Siddiqi, M. A., Bedognetti, D., El-Rifai, W., Frenneaux, M. P., Batra, S. K., *et al.* (2021). Tumor microenvironment: an evil nexus promoting aggressive head and neck squamous cell carcinoma and avenue for targeted therapy. Signal Transduct Target Ther *6*, 12.

Broz, P., and Monack, D. M. (2011). Molecular mechanisms of inflammasome activation during microbial infections. Immunol Rev *243*, 174-190.

Chang, C., and Werb, Z. (2001). The many faces of metalloproteases: cell growth, invasion, angiogenesis and metastasis. Trends Cell Biol *11*, S37-43.

Chen, P. Y., Wei, W. F., Wu, H. Z., Fan, L. S., and Wang, W. (2021). Cancer-Associated Fibroblast Heterogeneity: A Factor That Cannot Be Ignored in Immune Microenvironment Remodeling. Front Immunol *12*.

Chen, T., Li, Y., Sun, R., Hu, H., Liu, Y., Herrmann, M., Zhao, Y., and Muñoz, L. E. (2021). Receptor-Mediated NETosis on Neutrophils. Front Immunol *12*.

Chen, Y., Wu, F. H., Wu, P. Q., Xing, H. Y., and Ma, T. (2022). The Role of The Tumor Microbiome in Tumor Development and Its Treatment. Front Immunol *13*.

Chou, M. Y., and Yang, M. H. (2021). Interplay of Immunometabolism and Epithelial-Mesenchymal Transition in the Tumor Microenvironment. Int J Mol Sci *22*.

Coffelt, S. B., Wellenstein, M. D., and de Visser, K. E. (2016). Neutrophils in cancer: neutral no more. Nat Rev Cancer *16*, 431-446.

Cools-Lartigue, J., Spicer, J., McDonald, B., Gowing, S., Chow, S., Giannias, B., Bourdeau, F., Kubes, P., and Ferri, L. (2013). Neutrophil extracellular traps sequester circulating tumor cells and promote metastasis. J Clin Invest *123*, 3446-3458.

Dominguez, C., David, J. M., and Palena, C. (2017). Epithelial-mesenchymal transition and inflammation at the site of the primary tumor. Semin Cancer Biol *47*, 177-184.

Dumitru, C. A., Fechner, M. K., Hoffmann, T. K., Lang, S., and Brandau, S. (2012). A novel p38-MAPK signaling axis modulates neutrophil biology in head and neck cancer. J Leukoc Biol *91*, 591-598.

Dumitru, C. A., Bankfalvi, A., Gu, X., Eberhardt, W. E., Zeidler, R., Lang, S., and Brandau, S. (2013). Neutrophils Activate Tumoral CORTACTIN to Enhance Progression of Orohypopharynx Carcinoma. Front Immunol *4*.

Durand, M. L., Yarlagadda, B. B., Rich, D. L., Lin, D. T., Emerick, K. S., Rocco, J. W., and Deschler, D. G. (2015). The time course and microbiology of surgical site infections after head and neck free flap surgery. Laryngoscope *125*, 1084-1089.

El-Kenawi, A., Hänggi, K., and Ruffell, B. (2020). The Immune Microenvironment and Cancer Metastasis. Cold Spring Harb Perspect Med *10*.

Fridlender, Z. G., and Albelda, S. M. (2012). Tumor-associated neutrophils: friend or foe? Carcinogenesis *33*, 949-955.

Furumaya, C., Martinez-Sanz, P., Bouti, P., Kuijpers, T. W., and Matlung, H. L. (2020). Plasticity in Pro- and Anti-tumor Activity of Neutrophils: Shifting the Balance. Front Immunol *11*.

Giese, M. A., Hind, L. E., and Huttenlocher, A. (2019). Neutrophil plasticity in the tumor microenvironment. Blood *133*, 2159-2167.

Gong, L., Cumpian, A. M., Caetano, M. S., Ochoa, C. E., De la Garza, M. M., Lapid, D. J., Mirabolfathinejad, S. G., Dickey, B. F., Zhou, Q., and Moghaddam, S. J. (2013). Promoting effect of neutrophils on lung tumorigenesis is mediated by CXCR2 and neutrophil elastase. Mol Cancer *12*, 154.

Goodman, B., and Gardner, H. (2018). The microbiome and cancer. The Journal of pathology *244*, 667-676.

Guo, S., and Deng, C. X. (2018). Effect of Stromal Cells in Tumor Microenvironment on Metastasis Initiation. Int J Biol Sci *14*, 2083-2093.

Gupta, G. P., and Massagué, J. (2006). Cancer metastasis: building a framework. Cell *127*, 679-695.

Hedrick, C. C., and Malanchi, I. (2022). Neutrophils in cancer: heterogeneous and multifaceted. Nat Rev Immunol *22*, 173-187.

Helmink, B. A., Khan, M. A. W., Hermann, A., Gopalakrishnan, V., and Wargo, J. A. (2019). The microbiome, cancer, and cancer therapy. Nature Medicine *25*, 377-388.

Hoon, D. S., Ferris, R., Tanaka, R., Chong, K. K., Alix-Panabières, C., and Pantel, K. (2011). Molecular mechanisms of metastasis. J Surg Oncol *103*, 508-517.

Jorch, S. K., and Kubes, P. (2017). An emerging role for neutrophil extracellular traps in noninfectious disease. Nat Med *23*, 279-287.

Kanzaki, R., and Pietras, K. (2020). Heterogeneity of cancer-associated fibroblasts: Opportunities for precision medicine. Cancer science *111*, 2708-2717.

Kim, I. S., and Zhang, X. H. (2016). One microenvironment does not fit all: heterogeneity beyond cancer cells. Cancer Metastasis Rev *35*, 601-629.

Kim, S., Kim, H. E., Kang, B., Lee, Y. W., Kim, H., and Chung, D. K. (2017). Lipoteichoic Acid Isolated from Staphylococcus aureus Induces Both Epithelial-Mesenchymal Transition and Wound Healing in HaCaT Cells. J Microbiol Biotechnol *27*, 1820-1826.

Klein, C. A. (2020). Cancer progression and the invisible phase of metastatic colonization. Nat Rev Cancer *20*, 681-694.

Lambert, A. W., Pattabiraman, D. R., and Weinberg, R. A. (2017). Emerging Biological Principles of Metastasis. Cell *168*, 670-691.

Lerman, I., and Hammes, S. R. (2018). Neutrophil elastase in the tumor microenvironment. Steroids *133*, 96-101.

Liang, W., and Ferrara, N. (2016). The Complex Role of Neutrophils in Tumor Angiogenesis and Metastasis. Cancer immunology research *4*, 83-91.

Liu, Y., and Liu, L. (2020). The pro-tumor effect and the anti-tumor effect of neutrophils extracellular traps. Biosci Trends *13*, 469-475.

López-Soto, A., Gonzalez, S., Smyth, M. J., and Galluzzi, L. (2017). Control of Metastasis by NK Cells. Cancer Cell *32*, 135-154.

Magalhaes, M. A., Glogauer, J. E., and Glogauer, M. (2014). Neutrophils and oral squamous cell carcinoma: lessons learned and future directions. J Leukoc Biol *96*, 695-702.

Mantovani, A., Allavena, P., Sica, A., and Balkwill, F. (2008). Cancer-related inflammation. Nature *454*, 436-444.

Masucci, M. T., Minopoli, M., Del Vecchio, S., and Carriero, M. V. (2020). The Emerging Role of Neutrophil Extracellular Traps (NETs) in Tumor Progression and Metastasis. Front Immunol *11*.

McFarlane, A. J., Fercoq, F., Coffelt, S. B., and Carlin, L. M. (2021). Neutrophil dynamics in the tumor microenvironment. J Clin Invest *131*.

Micalizzi, D. S., Ebright, R. Y., Haber, D. A., and Maheswaran, S. (2021). Translational Regulation of Cancer Metastasis. Cancer research *81*, 517-524.

Mukaida, N., Sasaki, S. I., and Baba, T. (2020). Two-Faced Roles of Tumor-Associated Neutrophils in Cancer Development and Progression. Int J Mol Sci *21*.

Nejman, D., Livyatan, I., Fuks, G., Gavert, N., Zwang, Y., Geller, L. T., Rotter-Maskowitz, A., Weiser, R., Mallel, G., Gigi, E., *et al.* (2020). The human tumor microbiome is composed of tumor type-specific intracellular bacteria. Science *368*, 973-980.

Ng, L. G., Ostuni, R., and Hidalgo, A. (2019). Heterogeneity of neutrophils. Nat Rev Immunol *19*, 255-265.

Nicolás-Ávila, J., Adrover, J. M., and Hidalgo, A. (2017). Neutrophils in Homeostasis, Immunity, and Cancer. Immunity *46*, 15-28.

Nieto, M. A., Huang, R. Y., Jackson, R. A., and Thiery, J. P. (2016). EMT: 2016. Cell *166*, 21-45.

Nisar, S., Yousuf, P., Masoodi, T., Wani, N. A., Hashem, S., Singh, M., Sageena, G., Mishra, D., Kumar, R., Haris, M., *et al.* (2021). Chemokine-Cytokine Networks in the Head and Neck Tumor Microenvironment. Int J Mol Sci *22*.

Papayannopoulos, V. (2018). Neutrophil extracellular traps in immunity and disease. Nat Rev Immunol *18*, 134-147.

Poutahidis, T., and Erdman, S. E. (2016). Commensal bacteria modulate the tumor microenvironment. Cancer Lett *380*, 356-358.

Qin, Y., Zheng, X., Gao, W., Wang, B., and Wu, Y. (2021). Tumor microenvironment and immune-related therapies of head and neck squamous cell carcinoma. Mol Ther Oncolytics *20*, 342-351.

Quail, D. F., and Joyce, J. A. (2013). Microenvironmental regulation of tumor progression and metastasis. Nat Med *19*, 1423-1437.

Rumgay, H., Murphy, N., Ferrari, P., and Soerjomataram, I. (2021). Alcohol and Cancer: Epidemiology and Biological Mechanisms. Nutrients *13*.

Schwabe, R. F., and Jobin, C. (2013). The microbiome and cancer. Nat Rev Cancer *13*, 800-812.

SenGupta, S., Hein, L. E., and Parent, C. A. (2021). The Recruitment of Neutrophils to the Tumor Microenvironment Is Regulated by Multiple Mediators. Front Immunol *12*.

Sepich-Poore, G. D., Zitvogel, L., Straussman, R., Hasty, J., Wargo, J. A., and Knight, R. (2021). The microbiome and human cancer. Science *371*.

Sharma, N., Bhatia, S., Sodhi, A. S., and Batra, N. (2018). Oral microbiome and health. AIMS Microbiol *4*, 42-66.

Shaul, M. E., and Fridlender, Z. G. (2017). Neutrophils as active regulators of the immune system in the tumor microenvironment. J Leukoc Biol *102*, 343-349.

Shiomori, T., Miyamoto, H., Udaka, T., Okochi, J., Hiraki, N., Hohchi, N., Hashida, K., Fujimura, T., Kitamura, T., Nagatani, G., *et al.* (2007). Clinical features of head and neck cancer patients with methicillin-resistant Staphylococcus aureus. Acta Otolaryngol *127*, 180-185.

Si, Y., Merz, S. F., Jansen, P., Wang, B., Bruderek, K., Altenhoff, P., Mattheis, S., Lang, S., Gunzer, M., Klode, J., *et al.* (2019). Multidimensional Imaging Provides Evidence for Down-Regulation of T cell Effector Function by MDSC in Human Cancer Tissue. Science immunology *4*.

Smith, C. K., and Trinchieri, G. (2018). The interplay between neutrophils and microbiota in cancer. J Leukoc Biol *104*, 701-715.

Smith, H. A., and Kang, Y. (2013). The metastasis-promoting roles of tumor-associated immune cells. J Mol Med (Berl) *91*, 411-429.

Steeg, P. S. (2006). Tumor metastasis: mechanistic insights and clinical challenges. Nat Med *12*, 895-904.

Sun, J., Tang, Q., Yu, S., Xie, M., Xie, Y., Chen, G., and Chen, L. (2020). Role of the oral microbiota in cancer evolution and progression. Cancer Med *9*, 6306-6321.

Teijeira, Á., Garasa, S., Gato, M., Alfaro, C., Migueliz, I., Cirella, A., de Andrea, C., Ochoa, M. C., Otano, I., Etxeberria, I., *et al.* (2020). CXCR1 and CXCR2 Chemokine Receptor Agonists Produced by Tumors Induce Neutrophil Extracellular Traps that Interfere with Immune Cytotoxicity. Immunity *52*, 856-871.

Templeton, A. J., McNamara, M. G., Šeruga, B., Vera-Badillo, F. E., Aneja, P., Ocaña, A., Leibowitz-Amit, R., Sonpavde, G., Knox, J. J., Tran, B., *et al.* (2014). Prognostic role of neutrophil-to-lymphocyte ratio in solid tumors: a systematic review and meta-analysis. J Natl Cancer Inst *106*.

Trellakis, S., Bruderek, K., Dumitru, C. A., Gholaman, H., Gu, X., Bankfalvi, A., Scherag, A., Hütte, J., Dominas, N., Lehnerdt, G. F., *et al.* (2011). Polymorphonuclear granulocytes in human head and neck cancer: enhanced inflammatory activity, modulation by cancer cells and expansion in advanced disease. Int J Cancer *129*, 2183-2193.

Vahle, A. K., Kerem, A., Oztürk, E., Bankfalvi, A., Lang, S., and Brandau, S. (2012). Optimization of an orthotopic murine model of head and neck squamous cell carcinoma in fully immunocompetent mice--role of toll-like-receptor 4 expressed on host cells. Cancer Lett *317*, 199-206.

Valastyan, S., and Weinberg, R. A. (2011). Tumor metastasis: molecular insights and evolving paradigms. Cell *147*, 275-292.

Veyel, D., Kierszniowska, S., Kosmacz, M., Sokolowska, E. M., Michaelis, A., Luzarowski, M., Szlachetko, J., Willmitzer, L., and Skirycz, A. (2017). System-wide detection of protein-small molecule complexes suggests extensive metabolite regulation in plants. Scientific Reports *7*.

Vitale, I., Shema, E., Loi, S., and Galluzzi, L. (2021). Intratumoral heterogeneity in cancer progression and response to immunotherapy. Nat Med *27*, 212-224.

Wan, L., Pantel, K., and Kang, Y. (2013). Tumor metastasis: moving new biological insights into the clinic. Nat Med *19*, 1450-1464.

Wang, Q., Li, T., Wu, W., and Ding, G. (2020). Interplay between mesenchymal stem cell and tumor and potential application. Hum Cell *33*, 444-458.

Whitmore, S. E., and Lamont, R. J. (2014). Oral bacteria and cancer. PLoS Pathog *10*.

Wong-Rolle, A., Wei, H. K., Zhao, C., and Jin, C. (2021). Unexpected guests in the tumor microenvironment: microbiome in cancer. Protein Cell *12*, 426-435.

Wu, L., Saxena, S., and Singh, R. K. (2020). Neutrophils in the Tumor Microenvironment. Adv Exp Med Biol *1224*, 1-20.

Yang, L., and Lin, P. C. (2017). Mechanisms that drive inflammatory tumor microenvironment, tumor heterogeneity, and metastatic progression. Semin Cancer Biol *47*, 185-195.

Yeung, K. T., and Yang, J. (2017). Epithelial-mesenchymal transition in tumor metastasis. Mol Oncol *11*, 28-39.

Yu, Z. K., Xie, R. L., You, R., Liu, Y. P., Chen, X. Y., Chen, M. Y., and Huang, P. Y. (2021). The role of the bacterial microbiome in the treatment of cancer. BMC Cancer *21*.

Zella, D., and Gallo, R. C. (2021). Viruses and Bacteria Associated with Cancer: An Overview. Viruses *13*.

Zhang, D., and Frenette, P. S. (2019). Cross talk between neutrophils and the microbiota. Blood *133*, 2168-2177.

Zhuang, X., Zhang, H., and Hu, G. (2019). Cancer and Microenvironment Plasticity: Double-Edged Swords in Metastasis. Trends Pharmacol Sci *40*, 419-429.

Zitvogel, L., Daillère, R., Roberti, M. P., Routy, B., and Kroemer, G. (2017). Anticancer effects of the microbiome and its products. Nat Rev Microbiol *15*, 465-478.

9. APPENDIX

TABLE 2: CHARACTERISTICS OF PATIENTS USED FOR TUMOR TISSUE STUDY

Patients' characteristics	**Numbers**	**% of total**
Gender		
male	41	75.9
female	13	24.1
Tumor localization		
orohypopharynx	54	100
Tumor size		
T1	1	1.9
T2	16	29.6
T3	25	46.3
T4	12	22.2
Lymph node metastasis		
N0	17	31.5
N1	10	18.5
N2a	4	7.4
N2b	10	18.5
N2c	12	22.2
N3	1	1.9

Distal metastasis		
M0	50	92.6
M1	4	7.4
Histological grade		
Grade 1	5	9.3
Grade 2	31	57.4
Grade 3	18	33.3

TABLE 3: LIST OF GENES SELECTED FOR METASTASIS-RELATED RNASEQ ANALYSIS

ABCG2	CCL20	CYP1A1	FN1	INHBA	MAST4	PIK3CA	SDC4	TGFA
ABLIM1	CCM2	CYP1B1	FN1	ITGA2	MDGA1	PIK3CD	SELENBP1	TGFB1
AC007686.4	CCND1	CYP26B1	FNDC3B	ITGA5	MET	PIK3R1	SEMA3A	THBD
ADAM8	CCND2	DAB2	FOS	ITGA6	METTL27	PIM1	SEMA3B	THBS1
ADORA2B	CCNE2	DAPP1	FOSL1	ITGB1	MINK1	PKP2	SERPINA1	THY1
AEN	CD24	DDIT4	FUT1	JAG1	MMP1	PLAK	SERPINB1	TIMP1
AGRN	CD44	DDR1	FUT3	JDP2	MMP13	PLAU	SERPINE1	TJP1

AHR	CD49C	DDR2	FYN	JUN	MMP3	PLAUR	SERPINE2	TLR6
AJUBA	CD55	DGKE	GAB2	KCNG1	MMP9	PLEK2	SESN2	TMEM156
AKAP12	CD82	DNAJA1	GADD45A	KCNN3	MMRN1	PLK2	SH2B2	TNFAIP3
AKNA	CDC25A	DSP	GALNT6	KDM4A	MPZL2	PLOD1	SH2B3	TNF-A
AL137003.2	CDCP1	DUSP1	GAP43	KDM6B	MRAS	PLOD2	SIAH2	TNFRSF21
ALDH1A1	CDH1	DUSP2	GATA3	KDM7A	MTSS1	PMAIP1	SLC1A4	TNFRSF8
ALDH1A3	CDH11	DUSP4	GCH1	KDM7A-DT	MXD1	PPIF	SLC29A3	TNFRSF9
ALDH6A1	CDH2	DUSP5	GEM	KIF5B	MYADM	PPP1R15A	SLC38A5	TNFSF9
AMOTL2	CDK12	DUSP6	GINS3	KLF6	MYC	PRDM1	SLC7A11	TP53
ANTXR2	CDKN1A	DUSP7	GJB3	KLHDC8B	MYORG	PRKCE	SLC8B1	TRIB1
ANXA4	CDKN2A	ECM1	GJB5	KRT15	NAV2	PSMB9	SMPD1	TRIB2
APOC1	CEBPB	EGFR	GNA15	KRT16A	NAV3	PTAFR	SNAI1	TRIB3
AQP3	CEBPG	EGR1	GSDMB	KRT17	NDRG1	PTEN	SNAI2	TRIM35

AREG	CES1	ELK3	GST-PHI	KRT18	NEAT1	PTGS1	SNPH	TRMU
ARNTL	CFD	ELMO1	H19	KRT7	NES1	PTGS2	SOCS3	TSC22D3
ARSD	CGA	EPCAM	HBEGF	KRT8	NF1	PTPRG	SOX4	TUBA1A
ASNS	CHAC1	EPHA2	HIF1A	KYNU	NFKB2	PTPRH	SOX9	TUFT1
ATF3	CHRM3	ERBB2	HMOX1	LAD	NFKBIA	PTPRM	SP140	TWIST1
ATF5	CLDN1	ERBB4	HRAS	LAMA3	NKX3-1	PTX3	SPP1	UBASH3B
ATP8A1	CLDN11	EREG	HS3ST1	LAMB2	NOTCH1	RAC2	SPRY4	UCHL1
ATXN1	CLDN4	ERN1	HSPA1A	LAMC2	NOTCH2	RAET1E	SRGN	UGCG
BBC3	CLDN7	ERRFI1	HSPA1B	LATS2	NOTCH2NLA	RARB	STC1	ULBP2
BDKRB2	CLIP2	ETS1	HYAL1	LIMA1	NR1D1	RASAL2	STC2	ULK4
BDNF	COL10A1	ETV5	ID2	LIN7A	NR1D2	RASGEF1A	STEAP1	UNG
BEND7	COL1A2	EXO1	IER3	LMO4	NRCAM	RASSF2	STK40	UPP1
beta-NGF	COL4A5	EYA4	IGF1R	LPAR3	NTSR1	RELB	STRA6	VASH1

BIRC3	COL6A3	F2R	IGFBP-5	LRBA	NUAK 2	RHOB	STX1A	VAV3
BIRC7	COL7A1	FBLN2	IGFBP-6	LRFN4	NXN	RIPK2	SUCNR 1	VEGFA
BMI1	CORO6	FBN1	IGFN1	LRRC19	PAX6	RND3	SYNGR 3	VEGF-C
BMP2	COX19	FCGR 2A	IGSF3	LURAP1 L	PCDH1 7	RPS6K A2	TC2N	VIM
BTG1	CRCP	FGF	IL11	LYPD3	PDE4D	RRM2	TCF7	WNT5A
C5AR1	CSRNP1	FGF5	IL1A	LYST	PDGFR A	RSPH3	TENAS CIN-C	WSCD1
CAK	CSRP2	FGFR1	IL1B	MAFF	PDLIM 4	S100A1 4	TFEB	XBP1
CARD1 0	CTNNB1	FGFR2	IL1R1	MAN1A 1	PGF	SAT1	TFPI2	ZEB1
CBLB	CXCL5	FGFR3	IL1RL1	MAP1B	PHLD A1	SCIN	TFRC	ZEB2
CCDC3 3	CXCL8	FLNA	IL24	MAP3K5	PHLDB 2	SDC1	TGASE	ZNF114

10. PRESENTATIONS

10.1. ORAL PRESENTATIONS

BIOME Graduate Seminar, Essen, 08.10.2018: **"Communication of tumor cells and stromal cells within the head and neck cancer microenvironment"**

Cellular and Molecular Immunology, Tumor and Signaling and Infectious Diseases BIOME annual retreat, Bonn, 05.11.2019: **"Inside the tumor microenvironment: Neutrophils as inducers of tumor progression and metastasis"**

BIOME Graduate Seminar, Essen, 30.11.2020: **"Bacteria enhance the pro-metastatic cross-talk of tumor cells and tumor-associated neutrophils"**

3rd International Symposium on Tumor-Host Interaction in Head and Neck Cancer, Essen, 28.01.2022: **"Bi-directional cross-talk of cancer cells and tumor-associated neutrophils triggers innate immune escape"**

10.2. POSTER PRESENTATIONS

1st European symposium on myeloid regulatory cells in health and disease, Essen, 01.11.2018–03.11.2018: **"Functional interplay in the tumor microenvironment: cross-talk between neutrophils, tumor cells and tumor-associated stromal cells"** Jagoda Szlachetko, Kirsten Bruderek, Stephan Lang, Alexander Hackel, Sven Brandau

Cellular and Molecular Immunology, Tumor and Signaling and Infectious Diseases BIOME annual retreat, Cologne, 08-09.11.2018: **"Functional interplay in the tumor microenvironment: cross-talk between neutrophils, tumor cells and tumor-associated stromal cells"** Jagoda Szlachetko, Kirsten Bruderek, Stephan Lang, Alexander Hackel, Sven Brandau

Tag der Forschung der Medizinischen Fakultät Universität Duisburg–Essen, Essen, 17.12.2018, **"Functional interplay in the tumor microenvironment: cross-talk between neutrophils, tumor cells and tumor-associated stromal cells"** Jagoda Szlachetko, Kirsten Bruderek, Stephan Lang, Alexander Hackel, Sven Brandau

2nd Essener, Translational Oncology Symposium (ETOS), Essen, 07.02.2019: „**Functional interplay in the tumor microenvironment: cross-talk between neutrophils, tumor cells and**

tumor-associated stromal cells" Jagoda Szlachetko, Kirsten Bruderek, Stephan Lang, Sven Brandau

53rd Annual Scientific Meeting of the European Society for Clinical Investigation (ESCI), Coimbra, Portugal, 22-24.05.2019: **„Cross-talk in the tumor microenvironment affects migration and biology of Tumor-Associated Neutrophils"** Jagoda Szlachetko, Yu Si, Kirsten Bruderek, Stephan Lang, Ronja Schirrmann, Sven Brandau

Tag der Forschung der Medizinischen Fakultät Universität Duisburg–Essen, Essen, 22.11.2019: „**Inside the tumor microenvironment: Who is helping tumor with progression and metastasis"** Jagoda Szlachetko, Lara-Jasmin Schröder, Sebastian Vollmer, Kirsten Bruderek, Stephan Lang, Sven Brandau

3rd Essener, Translational Oncology Symposium (ETOS), Essen, 06.02.2020: „**Inside the tumor microenvironment: Neutrophils as inducers of tumor progression and metastasis"** Jagoda Szlachetko, Sebastian Vollmer, Lara-Jasmin Schröder, Maike Busch, Nicole Dünker, Sven Brandau

Tag der Forschung der Medizinischen Fakultät Universität Duisburg–Essen, Essen, 27.11.2020: „**Bacteria enhance the pro-metastatic cross-talk of tumor cells and tumor-associated neutrophils"** Jagoda Szlachetko, Lara-Jasmin Schröder, Sebastian Vollmer, Maike Busch, Kirsten Bruderek, Stephan Lang, Nicole Dünker, Sven Brandau

Neutrophil 2021, online conference, Edinburgh, 31.05.2021–01.06.2021: „**Bi-directional cross-talk of cancer cells and tumor-associated neutrophils triggers innate immune escape"** Jagoda Szlachetko, Sebastian Vollmer, Sven Brandau

Tag der Forschung der Medizinischen Fakultät Universität Duisburg–Essen, Essen, 19.11.2021: "**Bi-directional cross-talk of cancer cells and tumor-associated neutrophils triggers innate immune escape"** Jagoda Szlachetko, Sebastian Vollmer, Sven Brandau

ACKNOWLEDGEMENTS

My PhD journey was definitely not fast and easy, but fortunately I had people in my life who helped me to get through it.

First of all, I would like to thank Prof. Sven Brandau. For the past five years you were leading me through my project, helping me when I got stuck and started overthinking. You taught me that funny part of science is not in answering the easy questions, but in being constantly surprised by your own results and drawing new hypotheses. Thanks for showing me what I am capable of as a scientist and respecting my introvert comfort zone during the meetings.

The practical part of my project would not be possible without a support of my lab mates. Special thanks to Sebastian Vollmer for suffering together with me through the EMT project. Your technical help (thousands opened eggs and scratched plates), endless conversations about everything and egg-cellent humour will never be forgotten. I want to thank Kirsten Bruderek for teaching me most of the lab methods used in this thesis and not shouting when I put my ordering in the book 5 minutes after the deadline. Also, she, together with Petra Altenhoff introduced me to the weird German culture and helped to survive the adaptation time 😊. Thanks to Alex Hackel and Yu Si, with whom I shared serious and less serious conversations both in the lab and over the cocktails after long experiments. Big thank you to Ronja Schirrmann for being the best office mate I could have imagined. I am really glad I could share PhD experience with you. Thanks for reading my abstracts, practicing my talks with me and trying to put some optimistic attitude in our office. Thanks to Lara-Jasmin Schröder for deciding to stay with me for her master thesis and performing all the *in ovo* experiments, which can be found in this thesis. Thanks to Antonio Hrvat and Christian Doreth for our board games meetings, where we could just pretend we don't talk about the work and complain about the experiments in the meantime. Thanks to Mathias Schmidt for endless science puns and litres of buffers prepared for me. Thanks to Kim Lamers, Xi Wang, Rebeka Bošnjaković, Benedict Antuamwine, Simon Lemm, Tanja Hardt-Knechtli, Larissa Loska and Francisca Hofmann Vega for an amazing atmosphere in the lab, surviving all my complaining and always being there to help.

Finally I would like to thank all my friends and family for the endless support I got from them over last years. Thanks to Mateusz, Monia, Justyna, Karo, Krzyś and Sebastian, you all knew how

challenging PhD journey can be and kept me fighting when I didn't see the light in the tunnel anymore.

Thanks to my amazing parents which always supported crazy dreams of their daughter and let me believe that I can achieve everything I can imagine. Mamuś, tatuś bardzo Wam dziękuję za wspieranie wszystkich moich szalonych pomysłów i sprawienie, że sama uwierzyłam, że mogę osiagnąć co tylko sobie wymarzę. Thanks to my sister and my grandparents which even if have no idea what exactly I am doing always made me feel loved and supported. Paula, baciu Krysiu, babciu Elu, dziadku Mańku bardzo wam dziękuję za wasze wsparcie i wiarę, że wreszcie skończę ten doktorat.

Last but not least, I wanted to thank my partner – Stefan. Thanks for your mental support and understanding when I had to suddenly change our plans because of my experiments, thanks for waiting hours in front of department when meetings got too long and for showing me that life outside science exist and can be also fun 😊

This PhD journey was definitely not an easy ride, but with all the amazing people I have in my life I survived and now cannot wait for what is waiting for me around the corner.

CURRICULUM VITAE

"The curriculum vitae is not included in the online version for data protection reasons."

"The curriculum vitae is not included in the online version for data protection reasons."

STATUTORY DECLARATIONS

Declaration:

In accordance with § 6 (para. 2, clause g) of the Regulations Governing the Doctoral Proceedings of the Faculty of Biology for awarding the doctoral degree Dr. rer. nat., I hereby declare that I represent the field to which the topic "Bacterial stimulation enhances the pro-metastatic cross-talk of neutrophils and tumor cells*"* is assigned in research and teaching and that I support the application of Jagoda Szlachetko.

Essen, date _____ _____ _____

Name of the scientific supervisor/member of the University of Duisburg-Essen

Signature of the supervisor/member of the University of Duisburg-Essen

Declaration regarding previous attempts to attain a doctoral degree:

I hereby declare that in accordance with the Regulations Governing the Doctoral Proceedings of the Faculty of Biology § 6 (para. 2, clause e) I have undertaken no previous attempts to attain a doctoral degree.

Name in block letters: …….

Essen, date: …… …….

(Signature of the doctoral candidate)

Declaration regarding the commercial procurement of a doctoral supervisor
(§ 6, para. 2, clause f)

I hereby declare the following:
The present doctoral proceedings were not initiated via commercial procurement. In particular, no organisation has been engaged by me that, for a fee, has procured a doctoral supervisor nor has fulfilled all or part of my obligations with regard to examinations. Any third party help used up to now or will continue to be used has been/is only to a scientifically justifiable extent and in keeping with the laws on examinations.

I am aware that any falsehoods regarding the above statement could exclude me from the admission to the doctoral proceedings or later lead to the termination of the proceedings or to the withdrawal of the doctoral title.

Name in block letters: …….

Essen, date: …… ……..

(Signature of the doctoral candidate)

DOI: 10.17185/duepublico/78679
URN: urn:nbn:de:hbz:465-20250108-144414-3